

Fall 2013

# Cloud To Cloud Registration For 3d Point Data

Darion Shawn Grant  
*Purdue University*

Follow this and additional works at: [https://docs.lib.purdue.edu/open\\_access\\_dissertations](https://docs.lib.purdue.edu/open_access_dissertations)



Part of the [Civil Engineering Commons](#), and the [Computer Sciences Commons](#)

---

## Recommended Citation

Grant, Darion Shawn, "Cloud To Cloud Registration For 3d Point Data" (2013). *Open Access Dissertations*. 161.  
[https://docs.lib.purdue.edu/open\\_access\\_dissertations/161](https://docs.lib.purdue.edu/open_access_dissertations/161)

This document has been made available through Purdue e-Pubs, a service of the Purdue University Libraries. Please contact [epubs@purdue.edu](mailto:epubs@purdue.edu) for additional information.

**PURDUE UNIVERSITY**  
**GRADUATE SCHOOL**  
**Thesis/Dissertation Acceptance**

This is to certify that the thesis/dissertation prepared

By DARION SHAWN GRANT

Entitled

CLOUD TO CLOUD REGISTRATION FOR 3D POINT DATA

For the degree of Doctor of Philosophy

Is approved by the final examining committee:

JAMES S. BETHEL

Chair

MELBA M. CRAWFORD

AHMED H. SAMEH

BOUDEWIJN J. VAN GELDER

To the best of my knowledge and as understood by the student in the *Research Integrity and Copyright Disclaimer (Graduate School Form 20)*, this thesis/dissertation adheres to the provisions of Purdue University's "Policy on Integrity in Research" and the use of copyrighted material.

Approved by Major Professor(s): JAMES S. BETHEL

Approved by: MICHAEL KREGER

Head of the Graduate Program

08/28/2013

Date

CLOUD TO CLOUD REGISTRATION FOR 3D POINT DATA

A Dissertation

Submitted to the Faculty

of

Purdue University

by

Darion Shawn Grant

In Partial Fulfillment of the

Requirements for the Degree

of

Doctor of Philosophy

December 2013

Purdue University

West Lafayette, Indiana

## ACKNOWLEDGEMENTS

Blessed be the God and Father of our Lord Jesus Christ, who has made this dissertation possible. To Him be all glory, both now and forever. He has been with me from the beginning through the end. He never failed me nor forsook me and all I have needed his hands have provided. I am grateful for his faithfulness.

I am greatly indebted to my immediate and extended family who provided continual support financially, emotionally and spiritually through this long journey. I say a special thank you to my parents (Mr. Ronald Grant and Mrs. Jane Grant), my twin sister (Avion) and my little sister and brothers (Candice, Bevon and Emile). To my aunts (Ms. Ruth Williams and Mrs. Lynette Wiltshire), you have also been with me through this long journey and I thank you for your support as well. I will not forget your sacrificial love through these many years. To my other relatives you have contributed significantly to the completion of this stage and I give a big thank you to Ms. Myrna Spears and family, Mrs. Disa Awah, Mr. Eric Thompson and family, Mrs. Rita Duke and family, Mrs. Glenda Roberts and family, Mr. Neil Forbes and all my other cousins, aunts and uncles.

I thank my fellow Christians for your incessant prayers which our God has answered. I am indeed blessed to have you brothers and sisters who have helped carry this burden. Thank you to the saints from Tobago, Bro. Roberts and family, Sis. Teckler Graham and family, Bro. Paul and family and the believers at Hilltop Gospel Hall. To the saints at Fresno Gospel Hall I thank you for your prayers. I am especially thankful to Sis. Ruth Lee and Bro. Hamid Kombali for your prayers and kind words. To my Christian family at Kossuth St. Baptist Church, you have contributed immensely to my spiritual growth over these years. I specifically thank Mr. Paul Briggs and family, Mr. Mikel Berger and family, Mr. Daryll Starr and family, Dr. Tyler Johnson and family, Mr. Ben Whipple and family, Ms. Sarah Menefee and the many others who have played a significant part in my life at Purdue and West Lafayette. To my ACF brothers and sisters I bless the Lord for you and I say thank you also for the refreshing times together in studying the Word. I say thanks to the Adedokuns, the Ajuwons, the Agbelies, the Mundias, the Ankudeys, the Badu-Tawiahs and the other families and friends at ACF.

To all my friends, I thank you for the many fun moments. The late nights studying, the road trips and the many laughs we shared will always remain with me. I give God thanks for your impact in my life. You all provided much needed balance to the stressful days and nights of studying. Thank you goes to Ghambir, Mopelola, Dahlia, Bismark, Nwamaka, Oluwaseyi, Abraham, Olusegun, Naomi, Yves, Alain, Sheran, Charity, Nnaemeka, Tenille, Saria, Vincent, Fally, Oluwatoba, Dolu, Tolu, Francis, Daniel, Kamwana, Temi, Amadin, Akuffo and Rosemary.

I also thank my lab mates for the discussions we had and the fun experiences with publications and presentations. You were great company and you made the daily research activities less tedious. Special thanks go to Dr. Jinha Jung, Dr. Wonkook Kim, Mr. James Monty, Dr. Li Ma, Dr. Lexie Yang, Dr. Wei Di, Dr. Magda Galloza, Dr. Junhwa Chi, Dr. Garrett Pignotti and to the other visiting scholars who were a part of our lab. I must make special mention to Dr. Rochon, Mr. Larry Biehl, Mr. Lawrence Theller, Mr. Chris Siebern, Dr. Jyoti Mathur, Dr. Andrew Tarko and Ms. Vicki Leavitt who supervised me at some time at Purdue. You all were excellent supervisors and I am grateful to have worked with you.

I conclude with a very special thank you to the faculty who served on my PhD committee. My advisors, Dr. Bethel and Dr. Crawford have assisted me greatly and have guided me from the beginning of this process. I thank you Dr. Crawford for being my academic mother and for holding my hand along the way. I thank you Dr. Bethel for your insightful comments and discussions. The other committee members, Dr. Sameh and Dr. van Gelder have enriched my PhD through stimulating discussions in the classroom and I am very appreciative of this. I am also very grateful for the advice from Dr. Mikhail. To the other faculty in the Geomatics Department (Dr. Steven Johnson and Dr. Jie Shan) I thank you for your assistance.

To the many others who have assisted in one way or the other I say thank you.

## TABLE OF CONTENTS

	Page
LIST OF TABLES .....	vii
LIST OF FIGURES .....	viii
LIST OF ABBREVIATIONS.....	x
LIST OF SYMBOLS .....	xii
ABSTRACT.....	xiv
CHAPTER 1. INTRODUCTION.....	1
1.1 Background of Point Cloud Data .....	2
1.2 Motivation.....	4
1.3 Objectives.....	6
1.4 Thesis Organization .....	7
CHAPTER 2. LITERATURE REVIEW .....	9
2.1 Pairwise Registration .....	11
2.1.1 ICP Point Methods .....	11
2.1.2 ICP Plane Methods .....	15
2.2 Global Registration .....	18
CHAPTER 3. PAIRWISE REGISTRATION .....	23
3.1 Symmetric Correspondence .....	24
3.2 General Least Squares Adjustment Model.....	27
3.2.1 Deterministic Model.....	27
3.2.2 Stochastic Model .....	31
3.2.2.1 Individual Point Uncertainty .....	31
3.2.2.2 Planar Element Uncertainty.....	35
3.2.3 Adjustment and Registration Results .....	37
3.3 P2P Implementation .....	39
3.3.1 Overlap Region Between Scans .....	39
3.3.2 Inliers .....	40
3.3.3 Correspondence Sets .....	41
3.3.4 Iteration Termination Sets .....	42
3.3.5 Algorithm .....	43
3.4 Evaluations and Discussion .....	46

	Page
3.4.1	Internal Evaluations..... 47
3.4.1.1	Analytical Comparisons ..... 47
3.4.1.2	Simulated Experiments..... 49
3.4.1.3	Experiment with Real Data..... 53
3.4.2	Comparisons with Chen and Medioni (1991) ..... 60
3.4.2.1	ISPRS Buddha Data..... 60
3.4.2.2	Computer Vision Data #1 ..... 62
3.4.2.3	Computer Vision Data #2 ..... 64
3.4.2.4	Purdue Data ..... 74
3.5	Conclusions on Pairwise Registration.....77
CHAPTER 4.	GLOBAL REGISTRATION..... 80
4.1	Simultaneous Global Adjustment (P2Pg) .....82
4.2	P2Pg Algorithm.....86
4.3	Evaluations and Discussion .....89
4.3.1	Global Registration by Sequential Pairwise Approach ..... 89
4.3.2	Global Registration by Simultaneous Approach ..... 95
4.4	Conclusions on Global Registration .....98
CHAPTER 5.	FINAL CONCLUSIONS AND RECOMMENDATIONS ..... 100
5.1	Thesis Summary.....100
5.2	Final Conclusions.....102
5.3	Recommendations .....103
LIST OF REFERENCES	..... 106
APPENDICES	
Appendix A	Jacobians of Condition Equations for P2P Method .....110
Appendix B	Redundancy Calculation for P2P Method.....112
Appendix C	Jacobians of Condition Equations for P2Pg Method .....113
Appendix D	Transformed Planar Element and its Partial Derivatives .....116
Appendix E	Registration Parameter Errors .....118
VITA.....	120
PUBLICATIONS	.....121



## LIST OF TABLES

Table	Page
3-1 Cumulative Distribution of Incidence Angles.....	58
3-2 Runtime Comparisons (P2P vs Chen method).....	64
3-3 Description of data obtained from Salvi et al. (2007). .....	68
3-4 Initial registration RMSE for the different parameters.....	68
3-5 Number of points for each scan of the TLS data (Neil Armstrong). .....	76
3-6 Registration RMSE for each scan pair of the Neil Armstrong Statue.....	76
4-1 Pairwise Registration RMSE in mm, for scan pairs of the Purdue data. ....	92
4-2 Global Registration RMSE in mm, for scan pairs of the Purdue data.....	92
4-3 Global registration RMSE (in mm). .....	98
E-1 Pairwise parameter errors for each scan pair of the Purdue data. ....	118
E-2 Global parameter errors for each registered scan of the Purdue data. ....	119

## LIST OF FIGURES

Figure	Page
3-1 Symmetric Correspondence.....	26
3-2 Influence of Incidence Angle on Laser Footprint.....	34
3-3 Influence of Incidence Angle on Point Precision..	50
3-4 Effect of Point Precision on “Equivalent” Weights.....	52
3-5 Relative Effect of Point Precision on “Equivalent” Weights. ....	52
3-6 Intensity Images of Buddha Data (Left and Right Views).....	54
3-7 Comparison of Reference Variances..	56
3-8 Reference Variance.....	58
3-9 Average improvement in reference variance.....	59
3-10 Final reference variance per registration method .....	59
3-11 Comparison of Registration Methods.....	62
3-12 Data used for simulated experiments.....	65
3-13 Registration RMSE bars for fractal data.....	69
3-14 Registration RMSE bars for wave data..	70
3-15 Registration RMSE bars for owl data.....	71
3-16 Registration RMSE bars for frog data..	72
3-17 Neil Armstrong statue and layout of scans and targets. ....	75
4-1 Registration Misclosure for different algorithms/software..	93

Figure	Page
4-2 View from scan 6 of Purdue data, registered by <b>Besl</b> . .....	94
4-3 View from scan 6 of Purdue data, registered by <b>P2P</b> .....	94
4-4 View from scan 6 of Purdue data, registered by <b>Cyclone</b> .....	95
4-5 Registration RMSE before and after refinement. ....	96
4-6 Distribution of global registration errors by P2P.....	97
4-7 Distribution of global registration errors by P2Pg.....	97
5-1 Example sparse matrices from pair#1 of Neil Armstrong Data. ....	105

## LIST OF ABBREVIATIONS

<b>Abbreviation</b>	<b>Meaning</b>
2D	Two dimensional
3D	Three dimensional
3DIM	3D Digital Imaging and Modeling
ACM	Association for Computing Machinery
ALS	Airborne Laser Scanning (or Scanner)
ASPRS	American Society of Photogrammetry and Remote Sensing
ASTM	American Society for Testing and Materials
DEM(s)	Digital Elevation Model(s)
GNSS	Global Navigation Satellite System
ICP	Iterative Closest Point (sometimes used for Iterative Closest Plane)
ICPlane	Iterative Closest Plane
ICPoint	Iterative Closest Point
ISPRS	International Society for Photogrammetry and Remote Sensing
k-d tree	k-dimensional tree
LiDAR	Light Detection And Ranging
LS3D	Least Squares 3D Surface Matching
MLS	Mobile Laser Scanning (or Scanner)

NIST	National Institute of Standards and Technology
P2P	Point-to-Plane registration method
P2Pg	Point-to-Plane simultaneous global registration method
PAMI	Pattern Analysis and Machine Intelligence
PCD	Point Cloud Data
POS	Position and Orientation System
RMS	Root Mean Square
RMSD	Root Mean Square Distance
RMSE	Root Mean Square Error
SNR	Signal to Noise Ratio
SPIE	International Society for Optical Engineering
TIN(s)	Triangulated Irregular Network(s)
TLS	Terrestrial Laser Scanning (or Scanner)
UTM	Universal Transverse Mercator
WGS84	World Geodetic System 1984
w.r.t.	with respect to

## LIST OF SYMBOLS

<b>Symbol</b>	<b>Meaning</b>
$A$	Jacobian of the condition equations w.r.t. the observations
$B$	Jacobian of the condition equations w.r.t. the parameters
$P, Q$	3D coordinates for two overlapping point clouds
$R, t$	3x3 rotation matrix and 3x1 translation vector
$R_p, R_q$	3x3 rotation matrices for in $P$ and $Q$ respectively
$R_1, R_2, R_3$	Elementary rotations about x-, y- and z- axes respectively
$a, b, c$	Direction cosines of a unit normal vector
$bv$	Laser beam vector of a point
$d$	Normal distance from the origin of a plane
$f$	Vector of misclosure terms (discrepancy vector)
$l$	Observation vector
$n$	The unit normal vector of a plane
$o$	Zero vector
$p_i, q_i$	Individual scanned points in $P$ and $Q$ respectively
$\tilde{p}_i, \tilde{q}_i$	Transformed scanned points from $P$ and $Q$ respectively
$p_e, n_p$	Planar element in $P$ and its unit normal vector
$\tilde{p}_e, n_{\tilde{p}}$	Transformed planar element in $P$ and unit normal vector

$\mathbf{q}_e, \mathbf{n}_q$	Planar element in $\mathbf{Q}$ and its unit normal vector
$\tilde{\mathbf{q}}_e, \mathbf{n}_{\tilde{q}}$	Transformed planar element in $\mathbf{Q}$ and unit normal vector
$[p_x, p_y, p_z]$	Row vector of Cartesian point coordinates of a point in $\mathbf{P}$
$\mathbf{t}_p, \mathbf{t}_q$	3x1 translation vectors for $\mathbf{P}$ and $\mathbf{Q}$ respectively
$t_x, t_y, t_z$	Translations parallel to the x-, y- and z-axes respectively
$\mathbf{v}$	Vector of correction terms to observations (residual vector)
$\Sigma$	Cartesian covariance matrix of one or more observations
$\alpha$	Incidence angle
$k$	Point-to-plane distance
$\sigma$	Precision of an observable quantity
$\sigma_0^2$	Apriori reference variance
$[\rho, \theta, \phi]$	Range, vertical angle and horizontal angle respectively
$\emptyset$	Null matrix
$\omega, \phi, \kappa$	Euler angles about x-, y- and z- axes respectively
$[.]^T$ or $(.)^T$	Matrix transposition
$(\bullet)$	The dot (or inner) product of two vectors
$\in$	Is a member (or subset) of
$\Delta$	Vector of correction terms to parameters (unknown vector)
$diag(\cdot)$	Diagonal operator to create a diagonal matrix
$\cos(\cdot), \sin(\cdot)$	Trigonometric functions of cosine and sine respectively
$\frac{\partial(\cdot)}{\partial(\cdot)}$	Partial derivative

## ABSTRACT

Grant, Darion Shawn. Ph.D., Purdue University, December 2013. Cloud To Cloud Registration For 3D Point Data. Major Professors: James Bethel and Melba Crawford.

The vast potential of digital representation of objects by large collections of 3D points is being recognized on a global scale and has given rise to the popularity of point cloud data (PCD). 3D imaging sensors provide a means for quickly capturing dense and accurate geospatial information that represent the 3D geometry of objects in a digital environment. Due to spatial and temporal constraints, it is quite common that two or more sets of PCD are obtained to provide full 3D analysis. It is therefore quite essential that all the PCD are referenced to a homogeneous coordinate frame of reference.

This homogeneity in coordinates is achieved through a point cloud registration task and it involves determining a set of transformation parameters and applying those parameters to transform one dataset into another reference frame or to a global reference frame. The registration task typically involves the use of targets or other geometric features that are recognizable in the different sets of PCD. The recognition of these features usually involves the use of imagery, either intensity images or true-color images or both. In this dissertation, cloud-to-cloud registration, which is also called surface matching or surface



registration is investigated as an alternative registration method, which has potential for improved automation and accuracy.

The challenge in cloud-to-cloud registration lies in the fact that PCD are usually unstructured and possess little semantics. Two novel techniques were developed in this dissertation, one for the pairwise registration of PCD and the other for the global registration of PCD. The developed algorithms were evaluated by comparing with popular approaches and improvements in registration accuracy up to four fold were obtained. The improvement obtained may be attributed to some of the novel considerations introduced in this dissertation. The main novel idea is the simultaneous consideration of the stochastic properties of a pair of scans via the symmetric correspondence.

## CHAPTER 1. INTRODUCTION

In recent years the interest in three dimensional (3D) coordinate data capture has seen rapid growth in a variety of research and applied communities. The vast potential of digital representation of objects by large collections of 3D points is being recognized on a global scale and has given rise to the popularity of point cloud data (PCD). These collections of 3D points are frequently on the order of hundreds of thousands or even more (Cheok, 2006). They provide a dense and accurate means for quickly capturing and representing the 3D geometry of objects in a digital environment. Along with the vast potential of PCD however, come numerous research challenges, one of which is point cloud registration (Lichti et al., 2008).

It is quite common with PCD that two or more sets of coordinate data are obtained with each dataset having its own coordinate frame of reference. The task of point cloud registration involves determining a set of transformation parameters and applying those parameters to transform one dataset into another reference frame or to a global reference frame (Cheok, 2006). The challenge lies in the fact that PCD are usually unstructured and possess little semantics. Thus it is virtually impossible to establish exact point correspondences between sets of PCD. Various methods exist to deal with this challenge and this dissertation explores the use of point-to-nearest plane correspondences. In this

dissertation, mathematical concepts are developed and described for the registration of PCD. These concepts were implemented in the form of computer algorithms, and the algorithms will be discussed briefly. Experimental results will then be presented and discussed to evaluate the developed concepts and the final conclusions and recommendations will also be included in this dissertation.

The remainder of this introduction chapter will give some background on PCD. Here, the prevalent methods currently being used for obtaining PCD will be discussed and some of the applications of PCD will be provided. The research motivation will then be presented, followed by the goals and objectives of the research work. The introduction chapter concludes with an outline of the thesis organization.

### 1.1 Background of Point Cloud Data

The wide-spread adoption of PCD can perhaps be attributed to three major driving forces. First, the technological advancements in ranging sensors and techniques have given rise to a large number of 3D imaging systems which provide alternative means of acquiring PCD. These systems acquire 3D coordinate data at rapid rates operating on the order of thousands of measurements per second or faster. They include laser scanners, 3D optical scanners, 3D range cameras, 3D flash LiDARs, stereo vision systems and other devices and processes that can deliver 3D coordinate data (Huber, 2011; Cheok, 2006). There is now great flexibility in the size, mobility, accuracy, acquisition rates, operating distances, and ultimately the cost of these 3D imaging systems. This choice in available sensors has

increased the commercial viability of adopting 3D imaging systems (King and Li, 2012; Sansoni et al., 2009) and by extension, PCD.

Another major driving force has been the notable progress in software processing tools for PCD. In the last five to ten years, the research community has experienced increased activity with numerous conferences, workshops and special issue journal publications which were focused on processing algorithms (Lichti et al., 2008, King and Li, 2012; Bretar et al., 2011; Lichti et al., 2006). The dissemination of PCD and software tools has greatly benefitted from the open source movement as researchers and developers actively participate in data and knowledge sharing. The direct result has been that a suite of software libraries and tools has become readily available for point cloud processing. Some examples include LAStools, libLAS, libE57, PCL, PDAL, ITK, MeshLab, and CloudCompare. Furthermore, there has been significant progress in the standardization of file formats to facilitate data interchange among the ever-growing user community. The two most popular public file formats are the LAS and E57 formats. The LAS format was developed by the American Society of Photogrammetry and Remote Sensing (ASPRS) about ten years ago, to store PCD from airborne laser scanning (ALS). Since then there have been many improvements and the fifth format specification (LAS 1.4) was released in November 2011. This specification now accommodates PCD from other platforms (ASPRS, 2011). The E57 file format is more generic in nature and was developed about five years ago by the American Society for Testing and Materials (ASTM) (Huber, 2011).

A third major driving force has been the increased appreciation by the ever-growing user community, of the potential of 3D digital representation of objects. 3D digital models of people, animals, plants, objects and sites are of great interest to scientists, engineers, medical personnel, persons in the entertainment industry, and even clothes retailers. The spectrum of applications is wide and includes digital terrain modeling, digital documentation of cultural heritage, forensics, robotics, medical imaging, computer vision, forest structure estimation, 3D printing, and city modeling, to name a few. Two of the more recent industrial applications of PCD are arguably the most strategically placed to propel the utilization of PCD even further. These applications are the entertainment and clothing industries. In the entertainment industry, PCD are being used in motion sensing associated with gaming devices such as the Kinect sensor (Kinect, 2013). In the clothing industry, PCD are being used to obtain the perfect fit in shoe size and clothes size (SPAR, 2012).

These three major driving forces have combined to make PCD nearly ubiquitous. There is still significant ground to cover in the processing of PCD. One of these areas is point cloud registration, which is the focus of this dissertation.

## 1.2 Motivation

3D imaging systems generally operate with two distinct characteristics. First, they can only capture 3D geometry of the portions of objects that are within their line of sight. In many applications, the line-of-sight limitation requires either that the 3D imaging system or the objects of interest be moved, to obtain a complete 3D digital model. For example,

terrestrial laser scanning (TLS) is an active laser-based 3D imaging system which operates on a tripod platform (Lichti et al., 2008). In a typical TLS project, the platform must be moved two or more times to capture the 3D geometry of the entire object space because there is often occlusion. In Esser and Mayer (2007), the authors reported the use of 1168 scanner setups (or tripod positions) in their attempt to digitally document early-Christian wall paintings at the Domitilla Catacomb in Rome, with TLS.

Second, the acquired 3D coordinates of objects are intrinsically referenced to the position and orientation of the system at the epoch of data capture. Some 3D imaging systems operate on mobile platforms, such as in ALS and mobile laser scanning (MLS). These mobile systems often include a positioning and orientation system (POS), which allows all the captured PCD to be georeferenced to a common coordinate frame (King and Li, 2012). The static based 3D imaging systems such as those used in TLS, and in the entertainment industry (Kinect, 2013) do not typically include POS, however. Thus, PCD obtained at different platform locations have to be merged (or registered) to have all the data in the same coordinate reference frame. In the case of turn table 3D imaging systems as used in computer vision, the objects are moved and the imaging system is static (Bergevin et al., 1996). In this application, the obtained PCD are relative to the position and orientation of the object being imaged. Thus, every time the object moves coordinate registration is required.

Point cloud registration is also required in mobile applications that utilize POS. An example is 3D city modeling. The PCD obtained from ALS capture the geometry from an

aerial perspective and building facades are occluded. PCD from other 3D imaging systems such as MLS and/or TLS are needed and must be merged with (or registered to) the PCD from ALS. In general, there exist many other applications that require registration of PCD, for example sensor calibration and accuracy assessment. Point cloud registration is therefore an absolutely essential process and impacts the final accuracy of 3D modeling and analyses that follow (Akca and Gruen, 2010, Jacobs, 2005).

### 1.3 Objectives

The research community has recognized the importance of point cloud registration and has devoted much attention to this topic over the past two decades (Lichti et al., 2008). The primary aim of most of the research done in this area has been to obtain a fully automated method. Cloud-to-cloud (or surface based) registration has been pursued by many researchers over the last two decades to fulfill this aim. This registration method may potentially reduce or remove the dependency on targets (or tie points) and utilize the accuracy potential of the PCD (Akca and Gruen, 2008). In cloud-to-cloud registration methods the transformation parameters are obtained by establishing correspondences between the disparate 3D coordinate data. These methods can be divided into two groups, coarse and fine registration methods. Coarse registration methods determine good initial approximations for the registration parameters between overlapping sets of PCD. Fine registration methods assume that initial registration parameters exist and they aim to improve these parameters.

The interest in this dissertation is in the so-called fine registration methods, since in many applications especially among the geomatics community, initial registration parameters are typically available. This dissertation presents mathematical concepts developed to improve the accuracy of cloud-to-cloud registration with two main objectives. The first objective is to improve the registration accuracy of a pair of overlapping PCD (i.e. pairwise registration). This is done by utilizing the stochastic properties of all observables that contribute to the determination of the registration parameters. This has been lacking in many existing approaches as researchers have made certain assumptions in their stochastic models and neglected certain properties that this dissertation includes.

The second objective of this research is to improve the registration accuracy of multiple sets of PCD (i.e. global registration). A common approach to registering multiple sets of PCD is to perform a series of individual pairwise registrations among overlapping pairs of PCD. This sequential pairwise registration has its advantages and disadvantages, one of which is that the final solution may not be globally optimal. An alternative simultaneous approach is developed in this research to address some of these disadvantages.

#### 1.4 Thesis Organization

The remainder of this thesis is organized as follows. Chapter two reviews the literature related to methods of obtaining PCD and as well as registration methods. The review on registration methods first looks at pairwise registration methods. This is followed by a review of the related work on global registration methods. Chapters three and four



introduce the proposed methods for cloud-to-cloud registration. The proposed pairwise approach is presented first in Chapter three, along with experimental results and discussions. Chapter four includes the proposed global approach with the experimental results and discussions. Final conclusions, future work and recommendations are discussed in Chapter five.

## CHAPTER 2. LITERATURE REVIEW

The objective of point cloud registration is to align disparate PCD into one common coordinate reference frame. This reference frame may be an established geodetic coordinate frame such as the world geodetic system 1984 (WGS84), universal transverse Mercator (UTM) or state plane coordinate system. Local and/or arbitrary coordinate frames may also be used as the reference frame. The task of registration involves determining a set of transformation parameters and applying those parameters to transform one dataset into another reference frame (Cheok, 2006). For this to be achieved there must exist a means of establishing correspondences among the disparate coordinate data sets. Perhaps one of the most popular registration methods is the use of targets or other features that are recognizable in the different sets of PCD (Akca and Gruen, 2008; Elkrachy, 2008; Jacobs, 2005). The recognition of these features usually involves the use of imagery, either intensity images or true-color images or both.

Cloud-to-cloud registration, which is also called surface matching or surface registration (Akca and Gruen, 2008; Akca, 2007, Audette et al., 1999), is an alternative method with the potential for improved automation and accuracy (Akca and Gruen, 2008). With cloud-to-cloud methods, correspondences are established based only on the 3D coordinate data and they require that the sets of PCD overlap each other. One category of these methods

aims to establish correspondences that determine good initial approximations for the transformation (or registration) parameters that are also globally optimal. This category is referred to as coarse registration. Examples of this category include the use of point signatures, spin images, normal distribution transforms and segmentation methods (Brenner et al., 2008; Matabosch, 2007).

Another category of cloud-to-cloud methods is called fine registration. In these methods it is assumed that approximate values of the transformation parameters exist. These values can be obtained from the 3D imaging system's acquisition mode or from the output of some prior coarse registration. An iterative scheme is then typically employed to refine these approximate values and minimize a registration error metric between the sets of PCD. Like coarse registration, fine registration methods also establish correspondence features among sets of PCD. These features can involve points and various geometric features or shapes that are derived from the points. Derivative geometries may include lines, planes, higher order surfaces, TINs, or DEMs.

The focus of this dissertation is on fine registration and the related literature will be discussed in terms of two different modes. These modes will be referred to as pairwise registration and global registration. In pairwise registration the algorithms are concerned with a single pair of overlapping PCD, while with global registration, multiple sets of PCD need to be registered.

## 2.1 Pairwise Registration

Fine registration for pairwise cloud-to-cloud registration has a long history in the literature. Although methods can be traced as far back as 30 years ago (see Potmesil (1983)), the seminal work was presented in the early 1990's. Three groups of researchers (Chen and Medioni, (1991), Besl and McKay, (1992), and Zhang (1992)) independently developed similar registration methods about the same time. The name given by Besl and McKay (1992) for their method was the Iterative Closest Point (ICP) method. The three presented methods involve the iterative minimization of an error metric between overlapping PCD. The methods of Besl and McKay (1992) and Zhang (1992) may be referred to as point-to-point methods. Their methods utilize the actual points from both sets of PCD. Chen and Medioni (1991) utilize points from one set of PCD and local tangent planes in the other. This method may be referred to as a point-to-plane method. These three methods are sometimes referred collectively in the literature as the ICP method. However in this research it is preferred to distinguish these two registration paradigms. The method by Chen and Medioni (1991) is referred to as an ICPlane method. The methods of Besl and McKay (1992) and Zhang (1992) are referred to as ICPoint methods.

### 2.1.1 ICPoint Methods

Besl and McKay (1992) developed a method aimed at registering PCD that describes a rigid object (the data) to some known surface model of that object (the model). The model may be originally represented by points, lines, curves, or parametric surface. Assuming the model can be decomposed into points, then for each point in the data the

closest model point is obtained. The rotation and translation parameters that minimize the Euclidean distance (or error) between the set of closest point correspondences are then determined. These least squares parameters are used to transform the data and thus update the point coordinates. The process of closest model point correspondence, least squares parameter estimation and data transformation is repeated until the change in the data point coordinates falls below some threshold. Besl and McKay (1992) showed that this iterative algorithm converges monotonically to a local minimum with respect to the mean square distance objective function. The authors used the quaternion approach for obtaining the least squares parameters. It is important to note that the stochastic properties of the sets of PCD were ignored by Besl and McKay (1992). Also, this approach performs most accurately when the data (PCD representing the rigid object) is a subset of the model (PCD representing the known surface model). Besl and McKay (1992) also included an accelerated method in their original work. This method monitors the changes in parameter space and performs extrapolation to help predict the local minimum parameters in fewer iterations.

Zhang (1992) presented a similar approach soon after Besl and McKay (1992) with one major difference. Zhang (1992) made no assumption that one set of PCD was obtained from a known surface model. Thus, the presented approach involves the filtering of closest point correspondences if their Euclidean distance is above some threshold. This filtering makes the approach by Zhang (1992) more robust against outliers and occlusions that are common in PCD registration. Two other minor characteristics of the method of Zhang (1992) are that k-dimensional (k-d) trees are used for efficient closest point

searches and the dual-quaternion method is used for obtaining the least squares parameters. One advantage of the dual-quaternion method is that the stochastic properties of the PCD are partially included (Zhang, 1992).

Over the last two decades many researchers have modified various fundamental aspects of the ICP methods by Besl and McKay (1992) and Zhang (1992). One aspect that has attracted attention is the closest point search. This is the most computationally demanding step of ICP methods (Simon et al., 1994). Simon et al. (1994) investigated different enhancement strategies including k-d trees, coupled and de-coupled parameter acceleration, closest point caching and closest surface point caching. Blais and Levine (1995) presented an approach that utilized uniform subsampling to obtain control points. The authors also filtered the closest point correspondences by Euclidean distance in a manner similar to Zhang (1992). But instead of k-d trees the authors project control points along their spherical direction (inverse calibration) to quickly obtain closest point correspondences. Lavalley and Szeliski (1995) precomputed a 3D distance map they called an octree spline that speeds up the distance computation required in the closest point search. Their octree spline is an extension to the classical octree structure and leverages the benefits of adaptive spline functions.

Audette and Peters (1999) refined the distance map proposed by Lavalley and Szeliski (1995) to produce a closest-point map, which provides explicit point pairs suitable for closed-form transformation computation. Greenspan and Godin (2001) developed an ordering theorem that prunes the correspondence search space and is more efficient than

the k-d tree method or Elias method. Langis et al. (2001) proposed a parallel implementation of the Besl and McKay (1992) method where the correspondence calculations are distributed among the available processors to reduce the overall computational time. Jost and Hugli (2002) proposed a coarse to fine matching approach which uses increasingly more of the PCD at each successive iteration. In a similar manner, Zinsser et al. (2003) developed a hierarchical control point selection method which uses increasingly more points at each hierarchy level. More recently, Kim and Kim (2010) proposed a fast ICP algorithm that consists of two acceleration techniques. They use a hierarchical model point selection and a logarithmic data point search. Liu et al. (2012) proposed to use a spherical depth map to facilitate uniform down-sampling of the PCD and remove redundant points. Other related work on improving the correspondence search may be found in the reviews of Liu et al. (2012), Akca (2007) and Liu (2006).

In addition to correspondence search, there have been improvements on other aspects of the fundamental ICP methods. Some of these aspects include robustness to occlusion and outliers, convergence to local minima, consideration of the stochastic properties of the PCD, registration accuracy, convergence rate, and parameter estimation. The related literature is quite extensive. The interested reader is referred to Akca (2007), Matabosch (2007), Bae (2006), Liu (2004) and Rusinkiewicz and Levoy (2001) for useful reviews on other ICP methods.

### 2.1.2 ICPlane Methods

Perhaps the most popular point-to-plane approach is that of Chen and Medioni (1991) and it has since become the benchmark ICPlane registration method. This approach primarily involves two steps. These steps are line-surface intersection to obtain correspondences and the estimation of 3D coordinate transformation parameters between corresponding pairs of points. The authors developed an iterative approach that utilizes point-to-closest-plane correspondences instead of closest point correspondences as in ICPoint methods. Given a pair of overlapping PCD that represent the same object, a set of points (control points) is selected from smooth regions of one of the PCD. These control points are projected along their local surface normals to intersect the surface described by the other PCD. This line-surface intersection is done in an iterative manner until the change in the coordinates of the intersection points falls below a threshold. Local tangent planes are obtained at each intersection point and the transformation parameters that minimize the Euclidean distance between control points and tangent planes are determined. These least squares parameters are then used to transform the control points. The process of line-surface intersection, point-to-plane minimization and control point transformation is repeated until the change in the control points falls below a threshold.

Because of the similarity of Chen and Medioni (1991) to the ICPoint methods of Besl and McKay (1992) and Zhang (1992) many of the improvements used on ICPoint methods have also been proposed for ICPlane methods. Gagnon et al. (1994) modified Chen and Medioni (1991) in terms of the selection of control points and the search method for



corresponding closest plane. The authors extract discontinuous points and discard them to obtain feasible control points. These discontinuous points are identified based on least-squares planar fitting of an 8-point local neighborhood. Occluded points are also discarded based on a visibility test. For the closest plane search a two dimensional (2D) parametric approach is adopted. Each pair of PCD is converted to a grid structure based on a bilinear interpolation of the unstructured PCD. A point in one set of PCD is then projected along its surface normal to the parametric surface of the other PCD and the intersection point is then obtained. Dorai et al. (1998) also presented an extension to Chen and Medioni (1991) in terms of the selection of control points. An iterative scheme is devised to remove the most incompatible control point. This incompatible point is determined by comparing the distance to its corresponding tangent point with all other distances between control points and their corresponding tangent points. At the end of this iterative verification process all control points have corresponding tangent points such that the distance constraint of rigid transformation is enforced. Park and Subbarao (2003) developed an approach that combined Chen and Medioni (1991) with the point-to-projection ICP approach of Blais and Levine (1995). The combined approach of Park and Subbarao (2003) called the contractive projection point method was aimed at reducing the computational time for obtaining the corresponding intersection point.

The photogrammetric literature includes various ICPPlane approaches that were not necessarily developed as extensions to Chen and Medioni (1991). Jaw (1999) presented an approach for aerial triangulation of photogrammetric images by using unstructured ALS data as the control surface. For each measured photo point a neighborhood search

was employed to obtain the nearest 3-points and the plane passing through these points were determined. The General Least Squares adjustment model was used to determine the object space coordinates of photo measured points. The adjustment model minimized the Euclidean distance between photo points and their corresponding plane. Jaw (1999) used, a diagonal weight matrix in the adjustment thus sacrificing the correlation among some of the observations. Maas (2000) organized ALS data into TINs, and the point-to-TIN elevation differences were used to determine registration parameters for strip matching. Schenk et al. (2000) presented a similar registration approach for ALS data. Here a study was done to compare the use of elevation differences with the use of surface normal differences. Habib et al. (2001) presented an approach called the Modified Iterative Hough Transform, where the 3D similarity registration parameters were determined through a 2-step process. First there was a sequential and iterative parameter determination through the robust Hough transform to establish point-to-plane correspondences – the matching step. Then, these correspondences were used in a simultaneous least squares adjustment – the least squares solution step.

More recently Akca (2007) presented the Least Squares 3D Surface Matching (LS3D) approach. This method was designed for 3D surface data and is an extension of 2D least squares image matching. Planes were obtained from 3-point or 4-point local neighborhoods through a neighborhood search method, and the registration incorporates full 3D geometry in the estimation of the transformation parameters. However, the stochastic properties of the local surface normals were neglected in the LS3D approach. Habib et al. (2010) presented an approach called ICPatch. The presented approach

follows closely on the surface normal minimization method of Schenk et al. (2000). Levin and Filin (2010) presented a similar approach to Jaw (1999), where close-range photogrammetric imagery were mentioned in the mathematical explanation, but no details were provided for implementation purposes.

Other ICPlane methods exist in the literature, for example, Sande et al. (2010). In this approach the planes are extracted by a segmentation process, which means that planar features involve neighborhoods of typically more than four points. In this research it is preferred to exclude such methods in the study, since segmentation is itself an extensive research field. The developed approach in this dissertation will involve the utilization of corresponding point and planar features obtained from 3-point neighborhood. ICPoint methods are attractive in that they require no feature extraction (Lee et al., 2012). However, ICPlane methods are more accurate and achieve faster convergence than ICPoint methods (Chen and Medioni, 1991).

## 2.2 Global Registration

Researchers in the registration community have long recognized that many applications of PCD require multiple sets of PCD to be registered. When more than two sets of PCD need to be registered, one approach is to perform a series of sequential pairwise registration of the overlapping sets of PCD. Only the sequential overlap is considered in this approach, and the ignored information (i.e. non-sequential overlap) may potentially improve the global registration (Williams et al., 1999; Bergevin et al., 1996).

Chen and Medioni (1991) proposed a concatenation approach which utilizes the geometric information of previously merged sets of PCD and avoids the error propagation of sequential pairwise registrations. In a scenario where three scans overlap the transformation parameters needed to register scan 2 to scan 1 are first obtained. Scan 2 is transformed to the coordinate frame of scan 1 to obtain a merged or concatenated dataset. The parameters needed to register scan 3 to the previously concatenated dataset are obtained in the typical pairwise approach. The concatenated dataset is then updated with the transformed result of scan 3. Gagnon et al. (1994) and Bergevin et al. (1996) presented a simultaneous approach that computes transformation parameters for all overlapping pairs of PCD. In the method of Chen and Medioni (1991) a concatenated scan cannot be modified. Thus, geometric information from subsequent scans that may improve the concatenated result is not utilized. This drawback was dealt with by the method of Gagnon et al. (1994) and Bergevin et al. (1996), and a better global distribution of errors was obtained. The approach of Gagnon et al. (1994) and Bergevin et al. (1996) is a global ICPlane approach, where all the scans are transformed simultaneously to a common reference frame. Once point-to-plane correspondences have been established for all overlapping scans then the transformation needed for each scan to be expressed in the reference frame is computed. Thus, given  $N$  scans to be registered,  $N-1$  transformation matrices will be obtained at each iteration, with one of the scans kept fixed (the reference frame). Pulli (1999) highlighted the demands of the previous methods both in terms of memory requirement and computational cost. The author proposed a two-step approach where all overlapping pairs of PCD are first registered, one pair at a time, using any pairwise registration method. The second step involves a

simultaneous registration that enforces pairwise constraints that were obtained from the pairwise registration step. These constraints minimize the motion of overlapping regions while non-overlapping regions are free to move.

Williams et al. (1999) presented a novel weighted least squares method to deal with the stochastic properties of points in cases where they are heteroscedastically and anisotropically distributed. The inclusion of weights for the PCD was previously missing in the literature where earlier authors assumed the sets of PCD to have isotropic, identically, independent, and normally distributed measurement errors (Williams et al., 1999). The weighted least squares method of Williams et al. (1999) determines the global set of transformation parameters that minimizes the difference between the measured point coordinates and their estimated (or adjusted) coordinate values. Scaioni and Forlani (2003) presented a semi-automatic procedure that simultaneously registers multiple laser scans, based on the photogrammetric aerial triangulation by independent models method. The work done here is regarded as semi-automatic as they rely on retro-reflective targets for the registration. The interest though, in this research, is in fully automatic registration. Sharp et al. (2004) build up a graph that describes the relationship between neighboring sets of PCD, and then decompose the graph into basis cycles. They solve the nonlinear optimization problem over each basis cycle in closed form, and the solutions for the constituent basis cycles are merged using an averaging technique. Beinat (2006) reported a general model derived from the Generalized Procrustes Analysis, to obtain the simultaneous global registration of a set of PCD. The method is able to simultaneously consider all pairs of corresponding points obtained by ICPoint or ICPlane algorithms.

The authors reformulate the transformation parameters so they relate the coordinates of each set of PCD to a mean common reference coordinate frame. This reference coordinate frame is the geometric centroid of globally registered sets of PCD.

Zhai et al. (2006) introduced a closure condition for the global registration of PCD that depict a closed-circle (or ring) geometry. In this work, it is assumed that the first and last scans can be mathematically related in two ways. One would be through a combination of the successive transformations between the first and last scans. The second would be through the overlap that exists between the first and last scans. The authors imposed the condition that both mathematical relations should result in the same transformed coordinates for the last scan, assuming that the first scan is the reference. One novel contribution by the authors was their determination of the pairwise registration parameters in a simultaneous adjustment model. Akca (2007) proposed a similar approach to that of Scaioni and Forlani (2003), except Akca (2007) did not use targets. Akca (2007) first obtained correspondences between scans by performing a pairwise LS3D on all overlapping scans. The correspondences are thinned (i.e. every  $n$ -th correspondence is selected), and then used as “fictitious” targets in a simultaneous photogrammetric block adjustment by independent models. Kang (2008) extended the work of Zhai et al. (2006) by introducing a self-closure constraint among the ring of scans. Kang (2008) uses a simultaneous adjustment as in Zhai et al. (2006) where the first scan (the reference) appears both at the beginning and the end of the sequential chain of scans. The global registration enforces self-closure in that the position of the first scan when transformed by the series of sequential sets of parameters does not change.

Other authors have proposed different global registration approaches. For example, Rabbani (2006) and Rabbani et al. (2007) combine registration and modeling in one estimation task. The discussed literature however provides an overview of the major global registration approaches that have been developed.

### CHAPTER 3. PAIRWISE REGISTRATION

The formal definition of pairwise registration begins by first assuming that there exist two partially overlapping sets of PCD (or scans)<sup>1</sup>. It is also assumed that the coordinate frames for these scans are different and registration is needed to obtain a homogenous 3D model. Let  $\mathbf{P}$  and  $\mathbf{Q}$  refer to the 3D point coordinates of the PCD for the two partially overlapping scans. These two scans are registered to the same coordinate frame by using the 3D 6-parameter rigid-body transformation (Cheok, 2006) such that

$$\mathbf{Q} = \mathbf{R}(\mathbf{P}) + \mathbf{t} \quad (3.1)$$

$$\mathbf{R} = R_3(\kappa) * R_2(\phi) * R_1(\omega); \quad \mathbf{t} = [t_x, t_y, t_z]^T$$

In Eq. (3.1)  $\mathbf{R}$  is the conventional 3D orthogonal rotation matrix formed by three sequential rotations ( $R_1, R_2, R_3$ ) about the x-, y-, and z-axes of the  $\mathbf{P}$  coordinate frame, by the angles  $\omega, \phi$ , and  $\kappa$ , respectively.  $\mathbf{t}$  is the vector of translations ( $t_x, t_y, t_z$ ) that are parallel to the x-, y-, and z-axes respectively, of the  $\mathbf{Q}$  frame. The six rigid-body transformation parameters are thus  $\omega, \phi, \kappa, t_x, t_y, t_z$ . These parameters describe the relative orientation of  $\mathbf{P}$  with respect to (w.r.t.)  $\mathbf{Q}$ .

Eq (3.1) represents a classical 3D coordinate transformation. This is essentially the 3D similarity (or conformal) coordinate transformation (Mikhail and Ackermann, 1976) with

---

<sup>1</sup> In this research the terms PCD and scans are used interchangeably, as many 3D imaging systems are based on laser scanning technology.



the scale parameter set to unity. The parameter solution can be obtained in a very straightforward manner if exact point correspondences exist. However, 3D imaging systems typically acquire unstructured PCD, and no exact point correspondence (or labeling) exists. Following the work of Chen and Medioni (1991), it has been established that PCD can still be registered without exact point correspondences. This knowledge is built on in this research and a new ICPlane method called the P2P registration method has been developed. The proposed method extends the works of Akca (2007), Jaw (1999) and Levin and Filin (2010). Particular attention is paid to the stochastic properties of the local surface normals which were neglected in the work of Akca (2007). A full weight matrix is employed instead of the diagonal version in Jaw (1999). Furthermore, the registration parameters are solved for, and not point coordinates thus forming a linear system of equations with fewer unknowns than in Jaw (1999). Also it is not assumed that any of the data represent control surfaces or are error free, as in Chen and Medioni (1991), Jaw (1999) or Levin and Filin (2010). Instead, in this work correspondences are established on both scans. This duality of correspondences is referred to as commutativity in Godin et al. (1994). In this research work, it is preferred to describe this duality as symmetric correspondence.

### 3.1 Symmetric Correspondence

Chen and Medioni (1991) selected control points in smooth areas from  $\mathbf{P}$  and perform an iterative line-surface intersection to obtain their corresponding locations in  $\mathbf{Q}$ . The correspondence approach proposed in the P2P method differs from this in three ways.

1. The restriction of using smooth areas is removed and all points in  $\mathbf{P}$  may potentially be used. Instead of focusing on selecting “suitable” control points, the P2P method emphasizes the use of a stochastic model which enables all points to potentially contribute to the parameter solution.
2. Point-to-plane correspondences are established on both scans (see Figure 3-1). Corresponding tangent planes (or planar elements) are obtained for scanned points both in  $\mathbf{P}$  and  $\mathbf{Q}$ . This introduction of symmetric correspondences increases the redundancy of the adjustment as well as handles the varying point density of the sets of PCD (Goddin et al., 1994). Another benefit of the symmetric correspondences is that the uncertainty of both scans is considered simultaneously.
3. No iterative line-surface intersection is done in the P2P method. Rather, like Akca (2007) the nearest three sampled points are used to form a planar element.

Let the individual scanned points of  $\mathbf{P}$  and  $\mathbf{Q}$  be represented by  $\mathbf{p}_i$ , and  $\mathbf{q}_i$  respectively. Considering first those scanned points in  $\mathbf{P}$ , each  $\mathbf{p}_i$  can be transformed by the current approximation of the transformation parameters to obtain the transformed point  $\tilde{\mathbf{p}}_i$ . A nearest neighbor search is done to obtain the three scanned points in  $\mathbf{Q}$  that are closest to  $\tilde{\mathbf{p}}_i$  in terms of Euclidean distance. This triplet of points is referred to as a planar element whose unit normal vector is then determined. The planar element and its unit normal vector are denoted by  $\mathbf{q}_e$  and  $\mathbf{n}_q$  respectively. In a similar manner, a planar element  $\mathbf{p}_e$  and its unit normal vector  $\mathbf{n}_p$  can be obtained from the three scanned points in  $\mathbf{P}$  that are closest to the transformed point,  $\tilde{\mathbf{q}}_i$  from  $\mathbf{Q}$ .

The transformed points  $\tilde{\mathbf{p}}_i$  and  $\tilde{\mathbf{q}}_i$  are given by

$$\tilde{\mathbf{p}}_i = \mathbf{R}(\mathbf{p}_i) + \mathbf{t}; \quad \text{and} \quad \tilde{\mathbf{q}}_i = \mathbf{R}^T(\mathbf{q}_i - \mathbf{t}) \quad (3.2)$$

with 
$$\mathbf{p}_i = [p_x, p_y, p_z]^T; \quad \text{and} \quad \mathbf{q}_i = [q_x, q_y, q_z]^T$$

Potentially one may thus have a correspondence set for each scanned point in  $\mathbf{P}$ . This correspondence set contains the transformed point, its hypothesized planar element, and the unit normal vector of that planar element:  $\{\tilde{\mathbf{p}}_i, \mathbf{q}_e, \mathbf{n}_q\}$ . Likewise one may potentially have for each point in  $\mathbf{Q}$  the correspondence set:  $\{\tilde{\mathbf{q}}_i, \mathbf{p}_e, \mathbf{n}_p\}$ , as depicted in Figure 3-1

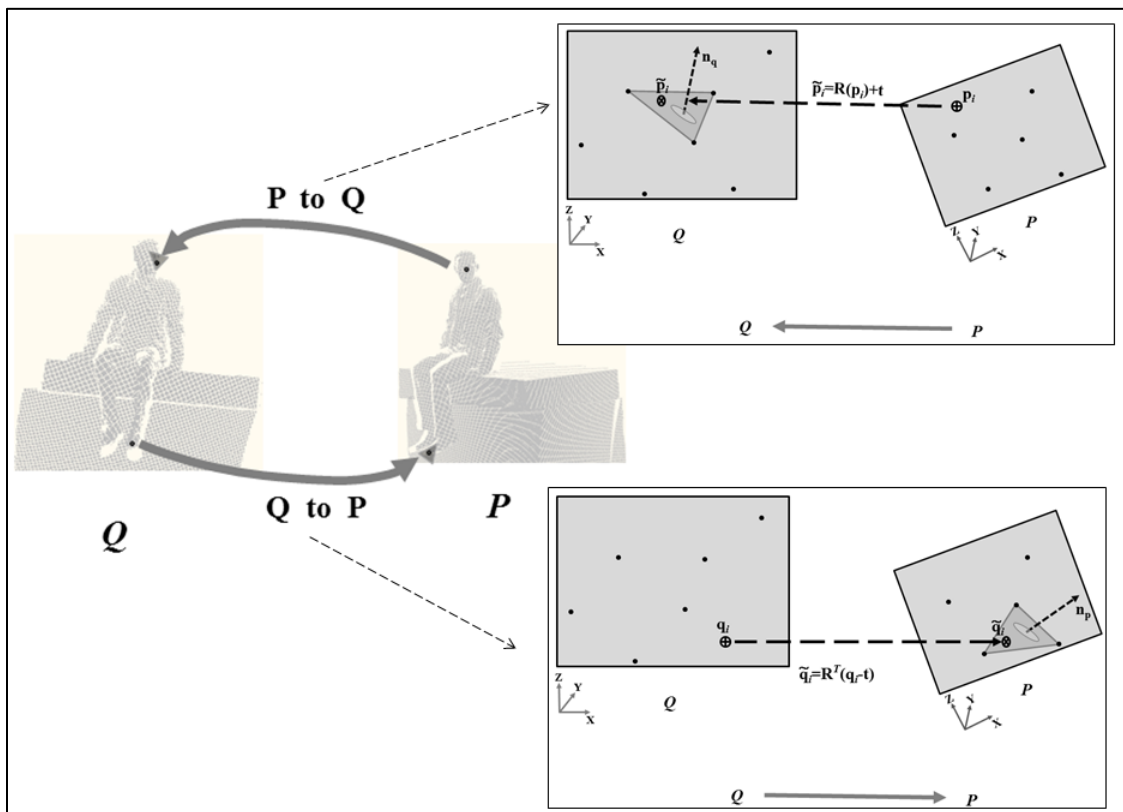


Figure 3-1 Symmetric Correspondence. Each transformed point is associated with a planar element and its unit normal vector.

### 3.2 General Least Squares Adjustment Model

The registration goal is to minimize the Euclidean distances between transformed points and their hypothesized corresponding planar elements. As was introduced by Chen and Medioni (1991), an iterative approach is necessary to refine the initial approximations to the transformation parameters because Eq. (3.1) is non-linear in relation to the parameters. The General Least Squares adjustment model<sup>2</sup> (Mikhail and Ackermann, 1976) is used for parameter estimation in the P2P method. This adjustment model involves both deterministic and stochastic components, and both are of importance in the registration of PCD.

#### 3.2.1 Deterministic Model

The mathematical formulation begins with the point-to-plane distance. Consider a plane with unit normal vector  $\mathbf{n}$ , whose direction cosines are  $\mathbf{a}, \mathbf{b}, \mathbf{c}$  and its normal distance from the origin  $\mathbf{d}$ . The equation of the plane is given by

$$\begin{aligned} \mathbf{a}x_0 + \mathbf{b}y_0 + \mathbf{c}z_0 + \mathbf{d} &= 0 \\ \Rightarrow \mathbf{d} &= -(\mathbf{a}x_0 + \mathbf{b}y_0 + \mathbf{c}z_0) \end{aligned} \tag{3.3}$$

In Eq. (3.3)  $x_0, y_0, z_0$  represent respectively the x-, y-, and z-coordinates of a point that lies on the plane. The signed distance  $k$  between an arbitrary point  $\mathbf{r}$ , and the plane with unit normal vector  $\mathbf{n}$  is

$$\begin{aligned} k &= \mathbf{a}r_x + \mathbf{b}r_y + \mathbf{c}r_z + \mathbf{d} \\ \mathbf{r} &= [r_x, r_y, r_z]^T \end{aligned} \tag{3.4}$$

---

<sup>2</sup> The General Least Squares adjustment model is also referred to in the literature as the Gauss-Helmert adjustment model, and as the Mixed Adjustment model.

If it is also known that the point  $\mathbf{u} = [u_x, u_y, u_z]^T$  lies on the plane then combining Eq. (3.3) and Eq. (3.4) gives

$$\begin{aligned} k &= \mathbf{a}r_x + \mathbf{b}r_y + \mathbf{c}r_z - (\mathbf{a}u_x + \mathbf{b}u_y + \mathbf{c}u_z) \\ \Rightarrow k &= (\mathbf{r} - \mathbf{u}) \cdot \mathbf{n} \end{aligned} \quad (3.5)$$

where  $(\bullet)$  is the dot (or inner) product of two vectors.

By symmetric correspondence, two sets of signed distances are obtained, one relating the correspondence sets in  $\mathbf{P}$  and another relating the correspondence sets in  $\mathbf{Q}$ . If  $\mathbf{P}$  and  $\mathbf{Q}$  are in perfect registration then the signed distances between scanned points and their corresponding planar elements will be zero. Mathematically, perfect registration may be expressed by the following two sets of condition equations which follow from Eq. (3.5):

$$\begin{aligned} F_1: (\tilde{\mathbf{p}} - \mathbf{q}) \cdot \mathbf{n}_q &= 0; & \mathbf{q} \in \mathbf{q}_e \\ F_2: (\tilde{\mathbf{q}} - \mathbf{p}) \cdot \mathbf{n}_p &= 0; & \mathbf{p} \in \mathbf{p}_e \end{aligned} \quad (3.6)$$

In Eq. (3.6)  $\mathbf{n}_q$  and  $\mathbf{n}_p$  represent the unit normal vectors of the planar elements  $\mathbf{q}_e$  and  $\mathbf{p}_e$  respectively.  $\mathbf{q}$  and  $\mathbf{p}$  represent any of the three points forming the planar elements  $\mathbf{q}_e$  and  $\mathbf{p}_e$  respectively.  $\tilde{\mathbf{p}}$  and  $\tilde{\mathbf{q}}$  represent a transformed point from  $\mathbf{P}$  and  $\mathbf{Q}$  respectively as defined in Eq. (3.2), but without the subscripts.

The correspondence sets in  $\mathbf{P}$  and  $\mathbf{Q}$  yield equations according to Eq.(3.6). The linearized form of Eq.(3.6) by Taylor series expansion gives the classical General Least Squares equation denoted in Mikhail and Ackermann (1976) as

$$\mathbf{A}\mathbf{v} + \mathbf{B}\Delta = \mathbf{f} \quad (3.7)$$

$\mathbf{A}$  is the Jacobian of the condition equations with respect to the observation

$\mathbf{B}$  is the Jacobian of the condition equations with respect to the parameter

$\mathbf{v}$  is the correction term of observations (residual vector)

$\Delta$  is the correction term of the parameters (unknown vector)

$\mathbf{f}$  is the misclosure term (discrepancy vector).

The known quantities of Eq.(3.7) are

$$\mathbf{A} = \begin{bmatrix} \mathbf{A}_1 \\ \mathbf{A}_2 \end{bmatrix}; \quad \mathbf{B} = \begin{bmatrix} \mathbf{B}_1 \\ \mathbf{B}_2 \end{bmatrix}; \quad \mathbf{f} = \begin{bmatrix} \mathbf{f}_1 \\ \mathbf{f}_2 \end{bmatrix} \quad (3.8)$$

where

$$\mathbf{A}_1 = [\mathbf{F}_1'(\mathbf{p}), \mathbf{F}_1'(\mathbf{q})]; \quad \mathbf{B}_1 = \mathbf{F}_1'(\Delta)$$

$$\mathbf{A}_2 = [\mathbf{F}_2'(\mathbf{p}), \mathbf{F}_2'(\mathbf{q})]; \quad \mathbf{B}_2 = \mathbf{F}_2'(\Delta)$$

$$\mathbf{f}_1 = -[\mathbf{F}_{1,0}]; \quad \mathbf{f}_2 = -[\mathbf{F}_{2,0}]$$

The observations are the individual scanned points in  $\mathbf{P}$  and  $\mathbf{Q}$ . These observations are combined into an observation vector  $\mathbf{l}$  such that for a pair of correspondence sets (one in  $\mathbf{P}$  and one in  $\mathbf{Q}$ ) one has  $\mathbf{l} = [\mathbf{p}, \mathbf{q}]^T$ . Here  $\mathbf{p}$  includes both the scanned points that form the planar element as well as the scanned point that is transformed and similarly for  $\mathbf{q}$ .  $\mathbf{F}_1'(\mathbf{p}), \mathbf{F}_1'(\mathbf{q})$  and  $\mathbf{F}_1'(\Delta)$  are the partial derivatives (or Jacobians) of the condition equation  $\mathbf{F}_1$  w.r.t.  $\mathbf{p}, \mathbf{q}$  and  $\Delta$  respectively. Similarly,  $\mathbf{F}_2'(\mathbf{p}), \mathbf{F}_2'(\mathbf{q})$  and  $\mathbf{F}_2'(\Delta)$  are the partial derivatives of the condition equation  $\mathbf{F}_2$  w.r.t.  $\mathbf{p}, \mathbf{q}$  and  $\Delta$  respectively. The detailed derivation of these Jacobians is given in Appendix A.

The unknown quantities of Eq.(3.7) are the residuals  $\mathbf{v}$ , and the parameter corrections  $\Delta$  to the six initial rigid body parameters,  $\omega, \phi, \kappa, t_x, t_y, t_z$ . The residuals may not always be of relevance in the current form. Alternatively it may be more meaningful to utilize the “equivalent” residuals  $\mathbf{A}\mathbf{v}$ , which refer to the point-to-plane distances for correspondence sets. The parameters are updated in an iterative fashion by repeatedly solving the following normal equation until convergence

$$\mathbf{N}\Delta = \mathbf{t} \quad (3.9)$$

$$\mathbf{N} = \mathbf{B}^T(\mathbf{A}\mathbf{Q}_{ll}\mathbf{A}^T)^{-1}\mathbf{B}; \quad \mathbf{t} = \mathbf{B}^T(\mathbf{A}\mathbf{Q}_{ll}\mathbf{A}^T)^{-1}\mathbf{f}; \quad \mathbf{Q}_{ll} = \frac{1}{\sigma_0^2}\Sigma$$

$\sigma_0^2$  is the apriori reference variance (typically set to 1)

$\Sigma$  is the Cartesian covariance matrix of the observations.

It must be noted that the correspondence set for a transformed point can potentially change at each iteration. Thus there is no iterating performed on the observations as may be done in the classical General Least Squares adjustment. Therefore, at each iteration only the parameters are improved, hence the reduced forms of  $\mathbf{f}_1$  and  $\mathbf{f}_2$  in Eq.(3.8). However, in cases where the residuals are large (used here loosely) it may be best to iterate on the observations as well. One may find that the residuals are large during the early iterations, especially if the initial registration parameters are not good approximations.

### 3.2.2 Stochastic Model

The stochastic model impacts the accuracy of the parameter solution in any weighted least squares adjustment. Various factors influence the precision of the individual scanned points (Soudarissanane et al., 2011; Romsek, 2008; Bae, 2006). These include the instrument's observational precision, geometric factors (e.g. incidence angle), radiometric factors (e.g. object reflectivity), and environmental factors (e.g. humidity). Each equation of the form in Eq.(3.6) involves two sets of points – the transformed points and their corresponding planar elements that are comprised of scanned points. Since these points are observations they contain observational error. The proposed P2P registration method incorporates the stochastic properties of both point clouds by quantifying the uncertainty of both the direct observations (individual points) and the derived quantities (planar elements).

#### 3.2.2.1 Individual Point Uncertainty

The uncertainty of individual points is captured in the covariance matrix of the observations which is denoted by  $\Sigma$  in Eq.(3.9). For a single point this covariance matrix is of dimension 3x3 and it reflects the impact of the various factors mentioned above. In the P2P method the instrument's precision and the incidence angle are considered, as these quantities are either provided (the precisions) or can be determined (the incidence angle).

The Cartesian and spherical coordinates of a scanned point  $\mathbf{r}$  are related by



$$\mathbf{r} = \begin{cases} r_x = \rho \cos(\theta) \cos(\varphi) \\ r_y = \rho \cos(\theta) \sin(\varphi) \\ r_z = \rho \sin(\theta) \end{cases} \quad (3.10)$$

In Eq.(3.10)  $[r_x, r_y, r_z]^T$  are the Cartesian coordinates. Let  $\mathbf{s} = [\rho, \theta, \varphi]^T$  be the spherical coordinates representing range, vertical angle and horizontal angle respectively. The spherical coordinates take values in the following intervals:  $\rho \in [0, \infty)$ ,  $\theta \in [-\pi/2, \pi/2]$ ,  $\varphi \in [0, 2\pi]$  where the angular terms are in radians. The trigonometric functions of cosine and sine are represented by  $\cos(\cdot)$  and  $\sin(\cdot)$  respectively. Given the precisions of the spherical coordinates and assuming<sup>3</sup> there are no correlations between these coordinates then the corresponding 3x3 spherical covariance matrix is

$$\Sigma_s = \text{diag}([\sigma_\rho^2, \sigma_\theta^2, \sigma_\varphi^2]) \quad (3.11)$$

where  $\text{diag}(\cdot)$  operates on a vector to create a square matrix whose diagonal elements are the elements of the vector.  $\sigma_\rho, \sigma_\theta, \sigma_\varphi$  are the precisions of the range, vertical angle and horizontal angle respectively.

Soudarissanane et al. (2011) reported that the incidence angle had a cosine effect on the precision of PCD that were acquired from TLS. The cosine of the incidence angle for a point is given by

$$\cos(\alpha) = \frac{\mathbf{bv} \cdot \mathbf{n}}{|\mathbf{bv}| * |\mathbf{n}|} \quad (3.12)$$

---

<sup>3</sup> There may be cases when the spherical coordinates are known to be correlated (especially the angular coordinates). In such cases a non-diagonal covariance matrix is warranted.

where  $\alpha$  is the incidence angle,  $\mathbf{bv}$  is the laser beam vector of the point and  $\mathbf{n}$  is the local surface normal at the point. The dot (or inner) product of two vectors and the scalar multiplication are represented respectively by  $(\bullet)$  and  $(*)$ .

For any scanned point with coordinates  $[\mathbf{x}, \mathbf{y}, \mathbf{z}]^T$  the laser beam vector is  $\mathbf{bv} = [\mathbf{x}, \mathbf{y}, \mathbf{z}]^T - [\mathbf{x}_0, \mathbf{y}_0, \mathbf{z}_0]^T$  where  $[\mathbf{x}_0, \mathbf{y}_0, \mathbf{z}_0]^T$  is the origin of the coordinate frame which is typically the zero vector  $[0,0,0]^T$ . The normal vector for a point is obtained by determining the plane that passes through its three nearest neighboring points. The issue of normal estimation for PCD is itself an area of open research with many proposed approaches. The optimal neighborhood size is an open question as the size affects the estimated normal in some cases. In this research the simplest option of a three-point neighborhood is chosen.

If the laser footprint is approximated by a circle, then the diameter of a point at non-normal incidence (i.e.  $\alpha \neq 0$ ) increases with the cosine of the incidence angle, such that  $d_2 \approx d_1 / \cos(\alpha)$  (Bitenc et al., 2010) as shown in Figure 3-2. The signal-to-noise (SNR) ratio of a laser return deteriorates with the cosine of the incidence angle, and the square of the range (Soudarissanane et al., 2011), which increases the uncertainty of the range.

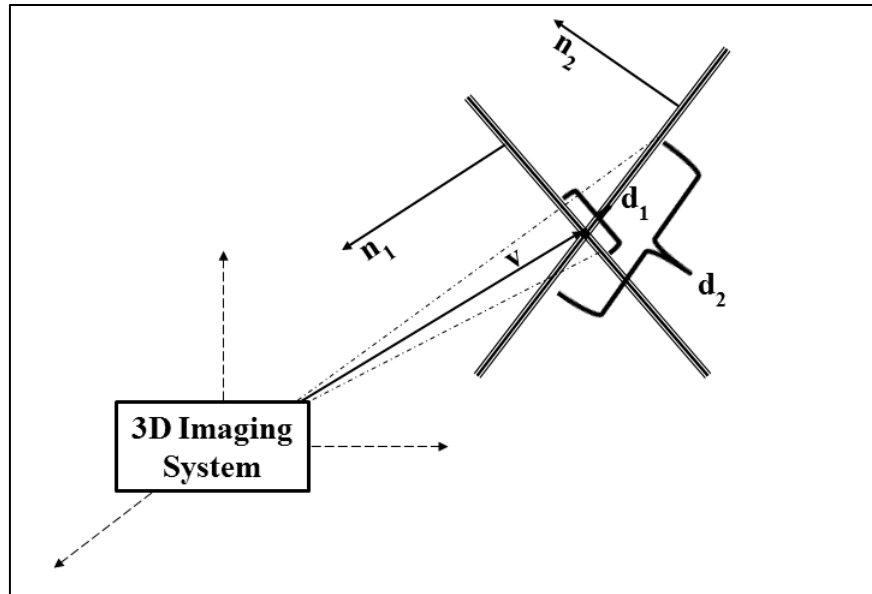


Figure 3-2 Influence of Incidence Angle on Laser Footprint. The footprint of a return at normal incidence ( $d_1$ ) is smaller than at non-normal incidence angle ( $d_2$ ).

Since a large number of 3D imaging systems employ laser scanning, in this work the effect of the incidence angle is included in the formulation. The precision of the range is thus divided by the cosine of the incidence angle. Soudarissanane et al. (2011) also studied the effect of increasing range on the SNR, but this is neglected in the implementation of this research, since most laser scanners have their range precision given in terms of a constant plus an additional term that varies with range. This additional term may have already been assigned to compensate for the range effect on the SNR. Furthermore, the incidence angle effect may also have an impact on the precision of the spherical angles. This impact may lead to off-diagonal correlation terms in the covariance matrix Eq.(3.11). However, these correlations are expected to be small and are thus ignored. The updated Eq.(3.11) which includes the cosine angle effect is given by

$$\Sigma_s = \text{diag} \left( \left[ (\sigma_\rho / \cos(\alpha))^2, \sigma_\theta^2, \sigma_\varphi^2 \right] \right) \quad (3.13)$$

The 3x3 covariance matrix of a scanned point can be obtained in Cartesian form by propagating Eq.(3.13) based on the relationship between spherical and Cartesian coordinates given in Eq.(3.10). By error propagation (Mikhail and Ackermann, 1976) one obtains the following

$$\Sigma_r = J_{r,s} * \Sigma_s * J_{r,s}^T \quad (3.14)$$

where

$$J_{r,s} = \begin{bmatrix} \cos(\theta)\cos(\varphi) & -\rho\cos(\theta)\sin(\varphi) & -\rho\sin(\theta)\cos(\varphi) \\ \cos(\theta)\sin(\varphi) & \rho\cos(\theta)\cos(\varphi) & -\rho\sin(\theta)\sin(\varphi) \\ \sin(\theta) & 0 & \rho\cos(\theta) \end{bmatrix}$$

$\Sigma_r$  is the covariance matrix of the observations mentioned in Eq.(3.9).

### 3.2.2.2 Planar Element Uncertainty

The normals of the planar elements are unique as each plane passes through three points. These normals can be determined by any of the simple methods such as the determinant method or the covariance approach as used by Bae (2006). Instead of these methods, a constrained linear system of equations is formulated, from which the Jacobian of the solution w.r.t. the three points is easily obtained. The motivation for using this method is that the Jacobian term captures the uncertainty of a planar element.

Given three non-collinear points one can obtain three equations of the form in Eq.(3.3). The unknown parameters of this system of equations are the direction cosines and the coordinates of the three points are the observations. The centroid of these three points lies

on the plane that passes through these points (Bae 2006). The coordinates of the centroid are thus chosen as  $x_0, y_0$  and  $z_0$ .

Eq.(3.3) can be expressed symbolically in a form similar to the classical General Least Squares adjustment expression given in Eq.(3.7). It is emphasized here however, that this is not a least squares adjustment, but rather simply the solution of a unique linear system of equations. The same symbolic usage of the terms of the General Least Squares adjustment model is adopted to explain the computation of the Jacobian term.

There are two degrees of freedom for the 3D plane and the linear system is constrained by setting the parameters to be the direction cosines of the plane. In other words, the 2-norm of the vector of parameters should be equal to unity. Thus one has (Mikhail et al., 2001, pg.354)

$$\mathbf{a}^2 + \mathbf{b}^2 + \mathbf{c}^2 = 1 \quad (3.15)$$

which can be expressed in the linearized form of

$$\mathbf{C}\Delta = \mathbf{g} \quad (3.16)$$

Expressing the linear system of equations of Eq.(3.3) in the form of Eq.(3.7) and combining it with Eq.(3.16) gives a constrained linear system. This constrained system requires only one iteration (for the case of three points) to determine the planar parameters. The constrained linear system is of the form (Mikhail et al. 2001, pg.405)

$$\begin{bmatrix} \mathbf{N} & \mathbf{C}^T \\ \mathbf{C} & 0 \end{bmatrix} \begin{bmatrix} \Delta \\ \lambda \end{bmatrix} = \begin{bmatrix} \mathbf{t} \\ \mathbf{g} \end{bmatrix}$$

$$\tilde{\mathbf{N}} \quad \tilde{\Delta} = \tilde{\mathbf{t}} \quad (3.17)$$

$$\mathbf{N} = \mathbf{B}^T(\mathbf{A}\mathbf{Q}_{ll}\mathbf{A}^T)^{-1}\mathbf{B}; \quad \mathbf{t} = \mathbf{B}^T(\mathbf{A}\mathbf{Q}_{ll}\mathbf{A}^T)^{-1}\mathbf{f}; \quad \mathbf{Q}_{ll} = \frac{1}{\sigma_0^2}\Sigma$$

$\sigma_0^2$  is the apriori reference variance (typically set to 1),

$\Sigma$  is the 9x9 diagonal covariance matrix of the observations.

The solution to Eq.(3.17) gives the direction cosines of the plane. Now by error propagation, the cross-cofactor matrix of the solution vector w.r.t. the observations ( $\mathbf{Q}_{\Delta l}$ ) is given by (Mikhail and Ackermann, 1976, pg.117)

$$\mathbf{Q}_{\Delta l} = -\mu\mathbf{B}^T(\mathbf{A}\mathbf{Q}_{ll}\mathbf{A}^T)^{-1}\mathbf{A}\mathbf{Q}_{ll} \quad (3.18)$$

where

$$\begin{bmatrix} \mathbf{N} & \mathbf{C}^T \\ \mathbf{C} & 0 \end{bmatrix} \begin{bmatrix} \mu & \eta^T \\ \eta & \gamma \end{bmatrix} = \begin{bmatrix} \mathbb{I}_3 & 0 \\ \mathbf{o}^T & 1 \end{bmatrix} \quad (3.19)$$

with  $\mathbb{I}_3$  being the identity matrix of size 3 and  $\mathbf{o}$  being a zero vector of size of 3. The Jacobian of the parameters w.r.t. the observations  $\mathbf{J}_{\Delta l}$  is then

$$\begin{aligned} \mathbf{Q}_{\Delta l} &= \mathbf{J}_{\Delta l}\mathbf{Q}_{ll} \\ \Rightarrow \mathbf{J}_{\Delta l} &= -\mu\mathbf{B}^T(\mathbf{A}\mathbf{Q}_{ll}\mathbf{A}^T)^{-1}\mathbf{A} \end{aligned} \quad (3.20)$$

For every contributing point, this 3x9 Jacobian term  $\mathbf{J}_{\Delta l}$  is included in the  $\mathbf{A}$  matrix of Eq.(3.7) and Eq.(3.8) as described in Appendix A.

### 3.2.3 Adjustment and Registration Results

In addition to the final estimated (or adjusted) parameters  $[\omega, \emptyset, \kappa, t_x, t_y, t_z]_{adjusted}$  other adjustment quantities can be obtained from the P2P method as a by-product of the

General Least Squares adjustment. These quantities include the covariance matrix of the estimated parameters  $\Sigma_{\Delta\Delta}$ , the transformed (or adjusted) point coordinates of the PCD  $\hat{\mathbf{l}} = [\hat{\mathbf{P}}, \hat{\mathbf{Q}}]^T$ , the covariance matrix of the adjusted coordinates  $\Sigma_{\hat{\mathbf{l}}\hat{\mathbf{l}}}$ , the residuals  $\mathbf{v}$  and the estimated reference variance  $\hat{\sigma}_0^2$  (Mikhail et al., 2001, Mikhail and Ackermann, 1976). It must be noted that the adjusted parameters are used to transform  $\mathbf{P}$  to give  $\hat{\mathbf{P}}$  based on Eq.(3.1). Since the parameters in Eq.(3.1) describe the transformation of  $\mathbf{P}$  relative to  $\mathbf{Q}$  it means that points in  $\mathbf{Q}$  are not transformed, i.e.  $\hat{\mathbf{Q}} = \mathbf{Q}$ . All the adjustment results may then be analyzed with the conventional post-adjustment analyses (Mikhail et al., 2001). These analyses include tests on the estimated reference variance, tests for blunders, computation of confidence region for the estimated parameters and computation of error ellipses for the adjusted coordinates.

The adjustment results and post-adjustment analyses may not be sufficient to describe the registration accuracy performance. In cases when the true parameters are known or can be determined, the absolute error of the estimated parameters can be obtained. In addition, the root mean square of the error (RMSE) between the adjusted point coordinates and the true coordinates can be determined. In most practical cases however, the absolute error is not possible since the true parameters are unknown. The final point-to-plane distances (i.e. after iteration termination) were utilized in Chen and Medioni (1991). Here it is proposed to use the root mean square (RMS) of these distances as part of the P2P registration accuracy assessment. The RMS of these distances will be abbreviated as RMSD in the remainder of this dissertation.

### 3.3 P2P Implementation

The mathematical concepts presented in sections 3.1 and 3.2 were implemented in a computer program using the Matlab ® high-level language. The program was used for numeric evaluations of the proposed P2P method which will be discussed in section 3.4. Some of the practical considerations are mentioned in this section for the benefit of the reader who is interested in implementing the P2P algorithm.

#### 3.3.1 Overlap Region Between Scans

Conceptually, a correspondence set can be obtained for each scanned point in  $\mathbf{P}$  and for each point in  $\mathbf{Q}$ . However, not all the scanned points will participate in the adjustment for several reasons. In the formulation of this research,  $\mathbf{P}$  and  $\mathbf{Q}$  are partially overlapping, thus only those points within the overlapping region are of interest. The exact boundary of this overlapping region is not known prior to pairwise registration, however. Assuming that the initial approximate transformation parameters are reasonable, it is expected that the overlapping region will not change much at each iteration, since this is a fine registration.

Overlapping points in  $\mathbf{P}$  are identified by first transforming the scanned points according to Eq.(3.2). For each transformed point, its nearest neighbor in  $\mathbf{Q}$  is found and the distance to this nearest neighbor is then determined. If the distance is above a threshold then this point is not in the overlap region. Similarly for points in  $\mathbf{Q}$  the distance to their nearest neighbor in  $\mathbf{P}$  is found and then compared with the threshold to determine the overlapping points. The choice of this threshold would depend on the quality of the initial



approximation to the transformation parameters, the density and distribution of the PCD.

The establishment of correspondence sets (see section 3.1) and the definition of the overlapping region involve point searching. This is very computationally expensive (Simon et al., 1994) and many approaches have been proposed to reduce the computational burden. Akca (2007) proposed the use of a boxing data structure where the PCD is partitioned into boxes. In this research a k-d tree is employed, since there may be huge disparity between the number of points in each box with the box structure (Zhang, 1992). The k-d tree is a data structure which utilizes a binary search tree and allows fast searching of k-dimensional data (Bentley, 1975). Other search methods were presented in Simon et al. (1994) for ICP methods and they may also be used for P2P and other ICP methods.

### 3.3.2 Inliers

In addition to non-overlapping points, there are also spurious points caused by geometric (e.g. edge effects), radiometric (e.g. highly reflective surfaces), and/or environmental (e.g. kinematic objects) factors, which need to be filtered. To identify these outliers it is assumed that the distances between transformed points and their corresponding planar elements follow a Gaussian distribution. Inlier transformed points can then be detected based on a threshold value such as (Bae, 2006)

$$\frac{|k_{inlier}|}{\sigma_k} \leq z(a/2) \quad (3.21)$$

$|k_{inlier}|$  is the absolute point-to-plane distance of an inlier transformed point

$\sigma_k$  is the sample standard deviation of the point-to-plane distances

$a$  is the confidence level, ( $a = 0.05$  is used in this research)

$z(a)$  is the standard normal distribution with confidence level of  $a$ .

Also, in the implementation of this research, planar elements with poor geometry (i.e. near collinear) are ignored. The condition number of the augmented normal matrix  $\tilde{N}$  in Eq.(3.17) is largely influenced by the geometric quality of a planar element. As the three points of a planar element become collinear, the condition number increases to infinity. Degenerate planar elements were identified with a threshold value of  $1E+13$  for the condition number. These correspondence sets were ignored.

### 3.3.3 Correspondence Sets

At least six unique correspondence sets are needed to determine all the rigid-body transformation parameters. In other words, multiple transformed points cannot share the same planar element, as this will lead to rank-deficiency in the A matrix of Eq.(3.7)<sup>4</sup> (Jaw, 1999). However, transformed points that are in close proximity to each other may have planar elements that share one or two (but not three) common vertices (or scanned points). In applications, multiple transformed points may share a planar element. One example is when there is a large disparity in point densities between point clouds. All such rank-

---

<sup>4</sup> When two transformed points are close to each other it is possible that the planar elements they are assigned to will share common vertices. In this scenario the associated condition equations become correlated. This correlation is visible in the equivalent cofactor matrix which will contain off-diagonal non-zero values. High correlation among condition equations leads to the A-matrix becoming rank-deficient (i.e. some equations in the A-matrix are linearly dependent). This rank-deficiency in the A-matrix renders the equivalent cofactor matrix to be singular.

deficient cases were handled by retaining the first transformed point that was assigned to a planar element. The other transformed points that share that planar element were ignored. The choice of the transformed point that should be used is a topic for future investigation as the current choice is purely ad hoc. The redundancy of the P2P adjustment may be calculated as described in Appendix B.

It must be emphasized that the planar elements contribute to the solution of the transformation parameters. In addition to unique correspondence sets, the planar elements should span the normal space for optimum registration results. In other words, the normal vectors of the planar elements should vary as much as possible (Levin and Filin, 2010; Schenk et al., 2000). The extent to which the normal vectors of planar elements vary is case dependent. As in other ICPlane methods the performance of the P2P method would be restricted in cases where there are not much variations within the overlapping region.

#### 3.3.4 Iteration Termination Sets

Any of the classical adjustment criteria can be used for iteration termination. Akca (2007) chose to terminate the iterations once the change in all parameters was smaller than a threshold. Since the parameters are of different types (i.e. angular and linear) it is advised that two sets of parameter thresholds be used if this option is selected. Chen and Medioni (1991) considered the change in the mean square of the point-to-plane distances (i.e. mean square error) to decide when the iterations should be terminated. As was mentioned by Chen and Medioni (1991) an alternative criterion is an absolute threshold on the mean square error itself.

In the proposed P2P method the RMS of change in coordinates of transformed points was used to terminate the iterations. At each iteration the updated transformation parameters are used to transform  $P$  and  $Q$  according to Eq.(3.2). These updated transformed coordinates are compared with the transformed coordinates obtained from the initial transformation parameters and the RMS is determined. If the RMS of the change in coordinates becomes smaller than a pre-defined threshold then the P2P algorithm is said to have converged and iterations are terminated. Change in transformed coordinates allows the use of one threshold despite the presence of parameters with linear and angular units. In addition to these methods it may also be necessary to set a maximum number of iterations to terminate the algorithm even if the RMS never falls below the threshold.

### 3.3.5 Algorithm

The inputs to the P2P algorithm are the 3D Cartesian coordinates of a pair of scanned points, the 3D imaging system's precision (assumed to be in terms of range and angles), and an initial set of rigid-body transformation parameters. The output of the algorithm includes the least squares estimate of the rigid-body transformation parameters, the registered pair of PCD with transformed coordinates, the registration error and the adjustment statistics.

It is assumed that the 3D imaging system operates a laser scanning mechanism where the range, horizontal and vertical angles are observed with their respective precisions. As described in section 3.2.2.1 these observables along with their precisions can provide a

3x3 Cartesian covariance matrix for each scanned point. If the 3D imaging system does not acquire spherical observables (e.g. in the case of stereo photogrammetric-derived PCD) then it is assumed that covariance information is still available for the PCD. In extreme cases where this covariance information is absent, then the observations can be assumed to be equally weighted and the 3x3 identity matrix can be used.

The algorithm involves nine main steps. Steps 1 through 4 are required only once and may be considered as the preprocessing steps. In some cases these steps may be the most time consuming and in other cases they may not even be needed. For example, step 1 may not be needed if the PCD is small (few thousands of points or less). Step 2 would be ignored if it is known that the pair of PCD are fully overlapping. Step 3 should be ignored if the 3D imaging system is not characterized by the incidence angle effect discussed in section 3.2.2.1. Step 4 can be ignored if covariance information is already available for the PCD. The iterative section of the algorithm (steps 5 to 9) provides the main processing component of the P2P method. Steps 5 to 9 are data independent.

---

### **P2P Algorithm for pairwise registration of a pair of PCD**

---

0. Inputs: - 3D coordinates of unstructured pair of PCD:  **$P$  and  $Q$**
- initial parameter approximations:  $[\omega, \vartheta, \kappa, t_x, t_y, t_z]_{initial}$
- observations' precision:  $[\sigma_\rho, \sigma_\theta, \sigma_\varphi]_P$  and  $[\sigma_\rho, \sigma_\theta, \sigma_\varphi]_Q$
-

1. Organize  $\mathbf{P}$  and  $\mathbf{Q}$  using a spatial data structure (e.g. k-d tree) to facilitate efficient point searching. This is strongly advised for PCD with tens of thousands of points or more.
  2. Identify and remove points in  $\mathbf{P}$  and  $\mathbf{Q}$  that are not in the overlapping region as discussed in section 3.3.1. In steps 3 to 8,  $\mathbf{P}$  and  $\mathbf{Q}$  represent only those points in the overlapping region.
  3. Compute the incidence angles for points on  $\mathbf{P}$  and  $\mathbf{Q}$  using Eq.(3.12).
  4. Obtain the 3x3 Cartesian covariance matrix for points on  $\mathbf{P}$  and  $\mathbf{Q}$  for example, using Eq.(3.14) if applicable (see earlier discussion in this section).
- 
5. For each scanned point obtain a correspondence set. This involves transforming the scanned point according to Eq.(3.2) with the current parameters. The transformed point's corresponding planar element is established as in section 3.1. The planar element's unit normal vector and its uncertainty are determined as given in section 3.2.2.2.
  6. Exclude outlier transformed points as in section 3.3.2. The distances between all transformed points and their corresponding planar elements are evaluated to identify and exclude outliers based on Eq.(3.21).
  7. Use all correspondence sets to populate the least squares matrices  $\mathbf{N}$  and  $\mathbf{t}$  in Eq.(3.9). The terms of these matrices are obtained as given in Eq.(3.7), Eq.(3.8), and Eq.(3.14).
  8. Solve the linear system in Eq.(3.9) to compute the correction to the parameters, and update the parameters.

9. Check for iteration termination according to section 3.3.4. If iterations should not be terminated then return to step 5. If termination criterion has been met then obtain registration and adjustment results according to section 3.2.3. Note that all the scanned points (including outliers and non-overlapping points) in  $\mathbf{P}$  are transformed to obtain  $\hat{\mathbf{P}}$ .

---

10. <u>Outputs</u> : - final (adjusted) parameters:	$[\omega, \vartheta, \kappa, t_x, t_y, t_z]_{adjusted}$
- registration and adjustment statistics	RMSE, RMSD, $\hat{\sigma}_0^2$
- registered pair of PCD	$\hat{\mathbf{P}}, \hat{\mathbf{Q}}$
- covariance matrices	$\Sigma_{\Delta\Delta}, \Sigma_{\hat{\mathbf{P}}}$

---

### 3.4 Evaluations and Discussion

The proposed P2P registration method was evaluated in two ways. The first mode of evaluation investigated the impact that various modifications to the stochastic model could have on pairwise registration. The second mode of evaluations involved the comparison of the P2P method with the ICPlane method of Chen and Medioni (1991). The results of these evaluations are presented and discussed in this section.

### 3.4.1 Internal Evaluations

If the stochastic properties of the planar elements are neglected,  $\mathbf{A}_1$  and  $\mathbf{A}_2$  in Eq.(3.8) are reduced. This has a direct impact on the weighting scheme, since the “equivalent” weight matrix  $\mathbf{W}\mathbf{e}$  for each the correspondence set is obtained by (Mikhail and Ackermann, 1976)

$$\mathbf{W}\mathbf{e} = (\mathbf{A}\mathbf{Q}_{ll}\mathbf{A}^T)^{-1} \quad (3.22)$$

In this section, the effect of point precision on  $\mathbf{W}\mathbf{e}$  is investigated analytically and experimentally. The experiments involve both simulated and real PCD. The proposed P2P adjustment model is referred to as the full model which carries both the terms from the transformed points and the planar elements. The model that carries only the terms from the transformed points is referred to as the reduced model.

#### 3.4.1.1 Analytical Comparisons

The “equivalent” cofactor matrix  $\mathbf{Q}\mathbf{e}$  is expressed as

$$\mathbf{Q}\mathbf{e} = \mathbf{A}\mathbf{Q}_{ll}\mathbf{A}^T \quad (3.23)$$

If  $\mathbf{A}$  and  $\mathbf{Q}_{ll}$  are partitioned such that

$$\mathbf{A} = [\mathbf{A}_p, \mathbf{A}_q] \text{ and } \mathbf{Q}_{ll} = \text{diag}([\mathbf{Q}_p, \mathbf{Q}_q]) \quad (3.24)$$

then one has

$$\begin{aligned} \mathbf{Q}\mathbf{e} &= \mathbf{A}_p\mathbf{Q}_p\mathbf{A}_p^T + \mathbf{A}_q\mathbf{Q}_q\mathbf{A}_q^T \\ &= \text{term1} + \text{term2} \end{aligned} \quad (3.25)$$

where  $\mathbf{A}_p = [\mathbf{F}_1'(\mathbf{p}), \mathbf{F}_2'(\mathbf{p})]^T$ ,  $\mathbf{A}_q = [\mathbf{F}_1'(\mathbf{q}), \mathbf{F}_2'(\mathbf{q})]^T$  (see section 3.2).  $\mathbf{Q}_p$ , and  $\mathbf{Q}_q$  are block diagonal cofactor matrices, with each participating point in  $\mathbf{P}$ , and  $\mathbf{Q}$



contributing a 3x3 diagonal covariance matrix which is then scaled by the apriori reference variance (see Eq.(3.9)).

Consider a single correspondence set of the form  $\mathbf{F}_1$  in Eq.(3.6), (i.e. one condition equation). Given one condition equation, the “equivalent” cofactor matrix becomes a scalar quantity. Let  $\mathbf{Qe}_1$ , and  $\mathbf{Qe}_2$  represent these scalar quantities for the full and reduced stochastic models, respectively. Thus, *term1* in Eq.(3.25) contains the contributions from the transformed point ( $\tilde{\mathbf{p}}_i$ ), and *term2* contains the contributions from the planar element ( $\mathbf{q}_e$ ). Since *term2* is positive one has<sup>5</sup>

$$\begin{aligned}\mathbf{Qe}_1 &= \textit{term1} + \textit{term2} \\ \mathbf{Qe}_2 &= \textit{term1} \\ \mathbf{Qe}_1 &> \mathbf{Qe}_2\end{aligned}\tag{3.26}$$

The precision of the points in  $\mathbf{q}_e$  impact *term2* in two ways, first in  $\mathbf{Q}_q$ , and second in  $\mathbf{A}_q$ . The first is obvious, the second is also easily seen when considering the Jacobian  $\left(\frac{\partial n_{q_i}}{\partial q_{e_i}}\right)$  in Eq.(A.1), which includes the precision of the points in  $\mathbf{q}_e$ .

The consequence of neglecting *term2* is that correspondence sets with transformed points of the same precision will be weighted equally, regardless of varying point precisions in their planar elements. Thus  $\mathbf{Qe}_1$  more accurately captures the relative difference between correspondence sets. The impact of this difference on point cloud

---

<sup>5</sup> Recall this is for one equation. For a system of linear equations *term1* and *term2* are matrices.

registration would be data dependent, and would be affected by the level of disparity between point precisions in the overlapping region.

#### 3.4.1.2 Simulated Experiments

Let the “equivalent” weights for full and reduced P2P be respectively  $\mathbf{W}e_1$ , and  $\mathbf{W}e_2$ , where

$$\mathbf{W}e_1 = \mathbf{Q}e_1^{-1} \text{ and } \mathbf{W}e_2 = \mathbf{Q}e_2^{-1} \quad (3.27)$$

Figure 3-3 illustrates the varying point precision of a sampled point at a range of 10 meters, and spherical angles both of 0 radians, whose observation standard deviations are respectively 1E-2 meters, 2E-5 radians, 2E-5 radians. This range of precision values is due to the incidence angle effect. For the experimental setup in this research, the functional model obtained from a correspondence set of the form  $\mathbf{F}_1$  in Eq.(3.6) is considered.

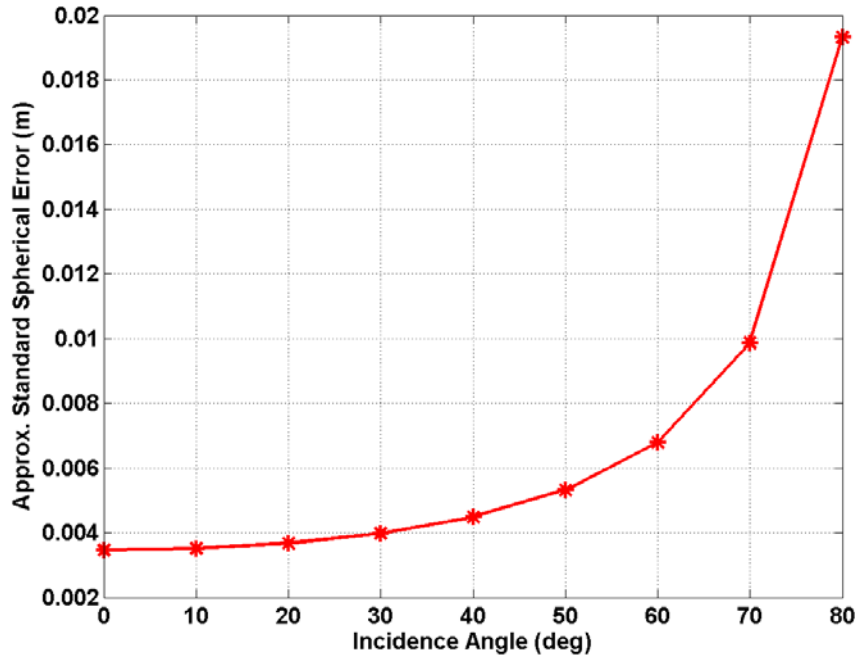


Figure 3-3 Influence of Incidence Angle on Point Precision. The point is observed at a range of 10 meters and the horizontal and vertical angles are zero radians. The standard deviations are 1E-2 meters, 2E-5 radians and 2E-5 radians respectively.

It is assumed that there are nine sets of correspondences of this form with the transformed points with incidence angles  $\alpha \in [0, 80]$  degrees, in increments of 10 degrees. For each transformed point it is further assumed that there are nine planar elements with each planar element consisting of triplets of points that have incidence angles  $\alpha \in [0, 80]$  degrees. Since planar elements consist of adjacent points the difference in incidence angles among the points in a planar element will be negligible. Thus it is also assumed that all the points in a planar element have the same incidence angle.

Next, the “equivalent” weights ( $W_{e_1}$ , and  $W_{e_2}$ ) for each of the 81 cases are compared.

As mentioned in Eq.(3.26)  $Q_{e_1} > Q_{e_2} \Rightarrow W_{e_2} > W_{e_1}$  for all the cases. Figure 3-4

shows the ratio of  $\mathbf{W}e_2:\mathbf{W}e_1$ , with each curve representing a different incidence angle for the transformed point ( $\tilde{\mathbf{p}}_i$  in Eq.(3.6)).

The first observation is that as the incidence angles of the transformed points increase, the ratio of  $\mathbf{W}e_2:\mathbf{W}e_1$  decreases. The second observation is that as the incidence angles of the planar elements increase, the ratio increases. For example, for planar elements with incidence angle less than 30 degrees the ratio is almost constant (between 1 and 1.5) for various incidence angles of the transformed points, but for angles above 70 degrees the ratio increases to a factor of almost ten.

The first conclusion from this illustration is that for planar elements of lower incidence angle the difference in the stochastic models is minimal or unnoticeable. The second conclusion however, is that for higher incidence planar elements, correspondences with larger disparity between incidence of the transformed point and that of the planar elements, have noticeably higher differences between the two models. For example a transformed point at 0 degrees and planar element at 80 degrees is weighted 14 times higher in  $\mathbf{W}e_2$  than  $\mathbf{W}e_1$ . This scenario is very common with TLS data where in the overlapping region the disparity in incidence angle between transformed points and planar elements is large. The full model more appropriately reduces the weight of these correspondences than the reduced model.

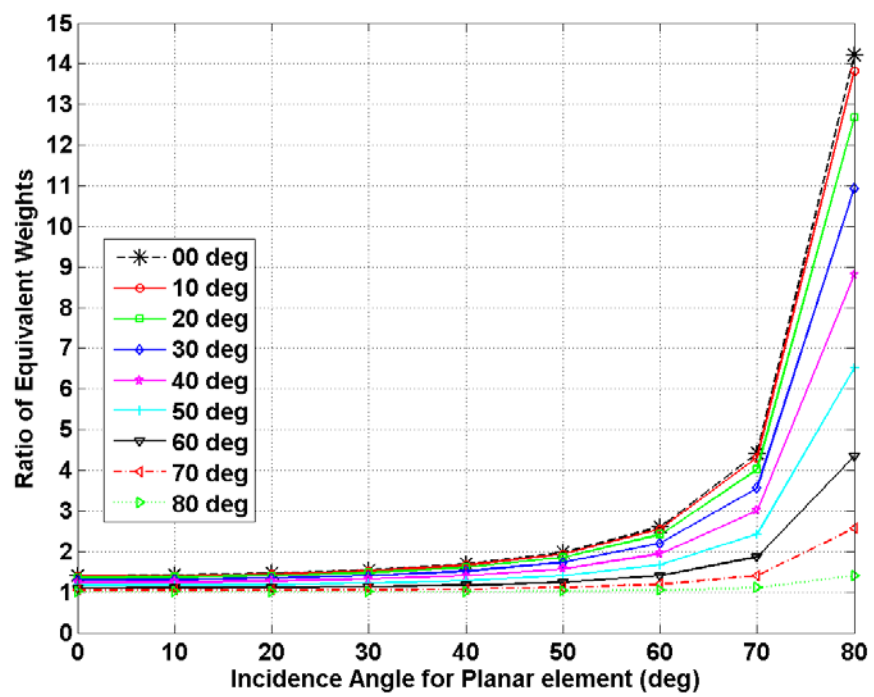


Figure 3-4 Effect of Point Precision on “Equivalent” Weights. Each curve represents the ratio of  $We_1(0):We_1(i)$  for a different incidence angle

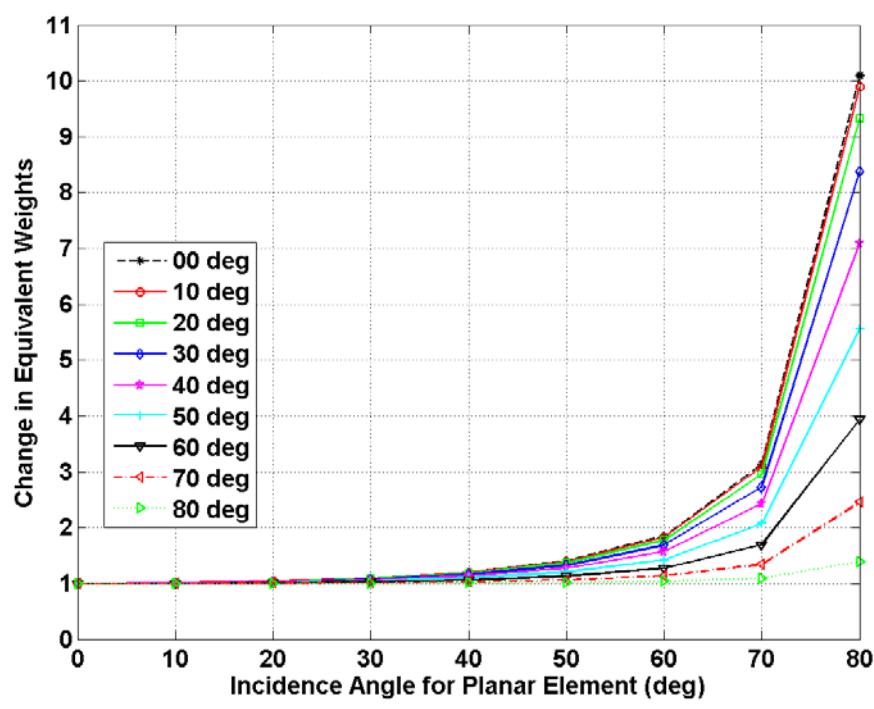


Figure 3-5 Relative Effect of Point Precision on “Equivalent” Weights. Each curve represents the ratio of  $We_2:We_1$  for a different incidence angle

As mentioned previously, the reduced model weights all correspondence sets equally if their transformed points are of equal precision, regardless of the precisions of the planar elements, while the full model does not. Figure 3-5 illustrates the difference in relative weights when using the full model.

Using the same data as in Figure 3-4 the curves in Figure 3-5 show the ratio of the “equivalent” weights for planar elements at normal incidence ( $We_1(0)$ ) to weights for various other incidence angles ( $We_1(i)$ ). The figure reinforces the earlier observation that for higher incidence planar elements, those correspondences with larger disparity between incidence of transformed point and that of planar elements have smaller weights than those with smaller disparity.

#### 3.4.1.3 Experiment with Real Data

An experiment was performed on real PCD to evaluate the registration performance of the full P2P method against three modifications. The real PCD were obtained from the Working Group V/3 of the International Society for Photogrammetry and Remote Sensing (ISPRS). The data represent a TLS of a Buddha statue in Thailand described in Bae (2006). The point clouds were obtained with the Riegl LMS-Z210 scanner, whose range and angular precisions are respectively 2.5E-2 meters, and 4.7E-4 radians. Intensity images were obtained from the point clouds representing the left and right views of the

statue (see Figure 3-6). Four common points were identified on these images from which initial transformation parameter estimates were obtained.

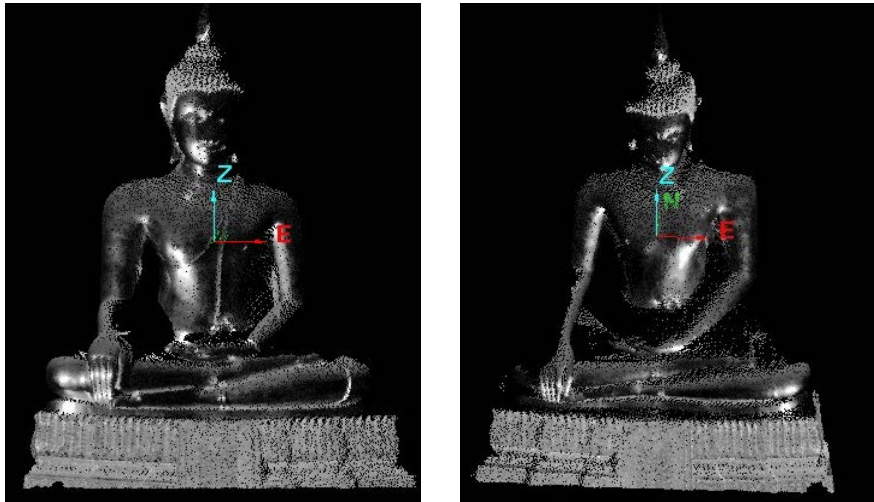


Figure 3-6 Intensity Images of Buddha Data (Left and Right Views)

The full P2P model was implemented as described in section 3.1 through section 3.3. Modifications were made to this model to investigate the effect of the incidence angle and local surface normals of the planar elements on the registration accuracy. The a posteriori reference variance was used as the metric to evaluate the models, as both the functional and stochastic models of an adjustment contribute to this metric. All variants of the P2P model had the same functional model: the only difference was in the stochastic model. The description of the full model and the variants are:

1. **P2P** - full model, *term1* and *term2* in Eq.(3.25) are included,
2. **P2Pr** - reduced model, *term2* in Eq.(3.25) is ignored,
3. **P2Pi** - full model as in **P2P**, but the incidence angle effect is ignored. Eq. (3.11) is used instead of Eq. (3.13) in computing the covariance matrix of points,

4. **P2Pri** - reduce model as in **P2Pr**, but the incidence angle effect is ignored as in **P2Pi**.

Figure 3-7 shows the aposteriori reference variances for the four models. As illustrated in the figure, **P2P** gave the smallest aposteriori reference variance, and the largest variance was obtained by the model which ignored both the incidence angle effect and *term2* (**P2Pri**).

The curve for **P2Pr** shows an improved variance compared to **P2Pri**, reflecting the contribution of the incidence angle effect. However, greater improvement was obtained when including *term2*, even if the incidence angle effect was ignored. The *F-test* for a confidence level of  $\alpha = 0.05$  indicated that the final variances for the three variants were statistically different from that of **P2P**.



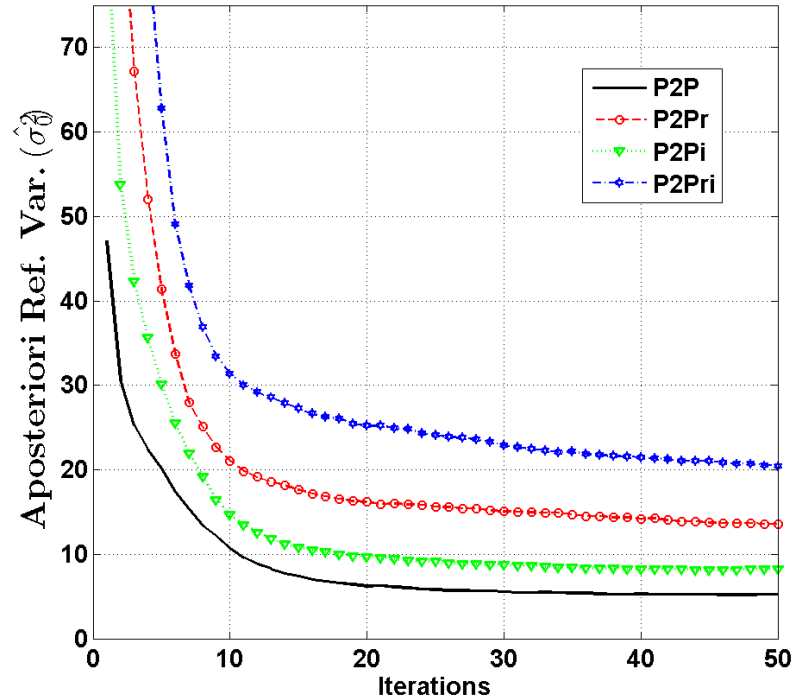


Figure 3-7 Comparison of Reference Variances. Values above 75 on the y-axis are not shown.

To further investigate the impact of the incidence angle sampled points which exceeded certain angle thresholds were removed. The filtering thresholds ranged from 90 degrees to 30 degrees at 5 degree decrements, where at 90 degrees, all the points were used (Figure 3-7). Thresholds of smaller angles were not used because more than 80% of the original points would be removed (Table 3-1).

The results were consistent with Figure 3-7 in that the highest to lowest variances were obtained by **P2P**, **P2Pi**, **P2Pr**, **P2Pri** respectively. An example of the filtered performance is given in Figure 3-8, which shows the results for the filtering threshold of 45 degrees. For incidence angles smaller than 55 degrees all the models showed an increase in the final a posteriori reference variance (Figure 3-9). The similarity of surface

normals can contribute to this increase. Figure 3-9 shows the average improvement in variance over the last 25 iterations, for the different filtering thresholds. Improvement represents the ratio of the variance for a P2P modification (e.g. **P2Pr**) to the **P2P** variance.

The improvement relative to **P2Pi** decreases near linearly with lower incidence angles, confirming that at lower incidence the difference between point precisions is minimal.

The improvement relative to **P2Pr** is near constant for higher incidence angles ( $\geq 70$  degrees), then increases with decreasing incidence angle. The increased improvement indicates that the impact of using only lower incidence angle points is greater on **P2Pr** than on **P2P**. The curve for **P2Pri** gives the combined effect of both the **P2Pr** and **P2Pi** curves.

The conclusion from this experiment is that the inclusion of the incidence angle effect as well as the precisions of the local surface normals impact the stochastic model so as to improve the a posteriori reference variance of the least squares adjustment. Filtering points with higher incidence angle must be considered carefully, as it may not always lead to improved reference variances.

Table 3-1 Cumulative Distribution of Incidence Angles. The columns with (L) refer to the Left View and those with (R) refer to the Right View.

Angle	Cum. Sum (L)	Cum. % (L)	Cum. Sum (R)	Cum. % (R)
00	100, 860	100	107, 451	100
10	98, 784	98	104, 934	98
20	91, 825	91	96, 870	90
30	78, 751	78	81, 953	76
40	57, 779	57	58, 638	55
50	35, 650	35	35, 087	33
60	19, 893	20	18, 799	17
70	9, 221	9	7, 981	7
80	1, 876	2	2, 037	2

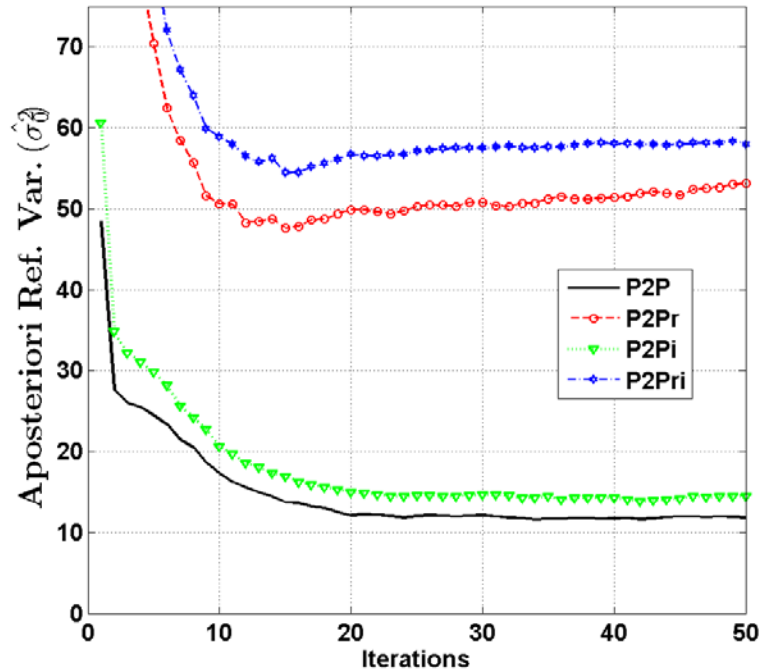


Figure 3-8 Reference variance – after filtering points with incidence angle greater than 45 degrees (values above 75 on the y-axis are not shown).

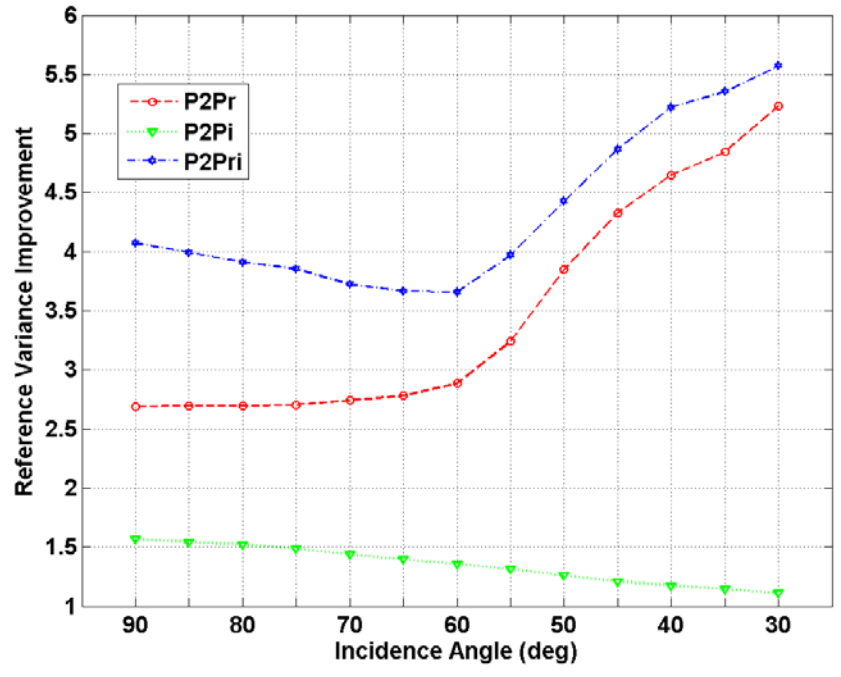


Figure 3-9 Average improvement in reference variance. Reference variances were obtained at iteration #50 for the different incidence angles.

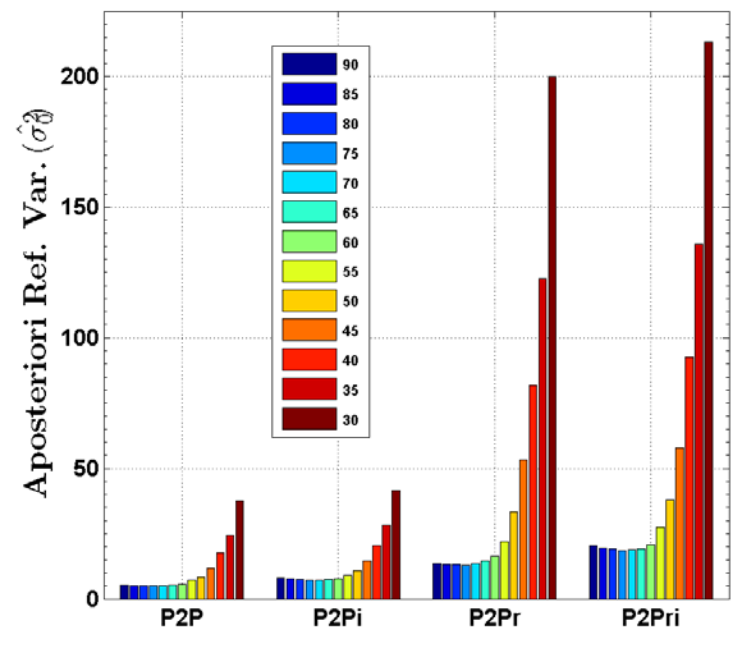


Figure 3-10 Final reference variance per registration method for different incidence angles

### 3.4.2 Comparisons with Chen and Medioni (1991)

The comparisons with the approach by Chen and Medioni (1991), referred to here as the Chen method, were done to provide some context in terms of the performance of the P2P method relative to established methods. The Matlab toolbox developed by Salvi et al. (2007) was used to perform the Chen registration. Both real and simulated data were used for the comparisons.

#### 3.4.2.1 ISPRS Buddha Data

The ISPRS Buddha data described in section 3.4.1.3 was used. This experiment involved some modifications on the P2P method to assess only the contribution of the planar elements to registration performance. For the P2P adjustment all points were weighted equally. For the Chen method correspondences were established by normal shooting on the right scan. That is, the intersection of the ray (or vector) originating at each point on the right scan in the direction of that point's normal vector with the surface on the left scan was determined (Rusinkiewicz, 2001). These intersection points were assigned as the correspondences of points in the right scan. The right scan was chosen to be the  $Q$  surface of the Chen method. For the P2P method, only correspondence sets of the form  $F_1$  in Eq.(3.6) were used (i.e. symmetric correspondence was not utilized). The metric used for comparison was the RMSD (see section 3.2.3), and Figure 3-11 gives the registration results.

The P2P registration was more accurate than the Chen registration by approximately 1.5cm for the ISPRS Buddha data. Interestingly, this improvement of about 50% was consistent throughout all 50 iterations of the evaluation. This improvement is related to two of the two major differences between the P2P and Chen methods.

- The P2P method includes the geometry of the planar elements whereas the Chen method uses only the intersection point on the planar element.
- The P2P method includes the stochastic properties of the planar elements. Although the points were weighted equally, the planar elements would still have different weights based on their geometric configurations and the differing incidence angles of the points. There is no inclusion of stochastic properties with the Chen method.

It is expected that further improvement would have been obtained should the symmetric correspondences and proper weighting of individual points be utilized in the P2P method. However, for this experiment the objective was to assess the impact of the planar elements on registration performance. The conclusion is that the consideration of the planar elements both in the deterministic and stochastic models of the P2P method improved the registration accuracy as compared with the Chen method.

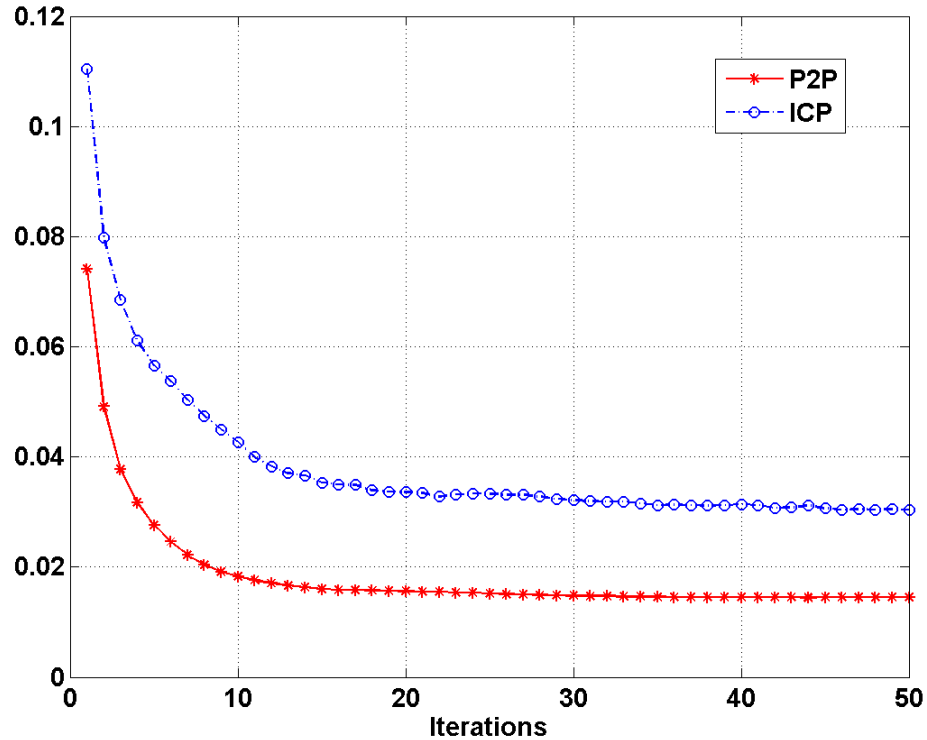


Figure 3-11 Comparison of Registration Methods.

#### 3.4.2.2 Computer Vision Data #1

The two major performance criteria for registration algorithms are perhaps registration accuracy and computational complexity. The computational complexity was not assessed in this dissertation, but the runtimes of the P2P and Chen methods were evaluated. The Matlab registration toolbox by Salvi et al. (2007) provided surface data which Salvi et al. (2007) used for evaluating various registration methods. Four of the surfaces (or scans) were used in these comparisons (see Figure 3-12, Table 3-2 and Table 3-3), and all were transformed with known parameters to obtain the “overlapping” (or “adjacent”) surface, then the registration methods were used to determine the parameters. The transformation parameters used by Salvi et al. (2007) were used in this experiment, which was a rotation

of 5 degrees about all three axes, and a shift of 0.2 units along the z-axis. The owl surface did not converge by the ICP method with this parameter set, and instead a transformation of 0.1 degree rotation about all axes, with a shift of 0.05 along the z-axis was used. No incidence angle effect was used for P2P, because the adjacent surface data were created, rather than observed. Unlike in section 3.4.2.1, here the symmetric correspondence of the P2P method was utilized.

No noise was added to the data, and the Chen and P2P iterations were terminated when the RMSE of the correspondence was less than  $1E-3$  units. The correspondence RMSE is the norm of the difference between a transformed point and its known location. Table 3-2 gives the number of iterations needed for termination, and the mean time per iteration. The runtime comparisons are to provide some preliminary context in terms of computational performance, but are not meant to be strict evaluations. Both approaches were implemented in Matlab ® 7.11.0 on an Intel ® Core™, 2.13GHz, 3.00GB RAM PC. For correspondence search the Chen method utilized the box structure as in Akca (2007), and the P2P method utilized the k-d tree structure.

The Chen method's average runtime was less than that of the P2P method in all cases except for the frog surface, which was the most difficult for the Chen method. Although the P2P method was slower on average per iteration, the number of iterations needed for termination was between one-third and one-half that of the Chen method, resulting in a reduced overall computational time. Once more these experiments are to provide some preliminary context for the P2P method in terms of computational time, and no



conclusions of superiority are drawn. Instead these comparisons indicate that the P2P compares favorably with the Chen method in terms of computational time, for these surfaces.

Table 3-2 Runtime Comparisons (P2P vs Chen method). The highlighted values are from P2P registration and Chen's results are in parentheses.

<b>Surface</b>	<b># Points</b>	<b>#Iterations</b>	<b>Avg. Time per Iteration</b>
fractal	4096	<b>5</b> (11)	<b>1.99</b> (1.74)
wave	4096	<b>5</b> (13)	<b>2.14</b> (1.36)
owl	4902	<b>6</b> (18)	<b>2.49</b> (2.18)
frog	4977	<b>8</b> (23)	<b>2.43</b> (4.93)

#### 3.4.2.3 Computer Vision Data #2

The four datasets which were used section 3.4.2.2 were also used in this section (Figure 3-12, Table 3-2 and Table 3-3). No linear units were provided by Salvi et al. (2007) for the datasets, and meters were adopted for convenience. The fractal and wave datasets were synthetic, while the owl and frog datasets were acquired by a scanner on a turn-table. The fractal and wave data were scaled by factors of 20 and 5 respectively, to create data ranges that are closer to that of TLS data (see Table 3-3).

The accuracy performance of registration methods is affected by various conditions which include instrument noise, sampling density, initial approximations to the transformation parameters, and the presence of outliers. The data obtained from Salvi et al. (2007) were considered noise-free, and Gaussian noise was added to both the original

and transformed scans to simulate the precision of a TLS instrument. The spherical coordinates of each point were perturbed randomly with standard deviations of  $4E-3$

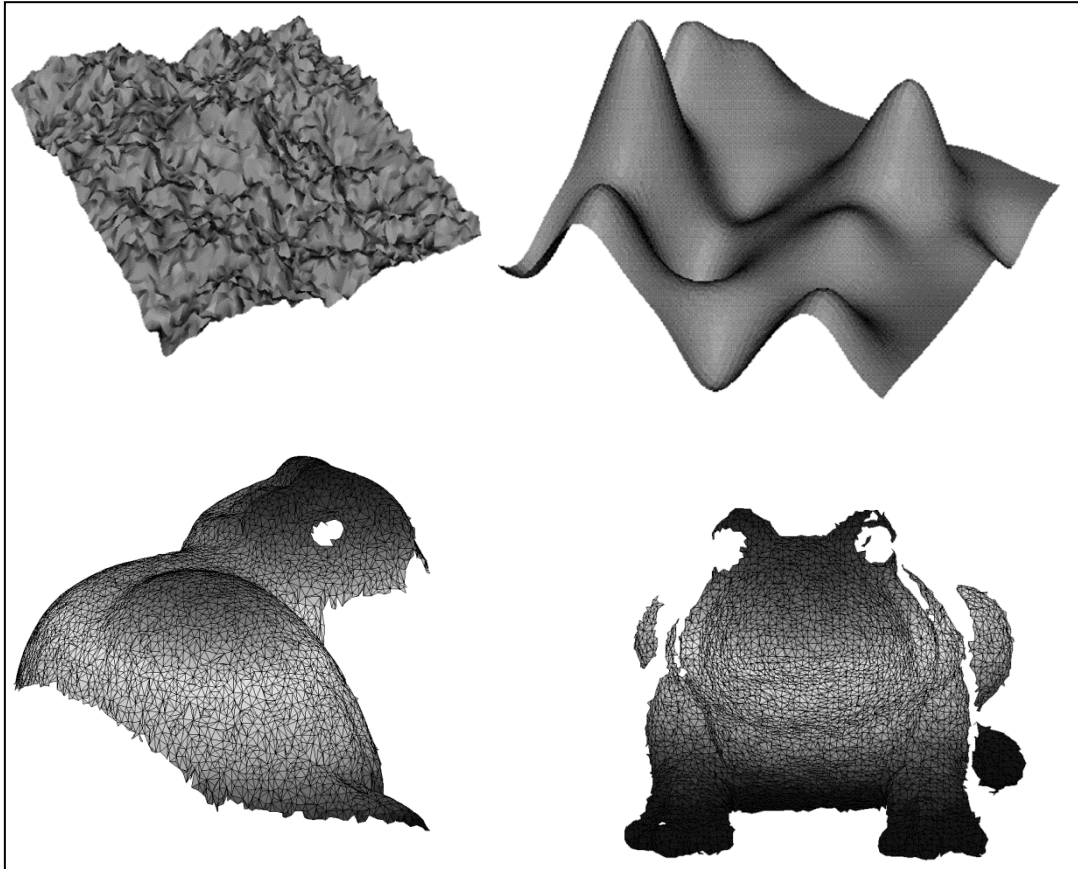


Figure 3-12 Data used for simulated experiments. From top left to bottom left in clockwise manner are Fractal, Wave, Owl, and Frog respectively. Fractal and Wave are synthetic. Owl and Frog are real laser scanning data.

meters and  $6E-5$  radians for linear and angular spherical coordinates, respectively. These standard deviations are realistic values as they represent the TLS precision of the instrument used for the real TLS data in section 3.4.2.4.

The lack of exact point correspondences between pairs of scans is the fundamental challenge of registration methods. To simulate this condition points were randomly removed from both the original and transformed scans. Sampling density also impacts registration accuracy (Salvi et al., 2007). For ICPlane methods, the sampling density is closely related to the sufficiency of the planar hypothesis for local neighborhoods. Three different sampling rates were used in the simulated experiments (75%, 50%, and 25%). Both the sampling rates and instrument noise were realized with a pseudo-random generator. Thus the experiment for each dataset was repeated 100 times and the means and standard deviations are given in Figure 3-13 through Figure 3-16. The results for the Chen method for the 75% sampling rate in Figure 3-15B were obtained from 33 runs. For the other 67 runs this method erroneously converged to local minima.

The initial pose is also an essential determining factor on the accuracy performance of registration methods. In general, the closer the initial approximations are to the “truth”, the better the registration method will perform. In the experiment three different sets of transformation parameters were used, which resulted in different initial registration RMSE values for each dataset as given in Table 3-4. Initial registration level 3 was not used for the owl data as this yielded an RMSE value that was unrealistically large. In Figure 3-13 through Figure 3-16 the subfigures A to C refer to the results from initial registration RMSE levels 1 to 3, respectively.

Other criteria such as outliers and overlap percentage were not included in this experiment. Since both the proposed P2P and the Chen methods are ICPlane methods the

same distance metric in Eq.(3.21) was used to identify outliers. In terms of overlap percentage, the more important factor is the variability in the values of local surface normals within the overlapping region rather than the percentage of overlap. Also, in these experiments the different sampling rates may also be thought of as simulating different overlap percentages.

The 75% sampling rate is probably the best of the three rates for representing the lack of exact point correspondences that exist in pairs of TLS data. At this sampling rate the errors for the P2P method were an order of magnitude smaller than those of the Chen method for the synthetic data (fractal and wave). For the real data (owl and frog) errors from the P2P method were smaller by a factor of approximately 4. These results were consistent for all the initial registration levels. This indicates that the different initial poses did not greatly affect the performance of either method. The improved accuracy of the P2P method indicates that this method better deals with inexact point correspondences between pairs of scans when the point density is high, and the surface is well sampled.

Table 3-3 Description of data obtained from Salvi et al. (2007).

	<b>Fractal</b>	<b>Wave<sup>6</sup></b>	<b>Owl</b>	<b>Frog</b>
<b># Pts</b>	4096	4096	4902	4977
<b>X Range (m)</b>	20.000	5.000	102.395	93.492
<b>Y Range (m)</b>	20.000	5.000	93.713	85.012
<b>Z Range (m)</b>	12.143	3.235	53.447	66.666

Table 3-4 Initial registration RMSE for the different rotation (column 2) and translation (column 3) transformation parameters.

<b>Level</b>	<b>Rot (rad)</b>	<b>Tran (mm)</b>	<b>Initial Registration RMSE (mm)</b>			
			<b>Fractal</b>	<b>Wave</b>	<b>Owl</b>	<b>Frog</b>
<b>1</b>	8.73e-5	5	8.7	8.7	114.4	9.8
<b>2</b>	1.75e-3	20	40.9	35.0	2282.6	98.3
<b>3</b>	8.73e-2	50	1104.5	283.0	N/A	4666.7

<sup>6</sup> The fractal and wave data were scaled by factors of 20 and 5 respectively to create data ranges that are closer to that of TLS data.

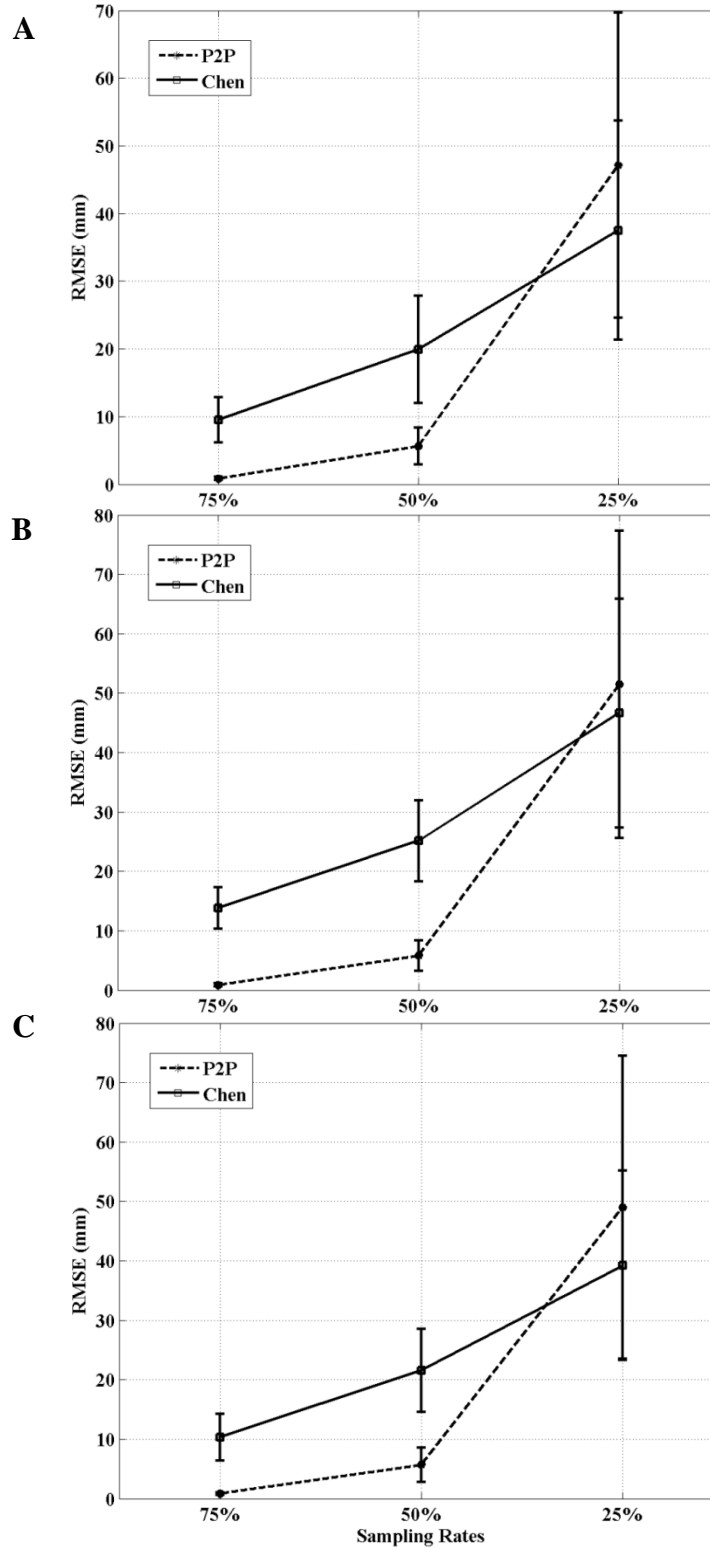


Figure 3-13 Registration RMSE bars showing mean and standard deviation in mm for fractal data. Results for the P2P method and the Chen method are given for different sampling rates. (A) to (C) are initial registration RMSE levels 1–3 respectively.

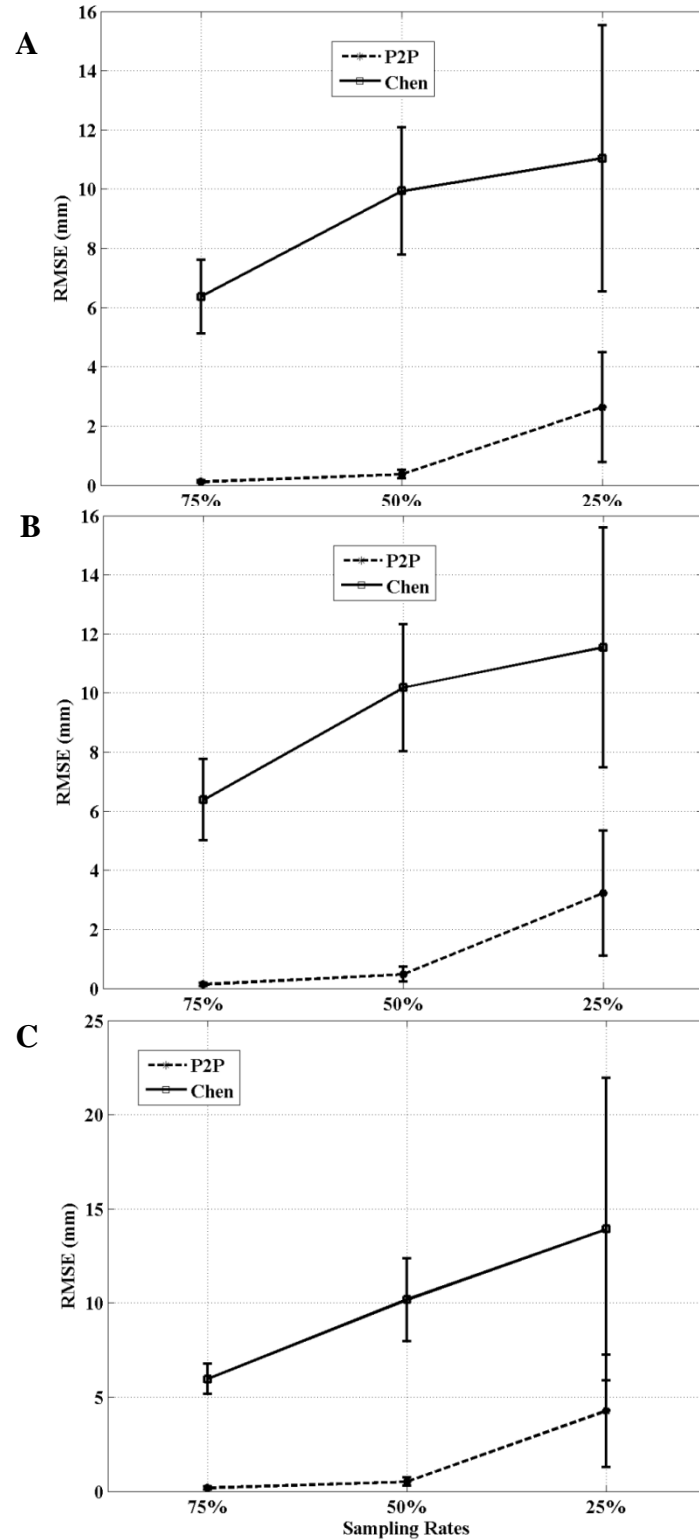


Figure 3-14 Registration RMSE bars showing mean and standard deviation in mm for wave data. Results for the P2P method and the Chen method are given for different sampling rates. (A) to (C) are initial registration RMSE levels 1–3 respectively.

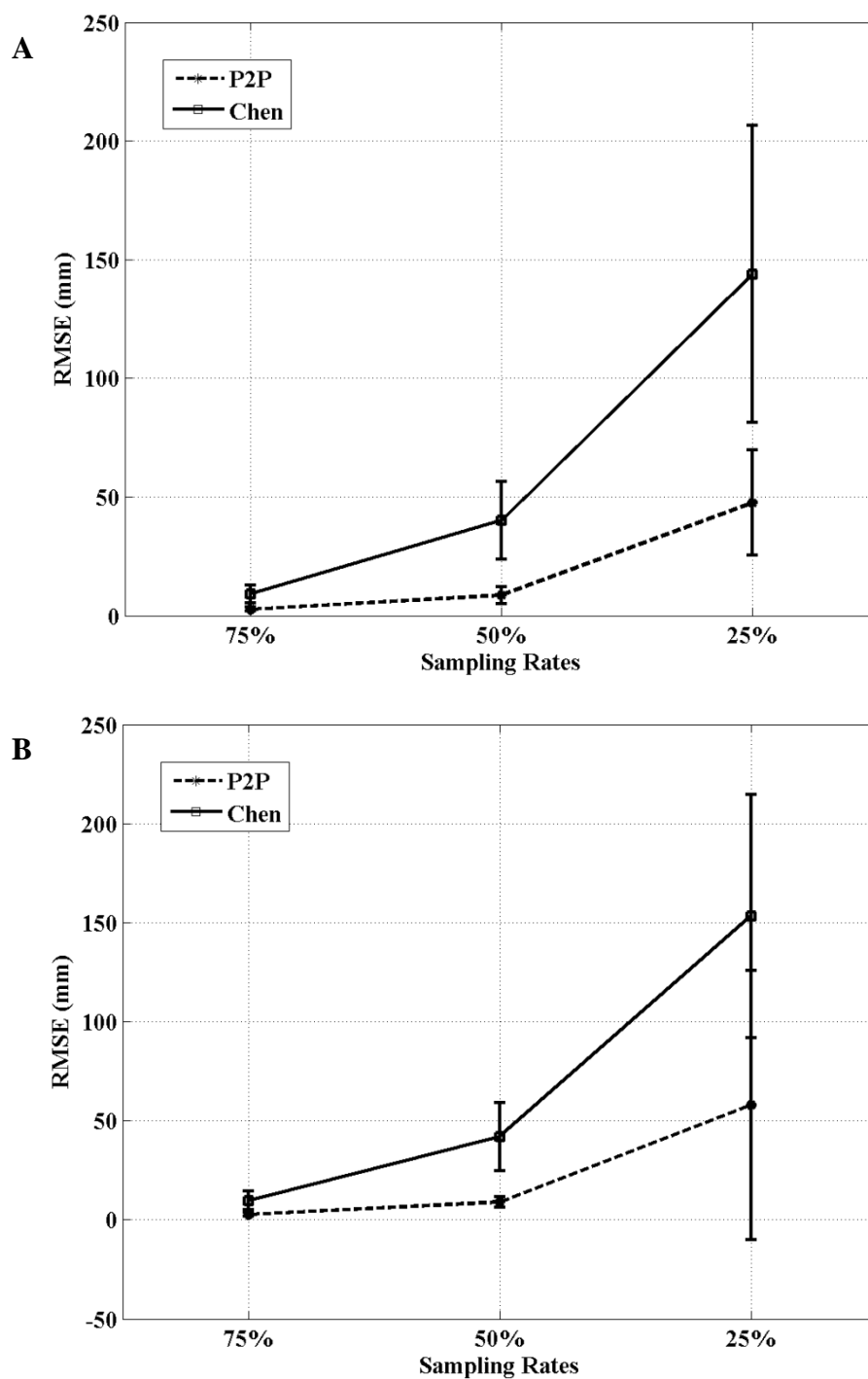


Figure 3-15 Registration RMSE bars showing mean and standard deviation in mm for owl data. Results for the P2P method and the Chen method are given for different sampling rates. (A) to (B) are initial registration RMSE levels 1–2 respectively. Note: both methods diverged for initial registration RMSE level 3. The Chen method also diverged for 75% sampling rate at initial registration RMSE level 2.



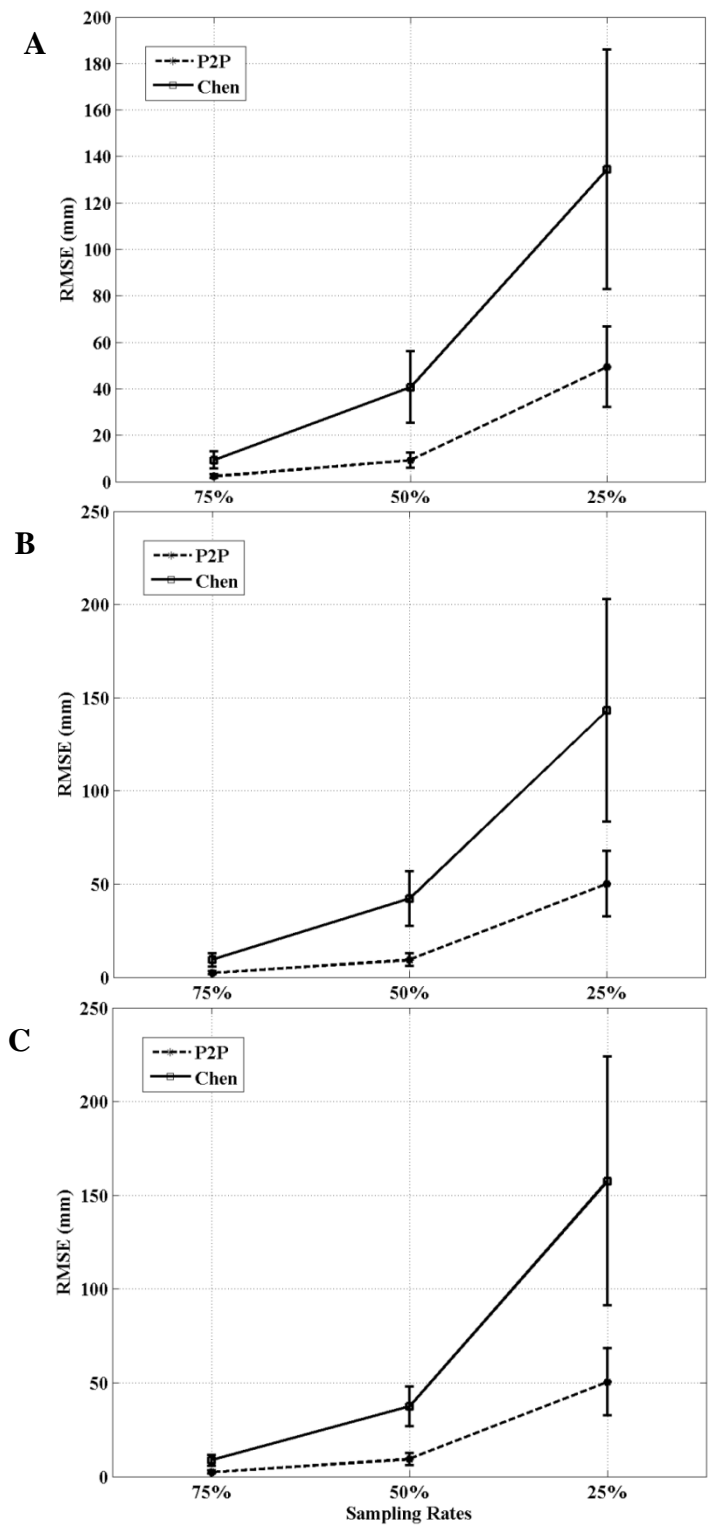


Figure 3-16 Registration RMSE bars showing mean and standard deviation in mm for frog data. Results for the P2P method and the Chen method are given for different sampling rates. (A) to (C) are initial registration RMSE levels 1–3 respectively.

The 50% sampling rate introduces the conditions of reduced overlap and potential under-sampling of the surface. These conditions are combined with the inexact point correspondences that occurred at the 75% rate. As can be expected, both methods performed worse than at the 75% rate. Errors from the P2P method were smaller than those of the Chen method by a factor of approximately 4, for all initial registration levels. This improvement of the P2P method was consistent with the results at 75%. This result indicates that the P2P method dealt better with cases of potential under-sampling and reduced overlap, than the Chen method.

The sampling rate of 25% presents an extreme case of the conditions mentioned at the 50% rate. Both methods had errors at the 50mm-and-above range, for all datasets and for all initial registration levels, except for the wave data. The wave data is predominantly a smoothly varying surface which is a possible explanation for the generally small errors by both methods. For the real data the P2P errors were smaller than the Chen method by a factor of approximately 4, which was consistent with the other sampling rates. There was a marked improvement in the Chen method for the fractal data, however. At all three initial registration RMSE levels the Chen method had smaller errors than the P2P method. The improvement here of the Chen method was by a factor of approximately 1.2. A possible explanation for this result can be based on the surface characteristics of the fractal data. With such low sampling density the local planar elements may not suffice to model the coarse fractal surface geometry. Since the P2P method is more dependent on the planar elements than the Chen method it follows that the Chen method would perform better here.

To summarize the results, it was found that the initial poses did not affect the registration performance of any of the methods, as they both yielded consistent results for all registration levels. The proposed P2P method was consistently more accurate than the Chen and Medioni (1991) method by a factor of approximately 4. The improved accuracy of the P2P method indicates that this method better deals with inexact point correspondences, reduced sampling rate and reduced overlap between pairs of scans. The only case where the Chen and Medioni (1991) method was more accurate was the 25% sampling rate of the fractal data. The improvement was by a factor of approximately 1.2 and was probably due to the fractal data being grossly under-sampled.

#### 3.4.2.4 Purdue Data

Real TLS data were obtained from a Leica Geosystems ScanStation 2. The original scans were filtered manually to remove major outliers such as people, cars, vegetation and the nearby buildings. The TLS data used in this research included eight scans of the Neil Armstrong statue on Purdue University's campus (see Figure 3-17 and Table 3-5). The statue has approximate dimensions of 2.2, 1.8, 2.6 meters (L, W, H). For each scan the ScanStation 2 was positioned at a distance of 5-10 meters from the statue to allow strong overlap (see overlap percentages in Table 3-6). The range and angular precisions of the instrument are  $4E-3$  meters and  $6E-5$  radians, respectively. Four Leica Geosystems pole targets were also scanned by each of the eight scan locations and these target coordinates were used to provide reference registration data for each pair of scans. Seven successive

pairs of scans were registered, with pair one consisting of scans 1 and 2, pair 2 consisting of scans 2 and 3, and so on. The registration RMSE values for both the proposed P2P method and the Chen method are given in Table 3-6.

The difference in RMSE between the proposed P2P method and that of Chen and Medioni (1991) was on the order of millimeters or less for each scan pair. Both methods provided good registration results for all scan pairs, except for scan pair 3 where the Chen method did not converge. Scan pair 2 was also difficult for the Chen method, with an

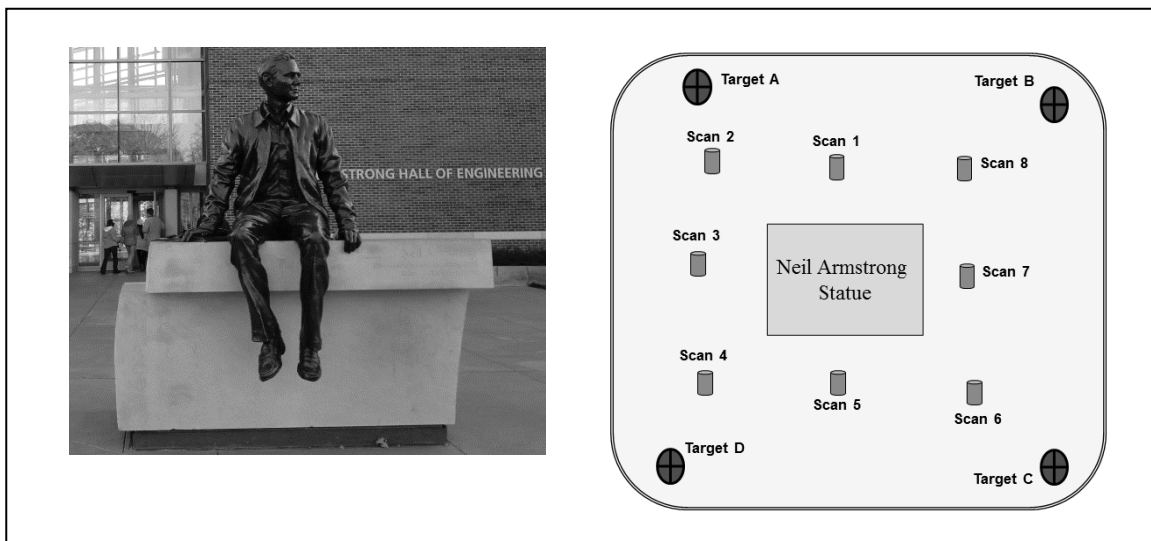


Figure 3-17 Left – View of Neil Armstrong statue at Purdue University from scan 1.  
Right – Layout of scans and targets.

Table 3-5 Number of points for each scan of the TLS data (Neil Armstrong statue).

<b>Scan</b>	<b>1</b>	<b>2</b>	<b>3</b>	<b>4</b>
# Pts	30,128	112,865	76,989	155,717
<b>Scan</b>	<b>5</b>	<b>6</b>	<b>7</b>	<b>8</b>
# Pts	157,839	141,630	86,299	104,183

Table 3-6 Registration RMSE for each scan pair of the Neil Armstrong Statue. The percentage overlap for the scans is given in the first column, in parentheses. For each pair the scan with the smaller index was regarded as Q. Thus 82% of scan 1 was in the overlap region for the registration of scan pair 1.

<b>Scan Pair (%P, %Q)</b>	<b>P2P_RMSE (mm)</b>	<b>Chen_RMSE (mm)</b>
<b>1 (52, 82)</b>	3.0	3.8
<b>2 (85, 47)</b>	1.5	8.0
<b>3 (35, 83)</b>	3.0	N/A
<b>4 (94, 71)</b>	1.7	2.5
<b>5 (77, 89)</b>	3.6	3.2
<b>6 (83, 32)</b>	3.6	4.7
<b>7 (64, 91)</b>	1.1	4.0
	<b>Mean = 2.5</b>	<b>Mean = 4.4</b>

improvement factor of approximately 5 obtained by the P2P method. Scan pairs 2 and 3 both involved scans with overlap percentages of 47 and 35 (for scans 2 and 4, respectively). Compared to the other overlap percentages this was low, and may be a

contributing factor to the performance of the Chen method. Scan pair 7 showed an improvement factor of approximately 4, which was consistent with the results of the simulated experiments. The other scan pairs showed smaller differences of about 1 mm between to two methods.

Scan pair 5 was the only pair where the Chen method gave a smaller error than the P2P method. The difference, however, was the smallest among all the scan pairs (0.4mm). Scan pairs 4 and 5 had the highest overlap percentage and these pairs gave the best results for the Chen method. This is not surprising as the P2P method is less affected by reduced overlap as indicated in the simulated experiments.

Overall, the proposed P2P method yielded more accurate registration results based on the RMSE metric, when compared with the Chen and Medioni (1991) method. The mean RMSE for the P2P method was smaller than that of Chen and Medioni (1991) by about 43% (P2P mean RMSE was 2.5 mm, Chen mean RMSE was 4.4 mm, ignoring scan pair 3). For four scan pairs the differences between the two methods were approximately 1mm. For two scan pairs the P2P method was more accurate by factors of approximately 4 and 5. For one scan pair the Chen method did not converge, but this scan pair was successfully registered with the proposed P2P method.

### 3.5 Conclusions on Pairwise Registration

This chapter focused on the so-called fine registration of a pair of PCD. Of specific interest were those methods that utilize corresponding point and plane features, as they

employ minimal processing of the original data during the registration task (Habib et al., 2010). A rigorous ICPlane registration approach called the P2P method was presented, which utilizes the General Least Squares adjustment model. As in any weighted least squares adjustment the stochastic model impacts the final solution. Thus, particular attention was paid to the stochastic properties of the estimated local surface normals which are neglected in the work of Akca (2007). A full weight matrix was employed instead of the diagonal version in Jaw (1999). The registration parameters were solved for and not point coordinates, thus forming a linear system of equations with fewer unknowns than in Jaw (1999). Also it is not assumed that any of the scans should be control surfaces, as in Jaw (1999) or Levin and Filin (2010) who used the ALS data as control data. Instead correspondences were established on both scans and the uncertainty of these scans were treated simultaneously.

Experiments were conducted with real and simulated PCD, and the registration accuracy of the proposed P2P method was compared against the well-established method of Chen and Medioni (1991). The proposed P2P method was consistently the more accurate of the two methods. The improvement indicated that the proposed P2P method was better able to deal with three conditions that impact registration accuracy: the lack of exact point correspondences, reduced overlap and potential under-sampling. It was also observed that the P2P method was comparable to the Chen method in terms of runtimes and in some cases converged faster.

The proposed P2P method can be further improved in terms of its accuracy, especially for cases where the surfaces are grossly under-sampled. A higher-order surface fitting scheme may be necessary in such cases. Future work involve assessing the computational burden of the proposed P2P method and conducting extensive comparisons with other published fine registration methods. Other implementation improvements that have been applied to ICPlane methods may also be applied to the P2P method and these will be explored to obtain a highly efficient version of P2P method. In addition, the proposed P2P approach can be extended for data of dimension greater than 3, so as to include the ancillary information that typically accompanies TLS data (e.g. intensity and RGB data).



## CHAPTER 4. GLOBAL REGISTRATION

Some applications require multiple sets of PCD to be registered in order for a complete 3D model to be obtained. For example, due to ranging and visibility restrictions, multiple scan stations are often required with TLS. Esser and Mayer (2007) reported on a large TLS campaign, where more than 1100 scan stations were required for an archeological documentation project. In these cases where multiple scans exist, a global registration is necessary to have all the scans transformed to a common reference coordinate frame.

Assuming that there are  $N$  overlapping scan pairs and each pair is related as given in Eq. (3.1) then one has

$$\begin{aligned} [Q = \mathbf{R}(P) + \mathbf{t}]_1 \\ [Q = \mathbf{R}(P) + \mathbf{t}]_2 \\ \vdots \\ [Q = \mathbf{R}(P) + \mathbf{t}]_N \end{aligned} \quad (4.1)$$

In Eq. (4.1), each  $[ \cdot ]_i$  row represents the 3D rigid-body transformation for the  $i$ -th scan pair and the symbols are as explained in Eq.(3.1). The transformation parameters  $\mathbf{R}$  and  $\mathbf{t}$  are local to each pair and the aim of global registration is to determine parameters that relate each scan to a common (or global) reference. After global registration one has for  $M$  scans

$$\begin{aligned}
\mathbf{Q} &= [\mathbf{R}(\mathbf{P}) + \mathbf{t}]_1 \\
\mathbf{Q} &= [\mathbf{R}(\mathbf{P}) + \mathbf{t}]_2 \\
&\vdots \\
\mathbf{Q} &= [\mathbf{R}(\mathbf{P}) + \mathbf{t}]_M
\end{aligned} \tag{4.2}$$

In Eq.(4.2), each row represents the transformation for a scan relative to the global reference coordinate frame, and thus these parameters are global.

As was discussed in section 2.2, global registration approaches may be grouped into two classes: sequential pairwise approaches and simultaneous approaches. The main advantage of sequential pairwise approaches is in the computational load. At any given time during the registration process, the computational load is greatly reduced as compared to the simultaneous approach. However, there are some disadvantages associated with sequential pairwise approaches.

Global registration by a sequential pairwise approach is generally susceptible to the propagation of errors. The transformation parameters for any scan are impacted by the parameters errors of all the preceding scans. In the case where the PCD is acquired in a ring structure such that the first and last scan share overlap, this propagation results in a misclosure error. That is, if the coordinate frame of the first scan is chosen as the reference after the series of sequential transformations, the first scan will have a rotation matrix that is not the identity matrix and a non-zero translation vector. Also, when there are multiple overlapping scans (i.e. redundant overlap) not all the overlap information can be used. The choice of sequential pairs to use can be haphazard and may not always yield a globally optimal solution.

Simultaneous approaches, although more computationally expensive aim at addressing these issues associated with the sequential pairwise approaches. The pairwise approach developed in Chapter 3 is extended for the global registration of multiple scans. Here it is proposed to accomplish this in a simultaneous adjustment that is closely related to the photogrammetric bundle-block adjustment. The developed method is coined the P2Pg registration method to indicate that it is a global extension of the developed P2P method of Chapter 3.

#### 4.1 Simultaneous Global Adjustment (P2Pg)

As presented in Chapter 3, the 3D points coordinates of a pair of overlapping scans may be represented symbolically as  $\mathbf{P}$  and  $\mathbf{Q}$ . The point-to-plane distances between correspondence sets in  $\mathbf{P}$  and  $\mathbf{Q}$  yield condition equations as given in Eq.(3.6) and repeated here for convenience

$$\begin{aligned} \mathbf{F}_1: (\tilde{\mathbf{p}} - \mathbf{q}) \cdot \mathbf{n}_q &= 0; & \mathbf{q} \in \mathbf{q}_e \\ \mathbf{F}_2: (\tilde{\mathbf{q}} - \mathbf{p}) \cdot \mathbf{n}_p &= 0; & \mathbf{p} \in \mathbf{p}_e \end{aligned} \quad (4.3)$$

In the context of a global adjustment, these condition equations need to be modified. For the global case, both  $\mathbf{P}$  and  $\mathbf{Q}$  need to be transformed to the reference frame, in both  $\mathbf{F}_1$  and  $\mathbf{F}_2$ . Also, the planar elements and their unit normal vectors are determined in the transformed reference space. The modified set of condition equations that arise for an overlapping pair of scans for the global adjustment is thus given by

$$\begin{aligned}
\mathbf{F}_1: (\tilde{\mathbf{p}} - \tilde{\mathbf{q}}) \cdot \mathbf{n}_{\tilde{q}} &= 0; & \tilde{\mathbf{q}} \in \tilde{\mathbf{q}}_e \\
\mathbf{F}_2: (\tilde{\mathbf{q}} - \tilde{\mathbf{p}}) \cdot \mathbf{n}_{\tilde{p}} &= 0; & \tilde{\mathbf{p}} \in \tilde{\mathbf{p}}_e
\end{aligned}
\tag{4.4}$$

$$\tilde{\mathbf{p}} = \mathbf{R}_p(\mathbf{P}) + \mathbf{t}_p \quad \tilde{\mathbf{q}} = \mathbf{R}_q(\mathbf{Q}) + \mathbf{t}_q$$

In Eq.(4.4),  $\tilde{\mathbf{p}}$  and  $\tilde{\mathbf{q}}$  are transformed points (i.e. they are in the global reference).  $\mathbf{R}_p, \mathbf{t}_p$  and  $\mathbf{R}_q, \mathbf{t}_q$  are the rotation and translation parameters for  $\mathbf{P}$  and  $\mathbf{Q}$  respectively, that transform their original scan points to the global reference. For the transformed point  $\tilde{\mathbf{p}}$  its correspondence set includes the transformed planar element  $\tilde{\mathbf{q}}_e$  (i.e. the closest three transformed points in  $\mathbf{Q}$ ) and its unit normal vector  $\mathbf{n}_{\tilde{q}}$ . Similarly for points in  $\mathbf{Q}$  each correspondence set contains  $\{\tilde{\mathbf{q}}, \tilde{\mathbf{p}}_e, \mathbf{n}_{\tilde{p}}\}$ . In the first set of condition equations  $\mathbf{F}_1$ ,  $\tilde{\mathbf{q}}$  represents any of the three points forming the planar elements  $\tilde{\mathbf{q}}_e$ . Likewise for  $\mathbf{F}_2$ ,  $\tilde{\mathbf{p}}$  represents any of the three points forming the planar elements  $\tilde{\mathbf{p}}_e$ .

The two sets of condition equations that are given in Eq.(4.4) can be linearized by Taylor series expansion to give the classical General Least Squares form of  $\mathbf{A}\mathbf{v} + \mathbf{B}\Delta = \mathbf{f}$  (Mikhail and Ackermann, 1976). The meaning of the symbols in this linearized form is as given in Eq.(3.7). For a pair of overlapping scans this linearized form is expressed as

$$\begin{bmatrix} \mathbf{A}_{1P}, & \mathbf{A}_{1Q} \\ \mathbf{A}_{2P}, & \mathbf{A}_{2Q} \end{bmatrix} \begin{bmatrix} v_P \\ v_Q \end{bmatrix} + \begin{bmatrix} \mathbf{B}_{1P}, & \mathbf{B}_{1Q} \\ \mathbf{B}_{2P}, & \mathbf{B}_{2Q} \end{bmatrix} \begin{bmatrix} \Delta_P \\ \Delta_Q \end{bmatrix} = \begin{bmatrix} \mathbf{f}_1 \\ \mathbf{f}_2 \end{bmatrix}
\tag{4.5}$$

where

$$\begin{aligned}
 \mathbf{A}_{1P} &= \mathbf{F}_1'(\mathbf{p}), & \mathbf{A}_{1Q} &= \mathbf{F}_1'(\mathbf{q}); & \mathbf{B}_{1P} &= \mathbf{F}_1'(\Delta_P), & \mathbf{B}_{1Q} &= \mathbf{F}_1'(\Delta_Q) \\
 \mathbf{A}_{2P} &= \mathbf{F}_2'(\mathbf{p}), & \mathbf{A}_{2Q} &= \mathbf{F}_2'(\mathbf{q}); & \mathbf{B}_{2P} &= \mathbf{F}_2'(\Delta_P), & \mathbf{B}_{2Q} &= \mathbf{F}_2'(\Delta_Q) \\
 \mathbf{f}_1 &= -[\mathbf{F}_{1,0}]; & & & \mathbf{f}_2 &= -[\mathbf{F}_{2,0}]
 \end{aligned}$$

In Eq.(4.5),  $\mathbf{F}_1'(\mathbf{p}), \mathbf{F}_1'(\mathbf{q}), \mathbf{F}_1'(\Delta_P)$  and  $\mathbf{F}_1'(\Delta_Q)$  are the partial derivatives (or Jacobians) of the condition equation  $\mathbf{F}_1$  w.r.t.  $\mathbf{p}, \mathbf{q}, \Delta_P$  and  $\Delta_Q$  respectively.  $\Delta_P$  and  $\Delta_Q$  are the parameter corrections to the initial rigid-body transformation parameters for scans  $\mathbf{P}$  and  $\mathbf{Q}$  respectively.  $v_P$  and  $v_Q$  are the residuals for points in  $\mathbf{P}$  and  $\mathbf{Q}$  respectively.  $\mathbf{F}_2'(\mathbf{p}), \mathbf{F}_2'(\mathbf{q}), \mathbf{F}_2'(\Delta_P)$  and  $\mathbf{F}_2'(\Delta_Q)$  are similarly the partial derivatives of the condition equation  $\mathbf{F}_2$  w.r.t.  $\mathbf{p}, \mathbf{q}, \Delta_P$  and  $\Delta_Q$  respectively. The detailed derivation of these Jacobians is given in Appendix C.

Given multiple scans, the unknown vector and correction vectors in Eq.(4.5) would have lengths equal to the number of scans. If the coordinate frame of one of the scans is chosen as the reference then the correction vector would have a length equal to one less than the number of scans. Each overlapping pair that is involved in the adjustment, contributes to the coefficient matrices  $\mathbf{A}$  and  $\mathbf{B}$ . The locations of these contributing terms in the coefficient matrices would be determined by the corresponding order of scan points in the residual vector.

A scenario of three scans may be considered, where there exist three overlapping pairs which are (1,2), (2,3) and (1,3). It is further assumed that the coordinate frame of scan 1 is set to be the reference (i.e. this scan is not to be transformed). Also, the adopted convention is that in a given scan pair, example (2,3),  $\mathbf{P}$  will represent the scan with the larger scan number, which is scan 3 in this case. For simplicity, the two-row expression in Eq.(4.5) is replaced by the following single-row expression

$$[\mathbf{A}_P, \mathbf{A}_Q] \begin{bmatrix} v_P \\ v_Q \end{bmatrix} + [\mathbf{B}_P, \mathbf{B}_Q] \begin{bmatrix} \Delta_P \\ \Delta_Q \end{bmatrix} = \mathbf{f} \quad (4.6)$$

where

$$\mathbf{A}_P = \begin{bmatrix} \mathbf{A}_{1P} \\ \mathbf{A}_{2P} \end{bmatrix}; \quad \mathbf{A}_Q = \begin{bmatrix} \mathbf{A}_{1Q} \\ \mathbf{A}_{2Q} \end{bmatrix}; \quad \mathbf{B}_P = \begin{bmatrix} \mathbf{B}_{1P} \\ \mathbf{B}_{2P} \end{bmatrix}; \quad \mathbf{B}_Q = \begin{bmatrix} \mathbf{B}_{1Q} \\ \mathbf{B}_{2Q} \end{bmatrix}; \quad \mathbf{f} = \begin{bmatrix} f_1 \\ f_2 \end{bmatrix}$$

Replacing  $\mathbf{P}$  and  $\mathbf{Q}$  by their corresponding scan numbers, the combined linearized system for the three overlapping scan pairs is given by

$$\begin{bmatrix} \mathbf{A}_1 & \mathbf{A}_2 & \emptyset \\ \emptyset & \mathbf{A}_2 & \mathbf{A}_3 \\ \mathbf{A}_1 & \emptyset & \mathbf{A}_3 \end{bmatrix} \begin{bmatrix} v_1 \\ v_2 \\ v_3 \end{bmatrix} + \begin{bmatrix} \mathbf{B}_2 & \emptyset \\ \mathbf{B}_2 & \mathbf{B}_3 \\ \emptyset & \mathbf{B}_3 \end{bmatrix} \begin{bmatrix} \Delta_2 \\ \Delta_3 \end{bmatrix} = \begin{bmatrix} \mathbf{f}(1, 2) \\ \mathbf{f}(2, 3) \\ \mathbf{f}(1, 3) \end{bmatrix} \quad (4.7)$$

$$\tilde{\mathbf{A}} \quad \mathbf{v} \quad + \quad \tilde{\mathbf{B}} \quad \Delta \quad = \quad \tilde{\mathbf{f}}$$

In this combined system, each row represents a pair of overlapping scans. For example the first row reflects the contributions of the overlap between scans 1 and 2. Both coefficient matrices  $\tilde{\mathbf{A}}$  and  $\tilde{\mathbf{B}}$  contain null matrices in each row which are represented by  $\emptyset$ . Since the coordinate frame of scan 1 was chosen to be the reference frame, the unknown vector only has parameter corrections for scan 2 and scan 3. The solution to this

combined system is obtained iteratively by solving the following normal equation until convergence

$$N\Delta = t \quad (4.8)$$

$$N = \tilde{\mathbf{B}}^T (\tilde{\mathbf{A}}\mathbf{Q}_{ll}\tilde{\mathbf{A}}^T)^{-1}\tilde{\mathbf{B}}; \quad t = \tilde{\mathbf{B}}^T (\tilde{\mathbf{A}}\mathbf{Q}_{ll}\tilde{\mathbf{A}}^T)^{-1}\mathbf{f}; \quad \mathbf{Q}_{ll} = \frac{1}{\sigma_0^2}\Sigma$$

$\sigma_0^2$  is the a priori reference variance (typically set to 1)

$\Sigma$  is the Cartesian covariance matrix of the observations (i.e. the scan points) as discussed in Chapter 3.

#### 4.2 P2Pg Algorithm

All the considerations that were discussed in section 3.3 apply to the global algorithm. Special attention must be given to the correspondence sets that are used. The combined linearized system of equations can include highly correlated observations. The P2Pg algorithm was used in this research as a refinement method after pairwise registration was performed with P2P. As such, the approach of Akca (2007) was adopted, where a small portion of the condition equations were used in the global adjustment. In this research 1% of the condition equations were used. This sub-sampling of the condition equations helped in avoiding rank-deficiency in the  $\tilde{\mathbf{A}}$ -matrix of Eq.(4.7) as the spacing between transformed points increased (see section 3.3.3). Also, this sub-sampling reduced the computational load of the P2Pg approach. The relatively high computational load is the main disadvantage of simultaneous global approaches. In addition, since a full pairwise registration was performed prior to the global refinement, only one or two iterations of P2Pg are expected. It must be further emphasized that the sub-sampling was

applied to the condition equations and not to the points. The latter will modify the point density of the PCD which is undesirable.

The algorithm involves seven main steps. The P2P approach is first used as a preprocessing step to provide the initial parameter approximations. If an initial pairwise registration is not done then the P2Pg algorithm will require more iterations for convergence. It must also be noted that it is advised that the unit normal vectors in Eq.(4.4) be computed in the original space and then rotated by the current rotation parameters as discussed in Appendix D. The P2Pg algorithm can be summarized as follows:

---

### **P2Pg Algorithm for global registration of multiple sets of PCD**

---

0. Inputs: - 3D coordinates of unstructured sets of PCD
    - initial set of parameter approximations obtained from P2P
    - observations' precision (as used in P2P)
- 
1. Transform each scan by its parameter approximations according to Eq.(4.4). All transformed scans will now be in the reference frame.
  2. Organize transformed scans using a spatial data structure (e.g. k-d tree) to facilitate efficient point searching.
  3. Establish correspondence sets and point-to-plane distances for each scan according to Eq.(4.4).



4. Identify and remove points that are not in the overlapping region. This can be done either by using the distance to closest transformed point or the point-to-plane distance.
5. Use every  $i$ -th correspondence set to populate the least squares matrices  $\mathbf{N}$  and  $\mathbf{t}$  in Eq.(4.8). The considerations for the sub-sampling rate include the quality of the parameter approximations, point densities and computational resources.
6. Solve the linear system in Eq.(4.8) to compute the correction to the parameters, and update the parameters.
7. Check for iteration termination. If iterations should not be terminated then return to step 1. If termination criterion has been met then obtain registration and adjustment results.

- 
8. Outputs: - final (adjusted) parameters and their covariance matrix
    - registration and adjustment statistics
    - registered sets of PCD and covariance matrix (if needed)
- 

One of the advantages of the P2Pg approach is that covariance information for the parameters is available. This is a distinguishing feature of simultaneous adjustment approaches. Also, as expressed in Eq.(4.5) and Eq.(4.6) one set of residuals per scan is obtained from P2Pg. When pairwise registrations are performed, scans that share overlap with more than one scan will have multiple sets of residuals. These residuals can be inconsistent (i.e. not the same) for a given scan. P2Pg provides consistent residuals for each scan, however. P2Pg also provides a solution with zero-misclosure. All the

overlapping scan pairs can potentially contribute to the final solution and since the reference scan is not included in the unknown vector it is never transformed.

### 4.3 Evaluations and Discussion

Two sets of global registration experiments were performed using the Purdue data described in section 3.4.2.4. First, a global registration was obtained by the sequential pairwise approach. The performance of the P2P algorithm was evaluated by comparisons with other registration methods in the context of sequential pairwise registration. Second, the P2Pg algorithm was used to refine the result that was obtained from the sequential P2P approach. This refined result was then evaluated by comparisons with other global registration methods.

#### 4.3.1 Global Registration by Sequential Pairwise Approach

The Purdue data comprises eight scans with each successive pair of scans sharing overlap. The first and last scan also shared overlap, which meant there was a total of eight scan pairs, [(1,2), (2,3), (3,4), (4,5), (5,6), (6,7), (7,8), (8,1)]. The sequential pairwise parameters were combined to obtain the global parameters for each scan. Thus, for example, to obtain the global parameters for scan 3, the pairwise parameters from pairs (1,2) and (2,3) were used. This was done for all scans, including scan 1 which shares overlap with scan 8. Since scan 1 was chosen as the reference, the global transformation for scan 1 should include the identity matrix for rotation and the zero vector for translation. Any other obtained transformation for scan 1 would result in a non-zero misclosure error, and it provided the basis for the first type of evaluation.

The P2P algorithm was compared with three registration methods in terms of their misclosure errors. The ICP method by Besl and McKay (1992) was implemented and used for comparisons. Although this method is a point-to-point registration method and not point-to-plane as P2P, it was used for comparisons because of its popularity. The cloud registration tools of two software packages were also used. The first software package was the open source, 3D point cloud and mesh processing software CloudCompare version 2.4. This software package includes a version of the ICP method of Besl and McKay (1992) in its fine registration (CloudCompare, 2013). The Leica Cyclone version 7.4.1 was the second software package used, which is a commercial package. Cyclone cloud registration tool requires the presence of point normals on both scans of a scan pair. This suggests that it uses some modification of the ICP method of Besl and McKay (1992) (Leica, 2013).

Pairwise registration parameters were determined for each of the eight scan pairs by all four registration methods (P2P, Besl, CloudCompare and Cyclone). These sequential pairwise parameters were then combined to obtain the global registration parameters for scans 2 through 8, with scan 1 being the reference. The registration parameters obtained from the use of targets were used as described in section 3.4.2.4 to obtain the registration errors for each of the four registration methods. The misclosure RMSE values are given in Figure 4-1 and the pairwise and global registration RMSE values are given in Table 4-1 and Table 4-2 respectively. The registered Purdue data was color coded by registration errors for the Besl, P2P and Cyclone methods and these results are given in

Figure 4-2, Figure 4-3 and Figure 4-4 respectively. The parameter errors are provided in Appendix D.

The pairwise registration results from CloudCompare were worse than the other methods by an order of magnitude, for scan pairs 1, 2 and 8, as shown in Table 4-1. It is uncertain what caused this poor performance. Both CloudCompare and Besl used the ICP method by Besl and McKay (1992), but possible areas where implementations differ are in the iteration termination and outlier removal. It is quite clear from Table 4-1 that P2P's pairwise registration RMSE was very consistent for all scan pairs. Scan pair 8 was the most problematic for the other methods but P2P's results were consistent with its results for the other pairs. It must be mentioned here that the iteration termination criteria used for P2P in this chapter was slightly different to that in chapter 3. Also for all registration methods, the registration was performed in a forward and backward approach and the best results reported here. A forward registration for scan pair  $(i, j)$  would be to find the parameters to transform scan  $j$  to scan  $i$ . A backward registration would be to find the parameters to transform scan  $i$  to scan  $j$ .

Table 4-1 Pairwise Registration RMSE in mm, for scan pairs of the Purdue data.

Pair	Besl	P2P	CloudCompare	Cyclone
1	3.5	1.4	28.6	0.9
2	1.6	0.9	10.2	3.5
3	3.4	1.6	7.4	3.8
4	1.3	1.1	7.2	1.7
5	1.1	1.3	5.0	2.9
6	1.9	1.5	3.6	3.9
7	2.9	2.9	4.9	3.8
8	5.7	2.4	46.2	8.7

Table 4-2 Global Registration RMSE in mm, for scan pairs of the Purdue data.

Scan	Besl	P2P	CloudCompare	Cyclone
2	3.5	1.4	28.6	0.9
3	4.4	2.3	35.4	3.2
4	7.9	2.8	35.7	6.7
5	8.4	3.4	27.1	7.9
6	8.5	4.2	28.4	9.2
7	7.9	5.3	31.2	7.3
8	5.9	3.0	29.3	4.5

The global registration errors are more of interest in this chapter. Again CloudCompare's performance was an order of magnitude worse than the other methods as shown in Table 4-2. Among the other three methods, the global registration RMSE by P2P was the best for all scans except for scan 2. It is known that the Chen and Medioni (1991) method is more accurate than the Besl and McKay (1992) method which explains why Cyclone's errors are smaller than Besl's. The P2P method showed marked improvement over Cyclone's tool in scan's 4, 5 and 6 (see Figure 4-2, Figure 4-3 and Figure 4-4) which can

be attributed to the increased stochastic consideration of the proposed P2P method. The misclosure RMSE in Figure 4-1 reflects the same results as Table 4-2.

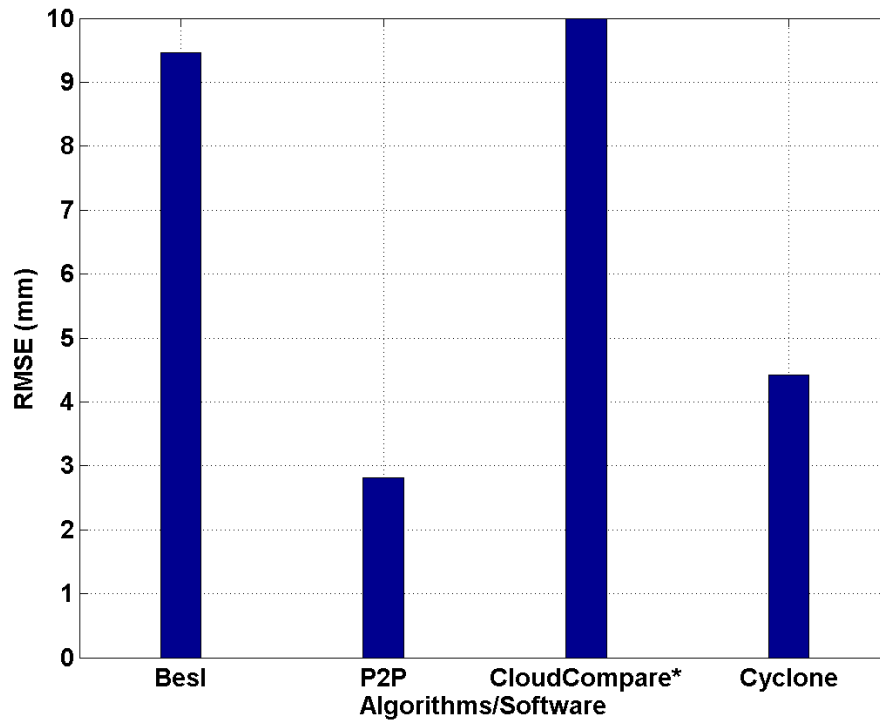


Figure 4-1 Registration Misclosure for different algorithms/software.  
(CloudCompare\*: the misclosure RMSE was 69.2mm).

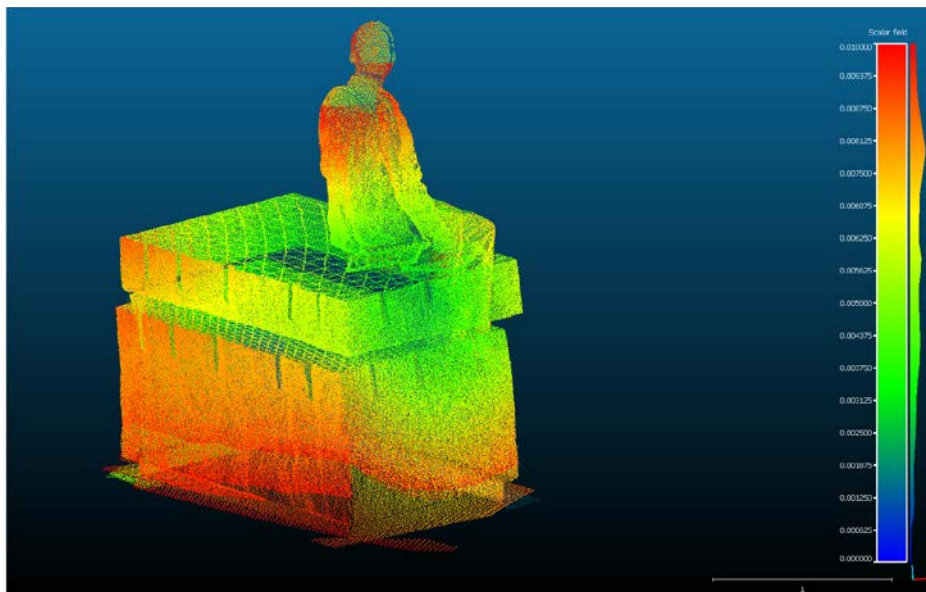


Figure 4-2 View from scan 6 of Purdue data, registered by **Best** and color-coded by registration errors. Error scale bar ranges from 0.00m (blue) to 0.01m (red).

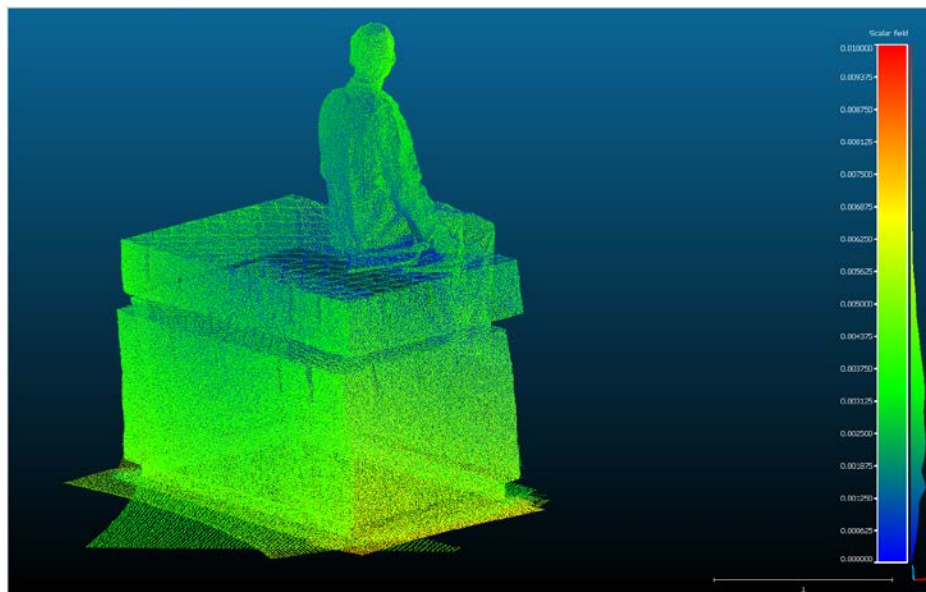


Figure 4-3 View from scan 6 of Purdue data, registered by **P2P** and color-coded by registration errors. Error scale bar ranges from 0.00m (blue) to 0.01m (red).

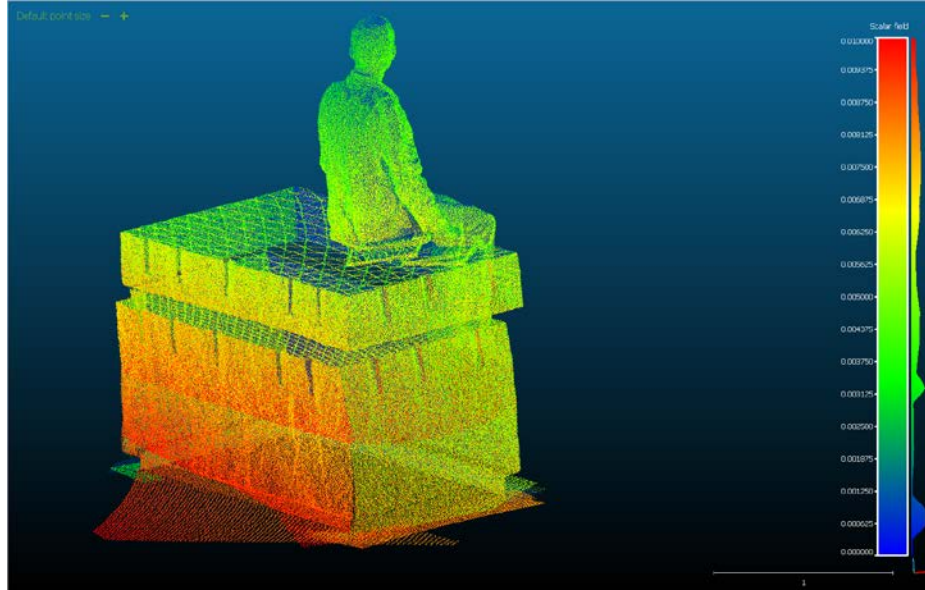


Figure 4-4 View from scan 6 of Purdue data, registered by **Cyclone** and color-coded by registration errors. Error scale bar ranges from 0.00m (blue) to 0.01m (red).

#### 4.3.2 Global Registration by Simultaneous Approach

The proposed P2Pg method was used to refine the results obtained from the global registration by sequential pairwise P2P. Cyclone also offers a global refinement tool and this was used to refine the sequential pairwise Cyclone results (called Cyclone-g). The registration RMSE values are given in Figure 4-5 for both of these methods, before and after refinement. Table 4-3 shows the global registration RMSE values for each scan both for the P2P algorithm and the P2Pg algorithm. Also, the distribution of the registration errors for P2P and P2Pg are given in Figure 4-6 and Figure 4-7. The parameter errors are included in Appendix E.

Both refinement methods (Cyclone-g and P2Pg) obtain global registration results that have no misclosure. However, it can be seen that unlike Cyclone-g, P2Pg achieved this



without increasing the registration RMSE values for each scan. In fact, as shown in Figure 4-6 and Figure 4-7 the proposed P2Pg method improved the distribution of the global registration errors. A look at the RMSE values for each scan in Table 4-3 shows that the proposed P2Pg method reduced the standard deviation of the RMSE values for the seven scans. In other words the P2Pg method better distributed the errors to obtain an improved global registration result.

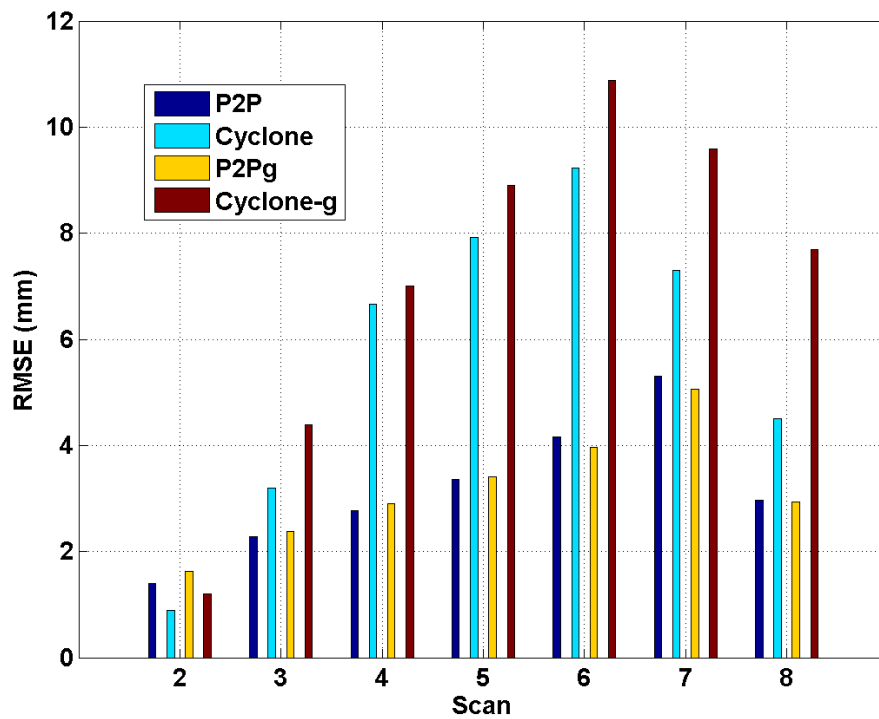


Figure 4-5 Registration RMSE before and after refinement.

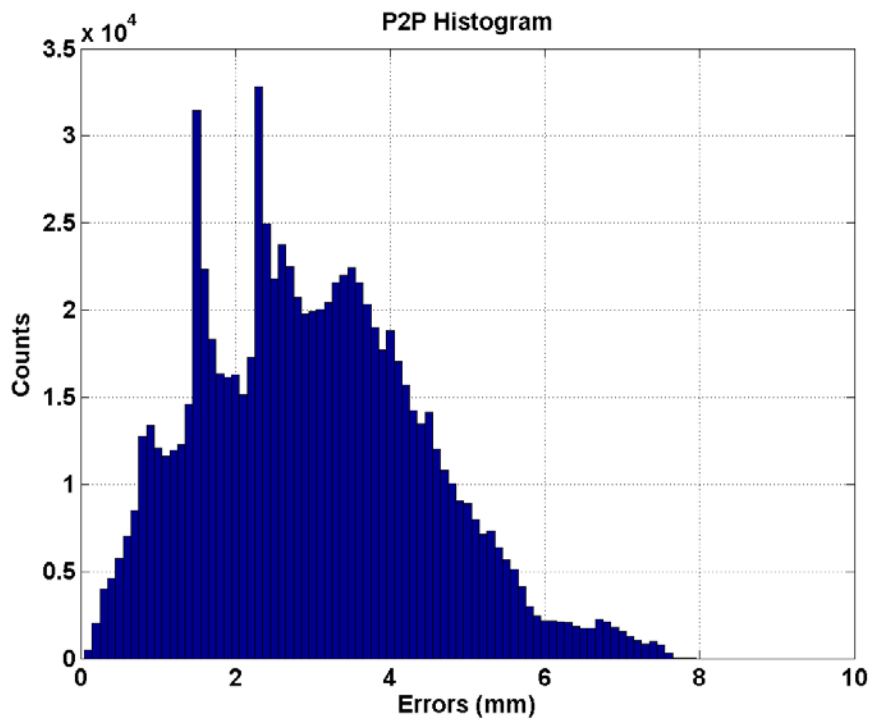


Figure 4-6 Distribution of global registration errors by P2P.

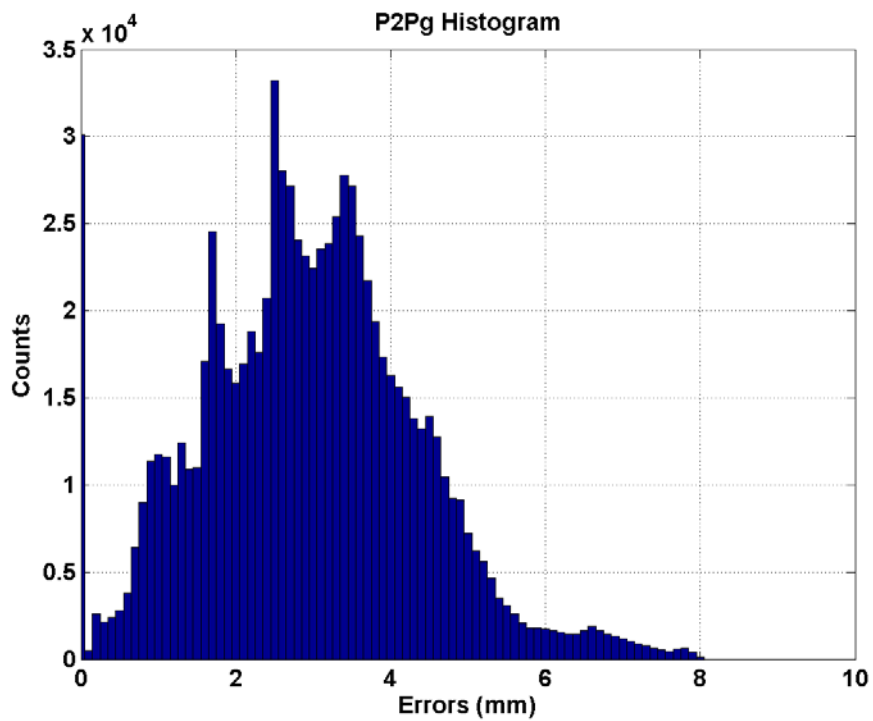


Figure 4-7 Distribution of global registration errors by P2Pg.

Table 4-3 Global registration RMSE (in mm).

Scan	<b>P2P_RMSE</b>	<b>P2Pg_RMSE</b>
2	1.4	1.6
3	2.3	2.4
4	2.8	2.9
5	3.4	3.4
6	4.2	4.0
7	5.3	5.1
8	3.0	2.9
Mean	3.18	3.18
Max	5.31	5.06
Std	1.28	1.11

#### 4.4 Conclusions on Global Registration

Global registration is an essential task with PCD, as some applications require multiple sets of PCD to be registered in order for a complete 3D model to be obtained. For example, due to ranging and visibility restrictions, multiple scan stations are often required with TLS. In the context of cloud-to-cloud registration the two common approaches for global registration are the sequential pairwise approach and a simultaneous global approach. The proposed P2P method was used in the sequential pairwise approach and evaluated by comparisons with other registration methods on a real TLS dataset. The global registration results of P2P were shown to be better than the other approaches.

An extension of the P2P approach was developed in this chapter which was called the P2Pg algorithm. This method was developed to provide global refinement to the P2P method and it determines global registration parameters in a simultaneous adjustment. The proposed approach presents many advantages which include the computation of consistent residuals for each scan (i.e. only one set of residuals is obtained for a registered scan). The P2Pg approach potentially includes all overlapping pairs in the adjustment, not only sequential pairs. Thus all information contribute to the final results and no haphazard selection of scan pairs is needed for the registration process. The computational load of the simultaneous approach may be circumvented when P2Pg is used as a refinement to the P2P. In this case, very good initial approximations would be available which mean only one or two iterations of P2Pg would be needed. Also, sub-sampling of the condition equations is a feasible option in this case.

## CHAPTER 5. FINAL CONCLUSIONS AND RECOMMENDATIONS

### 5.1 Thesis Summary

Point cloud data (PCD) have become very pervasive due to its use in many communities which include, but are not limited to, biomedical imaging, photogrammetric engineering, roadway and construction mapping, city modeling, automobile industry, autonomous navigation, robotics and computer vision. In some applications multiple sets of PCD are required to be registered in order for a complete 3D model to be obtained. For example, due to ranging and visibility restrictions, multiple scan stations are often required with terrestrial laser scanning (TLS). In these cases where multiple scans exist, a registration of the PCD is necessary to have all the scans transformed to a common reference coordinate frame.

The task of registration involves determining a set of transformation parameters and applying those parameters to transform one dataset into another reference frame (Cheok, 2006). For this to be achieved there must exist a means of establishing correspondences among the disparate coordinate data sets. Perhaps one of the most popular registration methods is the use of targets or other features that are recognizable in the different sets of PCD (Akca and Gruen, 2008; Elkrachy, 2008; Jacobs, 2005). The recognition of these features usually involves the use of imagery, either intensity images or true-color images

or both. Automatic registration methods that are independent of targets, and rather exploit the PCD, can reduce some of the current limitations of the use of targets. Cloud-to-cloud (or surface based) registration has been pursued by many researchers over the last two decades to fulfill this aim. In cloud-to-cloud registration methods the transformation parameters are obtained by establishing correspondences between the disparate 3D coordinate data. However, PCD are usually unstructured and possess little semantics. Thus it is virtually impossible to establish exact point correspondences between sets of PCD.

In this dissertation both pairwise and global cloud-to-cloud registration were addressed. Existing pairwise approaches do not consider the full stochastic model. This research sought to do that and showed improvement in accuracy over popular approaches. A rigorous point-to-plane registration approach was developed. Its formulation uses the General Least Squares adjustment model, with the scanned points on both surfaces being used as the model observations. The effect of the incidence angle is taken into account in the stochastic model, as well as the local surface normals, which are treated as derived quantities from the observations. Also it is not assumed that any of the scans should be control surfaces, as in Jaw (1999) or Levin and Filin (2010). Instead correspondences were established on both scans (symmetry) and the uncertainty of these scans was treated simultaneously.

The pairwise approach was then extended for the global registration of multiple scans. A simultaneous adjustment is proposed that is closely related to the photogrammetric

bundle-block adjustment. The proposed approach addresses the issue of some overlapping information which occurs in the sequential pairwise approach, when there is overlap between non-sequential scan pairs. Instead, the proposed approach utilizes all the available information from all scans so as to obtain a globally optimal parameter solution. Thus all information can contribute to the final results and no haphazard selection of scan pairs is needed in the registration process.

## 5.2 Final Conclusions

Experiments on pairwise registration were conducted with real and simulated PCD, and the registration accuracy of the proposed P2P method was compared against the well-established method of Chen and Medioni (1991). The proposed P2P method was consistently the more accurate of the two methods. The improvement indicated that the proposed P2P method was better able to deal with three conditions that impact registration accuracy: the lack of exact point correspondences, reduced overlap and potential under-sampling. It was also observed that the P2P method was comparable to the Chen method in terms of runtimes and in some cases converged faster than the Chen and Medioni (1991) method. The improved accuracy performance that was observed in these experiments can be attributed to the distinguishing feature of the P2P method. The symmetric correspondence enables the stochastic properties of both scans to be considered in the adjustment theory. This symmetric correspondence distinguishes the proposed P2P method from other fine, pairwise registration methods.

For global registration, two approaches were investigated. The commonly chosen method of sequential pairwise registrations was done with the proposed P2P method on real experimental data. Comparisons with other registration algorithms and software tools showed the P2P method to be the most accurate method. The proposed simultaneous global approach (called the P2Pg method) was shown to better distribute the registration errors among the overlapping scans. Also, this simultaneous global approach yields zero misclosure which is a desirable result from global registration. The P2Pg global refinement approach showed marked improvement in registration accuracy when compared to the global refinement tool in Cyclone.

The improved accuracy performance of both the P2P and P2Pg methods in these experiments suggests that these algorithms can be utilized in many of the applications where PCD exist.

### 5.3 Recommendations

The ICPlane method developed by Chen and Medioni (1991) has had many modifications since its development. Some of these modifications can be included in P2P, to improve areas such as the robustness and the search optimization. Also, both the P2P and P2Pg methods involve least squares matrices with sparse structure (see Figure 5-1), which may be exploited in the parameter solution process with iterative solvers. Another approach that may be considered is the re-ordering of the point order for the  $P$  and  $Q$  scans. Re-ordering schemes may compact the non-zero elements of some of the sparse least squares matrices and render a more efficient approach to parameter solution.



In addition to the linear algebra strategies it may be useful to adopt a coarse-to-fine strategy in the registration algorithm, especially for the P2Pg. This coarse-to-fine strategy may involve the use of a small percentage of the points in the early iterations which reduces the computational cost per iteration. The percentage of used points may then increase as the solution approaches convergence. As with all cloud-to-cloud registration methods, the success of these approaches and strategies would be data dependent. The overlap percentage impacts the final registration accuracy but perhaps more importantly would be the surface geometry within the overlapping regions. The P2P and P2Pg methods rely on having surfaces with sufficient variations in the directions of the unit normal vectors to be successful.

Future work include extensions from 3D to more dimensions to include intensity and RGB data. It may also be possible to even include multispectral data and have the registration be adopted in tasks such as manifold alignment for multispectral classification. In this case, a single point will be an  $n$ -dimensional point and the condition equations will involve minimizing the point-to- hyper-plane distances. In terms of the P2Pg method, the adjustment theory is flexible enough to include other data. These additional data may include targets, GNSS data, and other control information. Also, other geospatial data such as photogrammetric data may be included in the adjustment theory. This opens many options in terms of multi-sensor fusion. The synergy between PCD from LiDAR sensors and photogrammetry may be exploited by building on the current P2Pg mathematical model.

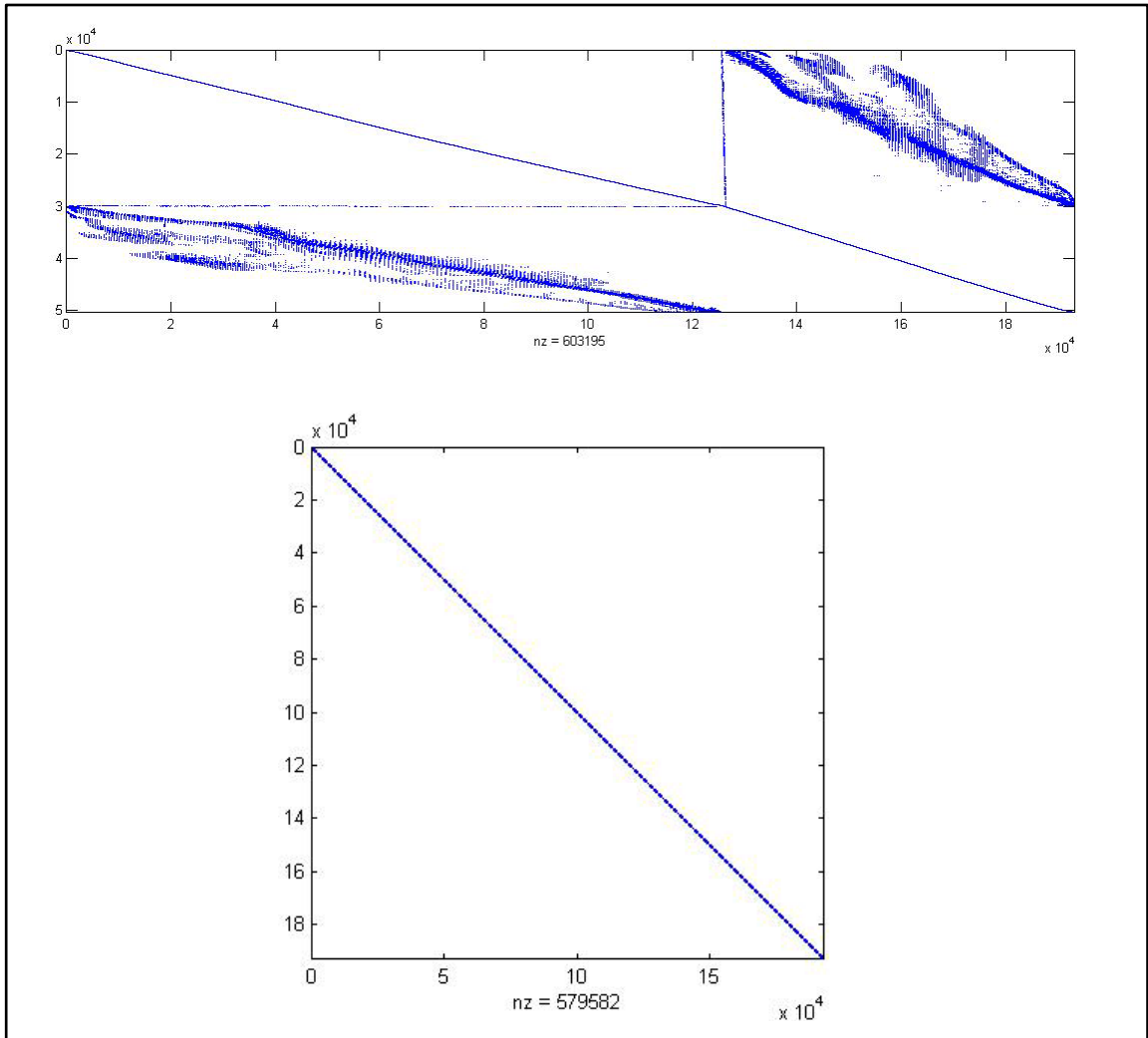


Figure 5-1 Example sparse matrices from pair#1 of Neil Armstrong Data.  
 Top – A-matrix, size = 50,346 x 193,194, non-zeroes = 603,195 (0.0062%)  
 Bottom – Q-matrix, size = 193,194, non-zeroes = 579,582 (0.0016%)

The algorithms developed in this research have the potential for being easily transferred to other communities. These communities utilize PCD and they include biomedical imaging, autonomous navigation, robotics and computer vision. These developed cloud-to-cloud registration approaches may potentially assist in autonomous navigation and also help towards autonomous mapping by reducing the need of control information.

## LIST OF REFERENCES

## LIST OF REFERENCES

- Akca, D., 2007. Least Squares 3D Surface Matching. Ph.D. Thesis, Swiss Federal Institute of Technology Zurich.
- Bae, K.-H., 2006. Automated Registration of Unorganised Point Clouds from Terrestrial Laser Scanners. Ph.D. Thesis, Curtin University of Technology.
- Bentley, J.L., 1975. Multidimensional binary search trees used for associative searching. *Communications of the ACM* 18(9), pp. 509–517.
- Bergevin, R., Soucy, M., Gagnon, H. and Laurendeau, D., 1996. Towards a general multi-view registration technique. *IEEE PAMI* 18(5), pp. 540–547.
- Bitenc, M., Lindenbergh, R., Khoshelham, K., vanWaarden, A.P., 2010. Evaluation of a laser land-based mobile mapping system for monitoring sandy coasts. *International Archives of Photogrammetry, Remote Sensing and Spatial Information Sciences* 38 (Part 7B), 92–97.

- Chen, Y., Medioni, G., 1991. Object modeling by registration of multiple range images. In: Proc. IEEE International Conference on Robotics and Automation, vol. 3, Sacramento, CA, 9–11 April, pp. 2724–2729.
- CloudCompare (version 2.4), 2013. [GPL software]. EDF R&D, Telecom ParisTech (2013). Retrieved from <http://www.danielgm.net/cc/> on 21st May, 2013.
- Cheok, G.S., 2006. In: Proceedings of the 3rd NIST Workshop on the Performance Evaluation of 3d Imaging Systems. NIST Interagency/Internal Report-7357.
- Esser, G., and I. Mayer, 2007. 3d-geometry and 3d-texture. Documenting early Christian wall paintings at the Domitilla Catacomb in Rome. Proceedings of 12th International Conference on “Cultural Heritage and New Technologies”, 5-7 November, Vienna, Austria.
- Godin, G., Rioux, M., Baribeau, R., 1994. Three-dimensional Registration Using Range and Intensity Information. In: Proc. SPIE 2350, Videometrics III, 279 (October 6, 1994).
- Huber, D., 2011. The ASTM E57 file format for 3D imaging data exchange. In: Proc. SPIE 7864, San Francisco, CA, 23 January.

Jaw, J.-J., 1999. Control Surface in Aerial Triangulation. Ph.D. Thesis, The Ohio State University.

Kinect, 2013. <http://www.microsoft.com/en-us/kinectforwindows/>, accessed on 22nd May, 2013.

Leica, 2013. <http://hds.leica-geosystems.com/>, accessed on 21st May, 2013.

Levin, S., Filin, S., 2010. Registration of terrestrial photogrammetric data using natural surfaces as control. *Photogrammetric Engineering and Remote Sensing* 76 (10), 1183–1193.

Lichti, D., Pfiefer, N., Maas, H.-G., 2008. ISPRS Journal of Photogrammetry and Remote Sensing theme issue “Terrestrial Laser Scanning”. *ISPRS Journal of Photogrammetry and Remote Sensing* 63 (1), 1–3.

Matabosch, C., 2007. Hand-held 3D scanner for large surface registration. Ph.D. Thesis, Universitat de Girona, Spain.

Mikhail, E.M., Ackermann, J.C., 1976. *Observations and Least Squares*. IEP-A Dun-Donnelley, New York.

- Mikhail, E.M., Bethel, J.S., McGlone, J.C., 2001. Introduction to Modern Photogrammetry. John Wiley & Sons, Inc., New York.
- Romsek, B.R., 2008. Terrestrial Laser Scanning: Comparison of Time-of-flight and Phase Based Measuring Systems. Master's thesis, Purdue University.
- Rusinkiewicz, S. and Levoy, M., 2001. Efficient Variants of the ICP Algorithm. In: Proc. 3DIM 2001, Quebec City, Canada, 28 May - 1 June.
- Schenk, T., Krupnik, A., Postolov, Y., 2000. Comparative study of surface matching algorithms. International Archives of Photogrammetry, Remote Sensing and Spatial Information Sciences 33 (Part B4), 518–524.
- Soudarissanane, S., Lindenbergh, R., Menenti, M., Teunissen, P., 2011. Scanning geometry: Influencing factor on the quality of terrestrial laser scanning points. ISPRS Journal of Photogrammetry and Remote Sensing 66 (4), 389–399.

## APPENDICES



Appendix A Jacobians of Condition Equations for P2P Method

The Jacobian terms in Eq.(3.8) for a single correspondence set in  $\mathbf{P}$  (i.e. one condition equation), are given by

$$\begin{aligned}
 \mathbf{F}_1'(\mathbf{p}_i) &= \frac{\partial \mathbf{F}_1}{\partial \tilde{\mathbf{p}}_i} * \frac{\partial \tilde{\mathbf{p}}_i}{\partial \mathbf{p}_i} = \mathbf{n}_{q_i}^T * \mathbf{R} && \in \mathbb{R}^{1,3} \\
 \mathbf{F}_1'(\mathbf{q}_i) &= \frac{\partial \mathbf{F}_1}{\partial \mathbf{n}_{q_i}} * \frac{\partial \mathbf{n}_{q_i}}{\partial \mathbf{q}_{e_i}} + \frac{\partial \mathbf{F}_1}{\partial \mathbf{q}_{e_i}} \\
 &= (\tilde{\mathbf{p}}_i - \mathbf{q}_j)^T * \frac{\partial \mathbf{n}_{q_i}}{\partial \mathbf{q}_{e_i}} - [\mathbf{n}_{q_i}^T, \mathbf{o}^T] && \in \mathbb{R}^{1,9} \\
 \mathbf{F}_1'(\Delta) &= \frac{\partial \mathbf{F}_1}{\partial \tilde{\mathbf{p}}_i} * \frac{\partial \tilde{\mathbf{p}}_i}{\partial \Delta} = \mathbf{n}_{q_i}^T * \left[ \frac{\partial \tilde{\mathbf{p}}_i}{\partial \Delta_1}, \frac{\partial \tilde{\mathbf{p}}_i}{\partial \Delta_2} \right] \\
 &= \mathbf{n}_{q_i}^T * \left[ \left( \frac{\partial \mathbf{R}}{\partial \omega} \mathbf{p}_i, \frac{\partial \mathbf{R}}{\partial \phi} \mathbf{p}_i, \frac{\partial \mathbf{R}}{\partial \kappa} \mathbf{p}_i \right), \mathbb{I}_3 \right] && \in \mathbb{R}^{1,6} \quad (\text{A.1})
 \end{aligned}$$

where

$\mathbb{I}_3$  is the identity matrix of size 3

$\mathbf{o}$  is a zero vector of length six

$\mathbf{R}$  is the conventional 3D orthogonal rotation matrix given in Eq.(3.1)

$\mathbf{n}_{p_i}$  is the normal vector of the planar element  $\mathbf{p}_e$  as given in Eq.(3.6)

$\mathbf{n}_{q_i}$  is the normal vector of the planar element  $\mathbf{q}_e$  as given in Eq.(3.6)

$\frac{\partial(\cdot)}{\partial(\cdot)}$  represents the partial derivative (or Jacobian)

$(\cdot)^T$  represents the transpose of a vector or matrix

$\tilde{\mathbf{p}}_i$  is the transformed point as given in Eq.(3.2)

$\Delta_1$  and  $\Delta_2$  represent the rotation and translation parameters respectively

The point  $\mathbf{q}_j$  in Eq.(A.1) refers to any of the sampled points forming the planar element  $\mathbf{q}_e$  as given in Eq.(3.6). In Eq.(A.1) the location of the zero terms for  $\mathbf{F}_1'(\mathbf{q}_i)$  must be consistent with that of the points in the planar element. If the first point is selected as  $\mathbf{q}_j$  then the zero terms will be as given in Eq.(A.1).

The Jacobian term  $\frac{\partial \mathbf{n}_{q_i}}{\partial \mathbf{q}_{e_i}}$  is the partial derivative of the local surface normal with respect to the planar element. This term is obtained from using the relevant rule of error propagation for multivariate cases (Mikhail and Ackermann, 1976) as described in Appendix B. This Jacobian captures the uncertainty of the local surface normals, and it impacts the stochastic model of the least squares adjustment.

By similar manipulations for a correspondence set in  $\mathbf{Q}$  one has

$$\begin{aligned} \mathbf{F}_2'(\mathbf{p}_i) &= (\tilde{\mathbf{q}}_i - \mathbf{p}_j)^T * \frac{\partial \mathbf{n}_{p_i}}{\partial \mathbf{p}_{e_i}} - [\mathbf{n}_{p_i}^T, \mathbf{o}^T] \\ \mathbf{F}_2'(\mathbf{q}_i) &= \mathbf{n}_{p_i}^T * \mathbf{R}^T \\ \mathbf{F}_2'(\Delta) &= \mathbf{n}_{p_i}^T * \left[ \left( \frac{\partial \mathbf{R}^T}{\partial \omega}(\mathbf{q}_i - \mathbf{t}), \frac{\partial \mathbf{R}^T}{\partial \phi}(\mathbf{q}_i - \mathbf{t}), \frac{\partial \mathbf{R}^T}{\partial \kappa}(\mathbf{q}_i - \mathbf{t}) \right), -\mathbf{R}^T \right] \end{aligned} \tag{A.2}$$

The terms for the differentiation of the rotation matrix can be found in Mikhail et al. (2001, pg.425). Also for  $\mathbf{F}_2$ , the partial differential of the transposed rotation matrix with respect to any of the rotation parameters is simply the transposed partial differential of the rotation matrix with respect to that parameter.

## Appendix B Redundancy Calculation for P2P Method

For a pair of scans,  $\mathbf{P}$  and  $\mathbf{Q}$  if four scanned points are selected from  $\mathbf{P}$ , then the number of unique planar elements that can be obtained is calculated from the binomial coefficient  $\binom{4}{3} = 4$ . If another four scanned points are selected from  $\mathbf{Q}$  there can be potentially four unique correspondence sets between the two point clouds. In other words, each unique planar element in  $\mathbf{P}$  has a corresponding unique transformed point from  $\mathbf{Q}$ .

Similarly, the four scanned points in  $\mathbf{Q}$  can also provide an additional four unique planar elements. If two of these planar elements are chosen then two additional unique correspondence sets can be obtained. This is done by associating two of the scanned points in  $\mathbf{P}$  with these additional planar elements in  $\mathbf{Q}$ .

By similar deduction it can be seen that any other combination of less than four points from each scan will fail to provide the minimum of six unique correspondence sets. Thus a minimum of eight points (four on each scan) is needed for P2P registration. The redundancy of the adjustment is therefore equal to  $3*(N_p+N_q-8)$ , where  $N_p$  and  $N_q$  are the number of contributing points from  $\mathbf{P}$ , and  $\mathbf{Q}$  respectively. These contributing points are inlier points within the overlapping region.

Appendix C Jacobians of Condition Equations for P2Pg Method

The Jacobian terms in Eq.(4.5) for a single correspondence set in the  $\mathbf{P}$  of a pair of overlapping scans (i.e. one condition equation, from one scan pair), are given by

$$\begin{aligned}
 \mathbf{F}_1'(\mathbf{p}_i) &= \frac{\partial \mathbf{F}_1}{\partial \tilde{\mathbf{p}}_i} * \frac{\partial \tilde{\mathbf{p}}_i}{\partial \mathbf{p}_i} = \mathbf{n}_{\tilde{q}_i}^T * \mathbf{R}_p && \in \mathbb{R}^{1,3} \\
 &= (\mathbf{R}_q * \mathbf{n}_{q_i})^T * \mathbf{R}_p \\
 \mathbf{F}_1'(\mathbf{q}_i) &= \frac{\partial \mathbf{F}_1}{\partial \mathbf{n}_{\tilde{q}_i}} * \frac{\partial \mathbf{n}_{\tilde{q}_i}}{\partial \mathbf{q}_{e_i}} + \frac{\partial \mathbf{F}_1}{\partial \tilde{\mathbf{q}}_{e_i}} * \frac{\partial \tilde{\mathbf{q}}_{e_i}}{\partial \mathbf{q}_{e_i}} && \in \mathbb{R}^{1,9} \\
 &= \left[ (\tilde{\mathbf{p}}_i - \tilde{\mathbf{q}}_j)^T * \mathbf{R}_q * \frac{\partial \mathbf{n}_{q_i}}{\partial \mathbf{q}_{e_i}} \right] - \left[ (\mathbf{R}_q * \mathbf{n}_{q_i})^T * \mathbf{R}_q, \mathbf{o}^T \right] \\
 \mathbf{F}_1'(\Delta_p) &= \frac{\partial \mathbf{F}_1}{\partial \tilde{\mathbf{p}}_i} * \frac{\partial \tilde{\mathbf{p}}_i}{\partial \Delta_p} = \mathbf{n}_{\tilde{q}_i}^T * \left[ \frac{\partial \tilde{\mathbf{p}}_i}{\partial \Delta_{p1}}, \frac{\partial \tilde{\mathbf{p}}_i}{\partial \Delta_{p2}} \right] \\
 &= (\mathbf{R}_q * \mathbf{n}_{q_i})^T * \left[ \left( \frac{\partial \mathbf{R}_p}{\partial \omega} \mathbf{p}_i, \frac{\partial \mathbf{R}_p}{\partial \phi} \mathbf{p}_i, \frac{\partial \mathbf{R}_p}{\partial \kappa} \mathbf{p}_i \right), \mathbb{I}_3 \right] && \in \mathbb{R}^{1,6} \\
 \mathbf{F}_1'(\Delta_q) &= \frac{\partial \mathbf{F}_1}{\partial \mathbf{n}_{\tilde{q}_i}} * \frac{\partial \mathbf{n}_{\tilde{q}_i}}{\partial \tilde{\mathbf{q}}_{e_i}} * \frac{\partial \tilde{\mathbf{q}}_{e_i}}{\partial \Delta_q} + \frac{\partial \mathbf{F}_1}{\partial \tilde{\mathbf{q}}_{e_i}} * \frac{\partial \tilde{\mathbf{q}}_{e_i}}{\partial \Delta_q} && \in \mathbb{R}^{1,6} \\
 &= \left[ (\tilde{\mathbf{p}}_i - \tilde{\mathbf{q}}_j)^T * \mathbf{R}_q * \frac{\partial \mathbf{n}_{q_i}}{\partial \mathbf{q}_{e_i}} * \left( \frac{\partial \tilde{\mathbf{q}}_{e_i}}{\partial \mathbf{q}_{e_i}} \right)^{-1} * \frac{\partial \tilde{\mathbf{q}}_{e_i}}{\partial \Delta_q} \right] - \\
 &\quad (\mathbf{R}_q * \mathbf{n}_{q_i})^T * \left[ \frac{\partial \mathbf{R}_q}{\partial \omega} \mathbf{q}_i, \frac{\partial \mathbf{R}_q}{\partial \phi} \mathbf{q}_i, \frac{\partial \mathbf{R}_q}{\partial \kappa} \mathbf{q}_i, \mathbb{I}_3 \right]
 \end{aligned}$$

(C.1)

In Eq.(C.1):

$\mathbb{I}_3$  is the identity matrix of size 3

$\mathbf{o}$  is a zero vector of length six

$\mathbf{R}_p, \mathbf{R}_q$  are the conventional 3D orthogonal rotation matrices given in Eq.(4.4)

$\mathbf{n}_{q_i}$  is the normal vector of the planar element  $\mathbf{q}_e$  as given in Eq.(3.6)

$\mathbf{n}_{\tilde{q}_i}$  is the normal vector of the planar element  $\tilde{\mathbf{q}}_e$  as given in Eq.(D.1)

$\tilde{\mathbf{q}}_e$  is the planar element obtained from transformed points in  $\mathbf{Q}$

$\frac{\partial(\cdot)}{\partial(\cdot)}$  represents the partial derivative (or Jacobian)

$(\cdot)^T$  represents the transpose of a vector or matrix

$\tilde{\mathbf{p}}_i, \tilde{\mathbf{q}}_i$  are the transformed points as given in Eq.(4.4)

$\Delta_p$  and  $\Delta_q$  represent the transformation parameters for  $\mathbf{P}$  and  $\mathbf{Q}$  respectively

$\Delta_{p1}$  and  $\Delta_{p2}$  represent the rotation and translation parameters respectively for  $\mathbf{P}$

The point  $\tilde{\mathbf{q}}_j$  in Eq.(C.1) refers to any of the transformed points forming the planar element  $\tilde{\mathbf{q}}_e$  as given in Eq.(4.4). In Eq.(C.1) the location of the zero terms for  $\mathbf{F}_1'(\mathbf{q}_i)$  must be consistent with that of the points in the planar element. If the first point is selected as  $\tilde{\mathbf{q}}_j$  then the zero terms will be as given in Eq.(C.1). The computation of the normal vector in the transformed coordinate space and the associated Jacobian terms are discussed in Appendix D.

By similar manipulations for a correspondence set in  $\mathbf{Q}$  of a pair of overlapping scans one has

$$\begin{aligned}
\mathbf{F}_2'(\mathbf{p}_i) &= \left[ (\tilde{\mathbf{q}}_i - \tilde{\mathbf{p}}_j)^T * \mathbf{R}_p * \frac{\partial \mathbf{n}_{p_i}}{\partial \mathbf{p}_{e_i}} \right] - [(\mathbf{R}_p * \mathbf{n}_{p_i})^T * \mathbf{R}_p, \mathbf{o}^T] && \in \mathbb{R}^{1,9} \\
\mathbf{F}_2'(\mathbf{q}_i) &= (\mathbf{R}_p * \mathbf{n}_{p_i})^T * \mathbf{R}_q && \in \mathbb{R}^{1,3} \\
\mathbf{F}_2'(\Delta_p) &= \left[ (\tilde{\mathbf{p}}_i - \tilde{\mathbf{q}}_j)^T * \mathbf{R}_p * \frac{\partial \mathbf{n}_{p_i}}{\partial \mathbf{p}_{e_i}} * \left( \frac{\partial \tilde{\mathbf{p}}_{e_i}}{\partial \mathbf{p}_{e_i}} \right)^{-1} * \frac{\partial \tilde{\mathbf{p}}_{e_i}}{\partial \Delta_p} \right] - \\
&\quad (\mathbf{R}_p * \mathbf{n}_{p_i})^T * \left[ \frac{\partial \mathbf{R}_p}{\partial \omega} \mathbf{p}_i, \frac{\partial \mathbf{R}_p}{\partial \phi} \mathbf{p}_i, \frac{\partial \mathbf{R}_p}{\partial \kappa} \mathbf{p}_i, \mathbb{I}_3 \right] && \in \mathbb{R}^{1,6} \\
\mathbf{F}_2'(\Delta_q) &= (\mathbf{R}_p * \mathbf{n}_{p_i})^T * \left[ \left( \frac{\partial \mathbf{R}_q}{\partial \omega} \mathbf{q}_i, \frac{\partial \mathbf{R}_q}{\partial \phi} \mathbf{q}_i, \frac{\partial \mathbf{R}_q}{\partial \kappa} \mathbf{q}_i \right), \mathbb{I}_3 \right] && \in \mathbb{R}^{1,6}
\end{aligned}$$

(C.2)

## Appendix D Transformed Planar Element and its Partial Derivatives

The planar element in Eq.(4.4) and its unit normal vector are given in the reference coordinate frame. These quantities are obtained from the transformed point coordinates. However, when the original sampled points are transformed to the reference coordinate frame, new (or false) incidence angles are introduced at each transformed point. This happens since the incidence angle is computed relative to the coordinate origin. For the transformed coordinates the new origin is that of the reference coordinate frame and not the origin of the local coordinate frame in which the point coordinates were obtained. These new (or false) incidence angles impact the stochastic model and it is thus preferred to compute unit normals for points in their original coordinate frame. The necessary transformed quantities can be obtained as follows.

$$\begin{aligned}
 \mathbf{n}_{\tilde{q}_i} &= \mathbf{R}_q * \mathbf{n}_q && \in \mathbb{R}^{3,1} \\
 \Rightarrow \frac{\partial \mathbf{n}_{\tilde{q}_i}}{\partial \mathbf{q}_{e_i}} &= \mathbf{R}_q * \frac{\partial \mathbf{n}_{q_i}}{\partial \mathbf{q}_{e_i}} && \in \mathbb{R}^{3,9}
 \end{aligned} \tag{D.1}$$

The left-hand side of Eq.(D.1) can alternatively be expressed as

$$\begin{aligned}
 \frac{\partial \mathbf{n}_{\tilde{q}_i}}{\partial \mathbf{q}_{e_i}} &= \frac{\partial \mathbf{n}_{\tilde{q}_i}}{\partial \tilde{\mathbf{q}}_{e_i}} * \frac{\partial \tilde{\mathbf{q}}_{e_i}}{\partial \mathbf{q}_{e_i}} \\
 \Rightarrow \mathbf{R}_q * \frac{\partial \mathbf{n}_{q_i}}{\partial \mathbf{q}_{e_i}} &= \frac{\partial \mathbf{n}_{\tilde{q}_i}}{\partial \tilde{\mathbf{q}}_{e_i}} * \frac{\partial \tilde{\mathbf{q}}_{e_i}}{\partial \mathbf{q}_{e_i}} \\
 \Rightarrow \frac{\partial \mathbf{n}_{\tilde{q}_i}}{\partial \tilde{\mathbf{q}}_{e_i}} &= \mathbf{R}_q * \frac{\partial \mathbf{n}_{q_i}}{\partial \mathbf{q}_{e_i}} * \left( \frac{\partial \tilde{\mathbf{q}}_{e_i}}{\partial \mathbf{q}_{e_i}} \right)^{-1} && \in \mathbb{R}^{3,9}
 \end{aligned} \tag{D.2}$$

And,

$$\left(\frac{\partial \tilde{\mathbf{q}}_{e_i}}{\partial \mathbf{q}_{e_i}}\right)^{-1} = \begin{bmatrix} \mathbf{R}_q & \emptyset & \emptyset \\ \emptyset & \mathbf{R}_q & \emptyset \\ \emptyset & \emptyset & \mathbf{R}_q \end{bmatrix}^{-1} \in \mathbb{R}^{9,9} \quad (\text{D.3})$$

Eq.(D.3) is in relation to the three points of a planar element.

Finally,

$$\begin{aligned} \frac{\partial \mathbf{n}_{\tilde{q}_i}}{\partial \Delta_q} &= \frac{\partial \mathbf{n}_{\tilde{q}_i}}{\partial \tilde{\mathbf{q}}_{e_i}} * \frac{\partial \tilde{\mathbf{q}}_{e_i}}{\partial \Delta_q} \\ \Rightarrow \frac{\partial \mathbf{n}_{\tilde{q}_i}}{\partial \Delta_q} &= \mathbf{R}_q * \frac{\partial \mathbf{n}_{q_i}}{\partial \mathbf{q}_{e_i}} * \left(\frac{\partial \tilde{\mathbf{q}}_{e_i}}{\partial \mathbf{q}_{e_i}}\right)^{-1} * \frac{\partial \tilde{\mathbf{q}}_{e_i}}{\partial \Delta_q} \in \mathbb{R}^{3,9} \end{aligned} \quad (\text{D.4})$$

where

$$\frac{\partial \tilde{\mathbf{q}}_{e_i}}{\partial \Delta_q} = \begin{bmatrix} \frac{\partial \mathbf{R}_q}{\partial \omega} q_1 & \frac{\partial \mathbf{R}_q}{\partial \phi} q_1 & \frac{\partial \mathbf{R}_q}{\partial \kappa} q_1 \\ \frac{\partial \mathbf{R}_q}{\partial \omega} q_2 & \frac{\partial \mathbf{R}_q}{\partial \phi} q_2 & \frac{\partial \mathbf{R}_q}{\partial \kappa} q_2 \\ \frac{\partial \mathbf{R}_q}{\partial \omega} q_3 & \frac{\partial \mathbf{R}_q}{\partial \phi} q_3 & \frac{\partial \mathbf{R}_q}{\partial \kappa} q_3 \end{bmatrix} \begin{pmatrix} \mathbb{I}_3 \\ \mathbb{I}_3 \\ \mathbb{I}_3 \end{pmatrix} \in \mathbb{R}^{9,6}$$



Appendix E Registration Parameter Errors

In both Table E-1 and Table E-2, the parameter errors are the differences in rotation values (in radians) and translation values (in meters) relative to the parameters obtained by using the target based registration. In Table E-2, Cyclone2 represents the refined Cyclone option.

Table E-1 Pairwise parameter errors for each scan pair of the Purdue data.

Pair	1	2	3	4	5	6	7	8
<b>Besl_om</b>	-2.8E-03	-1.5E-03	-2.6E-03	2.6E-04	9.7E-04	-1.0E-03	-2.4E-04	-3.6E-03
<b>Besl_ph</b>	4.9E-04	9.0E-04	3.0E-03	1.9E-04	-3.4E-05	4.9E-04	1.2E-03	-3.5E-03
<b>Besl_ka</b>	4.9E-04	-3.1E-04	1.5E-03	0.0E+00	2.0E-04	-8.1E-04	7.9E-04	1.7E-03
<b>Besl_Tx</b>	0.008	0.001	-0.003	0.000	0.001	0.002	0.000	0.010
<b>Besl_Ty</b>	-0.001	0.001	-0.013	0.001	0.001	0.002	-0.001	-0.007
<b>Besl_Tz</b>	-0.004	-0.003	0.022	-0.001	0.004	-0.001	0.004	-0.004
<b>P2P_om</b>	4.2E-04	-2.9E-04	-9.1E-04	-3.8E-05	1.1E-04	2.9E-04	-4.2E-04	-1.6E-04
<b>P2P_ph</b>	-1.4E-03	1.1E-04	1.0E-04	8.5E-05	2.4E-04	4.9E-04	-3.1E-04	8.8E-04
<b>P2P_ka</b>	-2.1E-04	-5.0E-04	4.9E-04	0.0E+00	2.0E-04	-6.0E-04	-6.1E-04	7.9E-04
<b>P2P_Tx</b>	-0.002	-0.001	-0.001	0.001	0.000	0.001	0.002	0.003
<b>P2P_Ty</b>	0.001	0.003	-0.004	0.000	0.002	0.002	0.005	-0.002
<b>P2P_Tz</b>	-0.008	-0.001	0.000	0.001	0.001	0.002	-0.003	0.005
<b>CloudC_om</b>	4.5E-03	4.3E-03	-1.6E-03	-1.5E-03	-5.6E-04	9.5E-05	2.1E-03	1.1E-02
<b>CloudC_ph</b>	-1.9E-02	-5.1E-03	1.0E-03	3.0E-03	4.2E-03	9.8E-04	-2.2E-03	8.9E-03
<b>CloudC_ka</b>	-3.2E-04	-1.2E-03	1.1E-03	2.6E-04	2.1E-04	-5.8E-04	2.0E-03	2.4E-04
<b>CloudC_Tx</b>	0.003	-0.002	-0.007	0.004	0.004	0.001	-0.003	0.022
<b>CloudC_Ty</b>	-0.008	0.004	-0.014	-0.004	0.003	-0.001	-0.011	-0.030
<b>CloudC_Tz</b>	-0.117	-0.007	0.008	0.002	0.018	0.003	-0.004	0.002
<b>Cyclone_om</b>	2.1E-04	-1.0E-04	-2.2E-03	5.2E-04	2.7E-04	-1.8E-03	-8.5E-04	-3.7E-03
<b>Cyclone_ph</b>	1.7E-04	4.3E-04	2.5E-03	-2.5E-04	8.3E-04	1.6E-03	1.1E-03	-1.9E-03
<b>Cyclone_ka</b>	3.3E-05	-1.4E-03	9.5E-04	2.2E-05	2.4E-04	-4.9E-04	9.2E-04	2.0E-03
<b>Cyclone_Tx</b>	0.000	-0.003	-0.001	0.000	-0.001	0.001	0.000	0.004
<b>Cyclone_Ty</b>	0.001	0.010	-0.007	0.001	0.001	0.004	-0.002	-0.002
<b>Cyclone_Tz</b>	0.001	0.001	0.019	-0.002	0.004	0.000	0.003	0.005

Table E-2 Global parameter errors for each registered scan of the Purdue data.

Scan	2	3	4	5	6	7	8
<b>Besl_om</b>	-2.8E-03	-2.3E-03	-4.8E-03	-7.3E-03	8.8E-03	5.4E-03	3.6E-03
<b>Besl_ph</b>	4.9E-04	3.6E-03	6.5E-03	-2.7E-03	2.6E-04	-5.6E-03	-5.7E-03
<b>Besl_ka</b>	4.9E-04	8.6E-05	1.6E-03	1.6E-03	1.8E-03	1.0E-03	1.8E-03
<b>Besl_Tx</b>	0.008	0.006	0.009	0.001	-0.005	-0.001	0.000
<b>Besl_Ty</b>	-0.001	0.002	0.015	0.010	0.005	-0.005	-0.008
<b>Besl_Tz</b>	-0.004	0.005	0.051	0.054	0.046	-0.001	-0.017
<b>P2P_om</b>	4.2E-04	-1.4E-03	-2.3E-03	1.4E-04	7.1E-04	2.5E-03	2.5E-03
<b>P2P_ph</b>	-1.4E-03	-8.7E-04	-8.4E-04	-2.3E-03	2.5E-03	1.7E-03	5.9E-04
<b>P2P_ka</b>	-2.1E-04	-8.0E-04	-3.0E-04	-3.0E-04	-8.6E-05	-6.6E-04	-1.3E-03
<b>P2P_Tx</b>	-0.002	-0.004	-0.001	0.000	-0.002	0.000	0.002
<b>P2P_Ty</b>	0.001	-0.002	-0.001	-0.002	-0.001	-0.001	0.005
<b>P2P_Tz</b>	-0.008	-0.010	-0.008	0.005	0.014	0.014	0.007
<b>CloudC_om</b>	4.5E-03	-1.1E-02	-1.3E-02	1.1E-02	-6.9E-03	1.0E-02	1.7E-02
<b>CloudC_ph</b>	-1.9E-02	-1.8E-02	-1.7E-02	-1.4E-02	2.1E-02	2.1E-02	1.5E-02
<b>CloudC_ka</b>	-3.2E-04	-1.8E-03	-6.7E-04	-2.3E-04	-1.9E-08	-7.3E-04	1.3E-03
<b>CloudC_Tx</b>	0.003	0.001	0.013	0.011	0.008	0.007	0.001
<b>CloudC_Ty</b>	-0.008	-0.011	-0.005	0.001	0.005	0.003	-0.005
<b>CloudC_Tz</b>	-0.117	-0.125	-0.137	-0.041	0.059	0.111	0.110
<b>Cyclone_om</b>	2.1E-04	1.5E-04	-2.0E-03	-2.7E-03	3.3E-03	1.5E-03	7.0E-04
<b>Cyclone_ph</b>	1.7E-04	3.7E-04	2.8E-03	-1.4E-03	1.3E-03	1.3E-04	7.7E-04
<b>Cyclone_ka</b>	3.3E-05	-1.4E-03	-4.5E-04	-4.4E-04	-1.8E-04	-6.5E-04	2.8E-04
<b>Cyclone_Tx</b>	0.000	-0.009	-0.003	-0.002	-0.001	0.002	0.000
<b>Cyclone_Ty</b>	0.001	-0.005	-0.005	-0.006	-0.006	-0.005	-0.005
<b>Cyclone_Tz</b>	0.001	0.001	0.021	0.020	0.021	0.004	0.003
<b>P2Pg_om</b>	2.2E-04	-9.5E-04	-2.1E-03	7.3E-05	4.0E-04	3.1E-03	2.3E-03
<b>P2Pg_ph</b>	-1.6E-03	-8.6E-04	-1.1E-03	-2.2E-03	2.6E-03	1.9E-03	6.9E-04
<b>P2Pg_ka</b>	-9.0E-05	-5.5E-04	-2.2E-04	-4.0E-04	4.3E-05	-1.1E-03	-1.2E-03
<b>P2Pg_Tx</b>	-0.001	-0.003	-0.001	0.000	-0.003	0.002	0.002
<b>P2Pg_Ty</b>	0.000	-0.002	-0.001	-0.003	-0.001	0.001	0.005
<b>P2Pg_Tz</b>	-0.010	-0.008	-0.010	0.004	0.013	0.015	0.007
<b>Cyclone2_om</b>	5.2E-04	-6.0E-04	-3.0E-03	-2.2E-03	3.3E-03	3.2E-03	2.9E-03
<b>Cyclone2_ph</b>	-8.0E-04	-3.6E-04	2.2E-03	-3.0E-03	3.4E-03	1.5E-03	1.5E-03
<b>Cyclone2_ka</b>	-2.8E-04	-1.8E-03	-9.7E-04	-9.8E-04	-7.4E-04	-1.9E-03	-1.5E-03
<b>Cyclone2_Tx</b>	-0.002	-0.011	-0.004	0.000	0.003	0.008	0.006
<b>Cyclone2_Ty</b>	0.000	-0.007	-0.008	-0.009	-0.008	-0.002	0.002
<b>Cyclone2_Tz</b>	-0.004	-0.005	0.016	0.021	0.031	0.015	0.012

VITA

## VITA

Darion Grant is a citizen of Trinidad and Tobago, and was born on September 10, 1977. He earned his Bachelor of Science Degree in the Department of Surveying and Land Information at the University of the West Indies, St. Augustine, Trinidad in June 2000. He was then employed as a Graduate Surveyor in his native island of Tobago until 2003, engaging in engineering and cadastral surveys. He then joined California State University, Fresno in August 2003 where he completed his Master of Science Degree in Geomatics in December 2005. The emphasis of his master's program was in Photogrammetry and his research work was in LiDAR. Darion joined the Department of Geomatics in the School of Civil Engineering at Purdue University in January 2006 to pursue a Degree of Doctor of Philosophy focusing on Photogrammetry, LiDAR and Computational Engineering. Prior to his graduation from Purdue in August 2013, he joined the School of Civil Engineering and Geosciences in Newcastle University, Newcastle upon Tyne, UK, as a Lecturer in Photogrammetry and Laser Scanning, in February 2013.

## PUBLICATIONS

## PUBLICATIONS

Grant, D., J. Bethel and M. Crawford, "Point-to-Plane Registration of Terrestrial Laser Scans." *ISPRS Journal of Photogrammetry and Remote Sensing* 2012, 72, pp: 16-26.

Grant, D., J. Bethel and M. Crawford, "Rigorous Point-to-Plane Registration of Terrestrial Laser Scans." In *Proc. ISPRS XXII Congress, August 25-September 01, Melbourne, Australia, 2012.*

Rochon, G.L., L. Biehl, S. Fall, D. Grant, T. Thiam, B. Araya, B.H. Mbongo, J. Jung, S. Ghani, M.A. Wahab, G.S. El Afandi, G. Altay, O. Ersoy, A.T. Valcarcel, and C.J. Gonzalez, "Real-Time Remote Sensing in Support of Ecosystem Services and Sustainability.", pp:217-223. In P.H. Liotta, et al., *Achieving Environmental Security: Ecosystem Services and Human Welfare* (ISBN 978-1-60750-578-5; August 2010, 296 pp., IOS Press, Amsterdam)

Grant, D., J. Bethel and M. Crawford, "A Correspondence-Based Strategy for Automatic Registration of Terrestrial Laser Scanning Data." In *Proc. ASPRS Annual Conference, April 26-30, San Diego, CA, 2010.*

Grant, D., J. Bethel and M. Crawford, "Direct Point Correspondence for LIDAR Strip Adjustment Using Iterative Network Matching." In Proc. 10th International Lidar Mapping Forum Conference, March 3-5, Denver, CO, 2010.

Rochon, G., M.A. Wahab, G.S. El Afandi, G. Altay, O.K. Ersoy, X.C. Song, L. Zhao, D. Niyogi, L.Biehl, D. Grant, B. Elleithy, M. Shokr, M.A. Mohamed, and T. El Ghazawi: "The Kamal Ewida Earth Observatory: A NATO Supported Real-time Remote Sensing Receiving Station being Established in Egypt with HPC-enabled Near-real-time Data Products for Mitigation of Environmental & Public Health Disasters." In Proc. IEEE IGARSS July 12-17, University of Cape Town, South Africa, 2009.

Tarko, A.P., J. Thomaz, and D. Grant, "Probabilistic Determination of Crash Locations in a Road Network with Imperfect Data.", Transportation Research Record: Journal of the Transportation Research Board 2009, 2102(1), pp: 76-84.

Tarko, A.P., D. Grant, and J. Thomaz, "Probabilistic Data Linking For Mapping Crashes In Large Networks." In Proc. 10th International Conference on Application of Advanced Technologies in Transportation, May 27- 31, Athens GREECE, 2008.